Molecular Study of Capsaicin in Aqueous and Hydrophobic Environments

Joseph W. Lambert

Thesis submitted to the Faculty of the
Virginia Polytechnic Institute and State University
in partial fulfillment of the requirements for the degree of

Master of Science
in
Chemical Engineering

Amadeu K. Sum, Chair
David R. Bevan
Eva Marand

June 8, 2006
Blacksburg, Virginia

Keywords: Capsaicin, Molecular Dynamics, Simulations, Lipid Bilayer, Octanol-water

Molecular Study of Capsaicin in Aqueous and Hydrophobic Environments

Joseph W. Lambert

Abstract

Anyone who has eaten spicy foods has experienced the adverse effects of capsaicin, the pungent chemical found in hot chili that causes a burning sensation. The specific action of capsaicin occurs by the activation of receptors in sensory neurons. This thesis investigates the interaction of capsaicin with model cell membranes representing the structure of neurons. In particular, we are interested in the changes induced by capsaicin to the structure and dynamics of membranes. Molecular dynamics simulations are used to study the molecular interactions. The first part of this study evaluates different molecular representations for capsaicin in an 1-octanol/water system. This inhomogeneous system is commonly used to determine the partition of compounds between hydrophilic and hydrophobic environments, as that found in biological membranes. The results of these simulations validate the OPLS united-atom force field as a reasonable molecular representation of capsaicin, as it describes the behavior of capsaicin both quantitatively and qualitatively in 1-octanol/water mixtures. In the second part, simulations are performed for capsaicin and model cell membranes consisting of dipalmitoylphosphatidylcholine and dipalmitoylphosphatidylethanolamine, two of the most commonly found lipids. Simulations investigated capsaicin in the aqueous and lipid phases. The results provide insight into the changes to the bilayers caused by capsaicin. Bilayers containing dipalmitoylphosphatidylethanolamine showed lower permeabilities to capsaicin than those composed of pure dipalmitoylphosphatidylcholine. Temperature is found to be an important factor in the permeability of capsaicin in the bilayer. Capsaicin in the bilayer concentrated in a region beneath the lipid/water interface, in which favorable hydrophilic and lipophilic interactions occur. The structure of the bilayer is not significantly changed at the concentrations of capsaicin considered. One important result from the simulations indicates that the interfacial density decreases with increasing capsaicin concentration in

the bilayer, supporting the experimental observations of increased permeability in bilayers exposed to capsaicin.

Dedication

To Janna, without your constant love and support, none of this would have been possible.

Acknowledgments

Soli Deo gloria!

The work contained in this dissertation would not be possible without the intellectual support of my adviser, professors, and fellow students. I would like to thank Professor Amadeu K. Sum for his guidance and support that led to a better understanding of this study, and my committee members: Professors David R. Bevan and Eva Marand. I am also grateful for the insight provided by my classmate Sukit Leekumjorn during the course of my studies at Virginia Tech. I would also like to acknowledge the computational resources provided by Virginia Tech Terascale Computing Facility (System X). As one of the first users of this system, almost unlimited time was granted for usage, without which, none of this thesis would be possible.

I also thank all of my parents: Pops, Mom, Miriam, Gary, Katie, and Bill. Your constant love, support, and prayers are appreciated and I owe much of my success to you.

And last but not least, the congregation of Redeemer Church, my family of brothers and sisters, whose fellowship has been a great service to my wife and I during our time at Virginia Tech.

Contents

List of Tables

List of Figures

Chapter 1

Introduction

1.1 Motivation

Most people probably know more about capsaicin and its physiological effects than they realize. The effects of capsaicin are well illustrated by culinary experiences of, for example, eating hot buffalo wings or spicy ethnic food. Ingestion of these foods is immediately followed by a burning sensation. A novice may drink a glass of water, only to find that the pain increases. A more experienced person will reach for ranch dressing or some other fatty food to "quench the fire." It is also common to see spicy food veterans that are indifferent to the hottest menu item. Some people suffer from osteoarthritis or rheumatoid arthritis and use creams containing capsaicin for its analgesic properties. These creams do not provide immediate relief (in fact the burning may be unbearable), but prolonged use can considerably reduce the chronic pain.

We can deduce a great deal of information about the physiological action of capsaicin by simply recalling these every day occurrences or reading the instructions and warning labels of topical creams containing capsaicin. Common warnings and side effects associated with these creams include:

- Avoid taking a hot bath or shower after application

- Do not use on broken or infected skin

- Avoid use near eyes or other sensitive areas

- Wash affected sensitive areas with soapy water

These warnings are similar to culinary experiences: water increases the pain while a fatty substance, like ranch dressing, milk, or yogurt, alleviates it. We know that capsaicin triggers a somatosensation (sense of touch), but what do these experiences teach us? In scientific terms, water and fat correspond to hydrophilic and hydrophobic environments, and on the level of sensory neurons, these environments are representative of the extracellular domain and the cell membrane of the neurons, respectively. Sensory neurons are members of the human peripheral central nervous systems (CNS), and as such, they are responsible for sensing changes that occur throughout the body. The CNS functions by relaying cellular signals, in the form of action potentials, from sensory neurons to the spinal cord, and ultimately to the brain [1]. This process begins when the chemical potential across sensory neurons is changed. A diagram of this pathway for the chemical activation of sensory neurons by capsaicin is shown in Figure 1.1.

Recently, our understanding of how the brain acquires and processes somatosensations has been revolutionized [2]. The cell membrane of sensory neurons is responsible for maintaining a chemical potential, or a state of non-equilibrium, between the intra- and extracellular domains. Changes in this potential are facilitated by embedded membrane proteins that regulate the transient flow of ions across the membrane. A change in the local concentration of ions, changes the chemical potential across the cell, and triggers the pain pathway [2]. With the completion of the genome project in 2003 and advances in crystallographic/spectroscopic methods, the sequence of all proteins and the structure of some are accessible. These advances greatly assist studies to understand the role of proteins in their biological function.

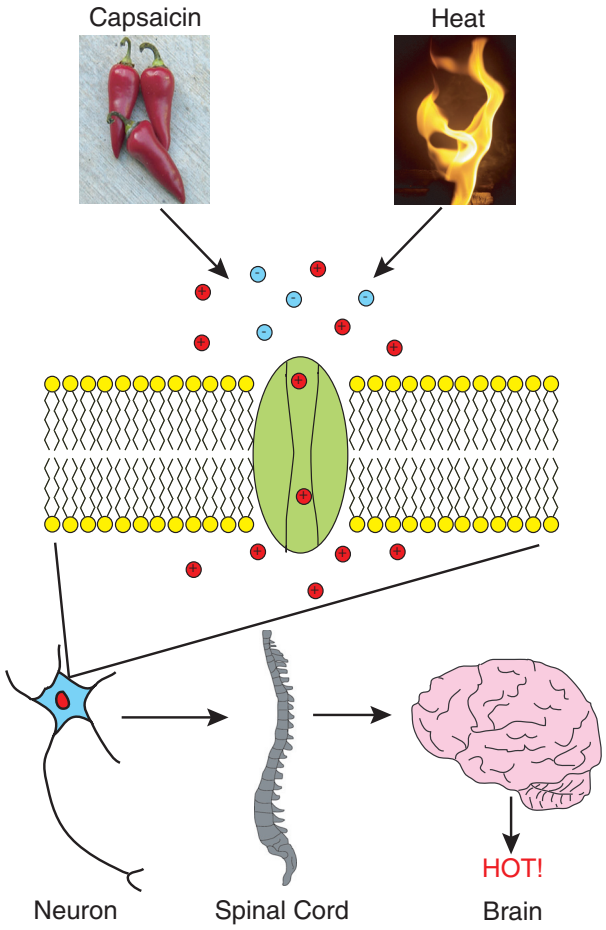

Figure 1.1: Diagram of the pain pathway initiated when sensory neurons are exposed to capsaicin or heat. When a chemical potential across sensory neurons is induced, a signal is transferred to the spinal cord and then to the brain in the form of action potentials. The brain senses the stimuli as "hot!"

Transient receptor potential (TRP) proteins are a family of embedded membrane proteins that are commonly expressed by sensory neurons. This family of proteins is involved in many sensory processes including gustatory, auditory, thermal, and pain sensations [3]. Recently, the TRP protein responsible for sensing capsaicin and noxious temperatures was isolated [4]. This protein was named the vanilloid receptor (TRPV1) because of its chemical activation by vanilloid functional groups. TRPV1 is a non-selective ion channel that transports about ten calcium ions for every sodium ion [4]. Exposure to capsaicin for prolonged periods of time causes a continuous influx of calcium ions that eventually leads to cell death [4]. For this reason, capsaicin not only desensitizes sensory neurons to itself, but to other stimuli as well. This behavior helps to explain the analgesic properties of capsaicin and the indifference of spicy food veterans to its effects.

The physiological effects of capsaicin are well known, but the specific interactions involving capsaicin, sensory neurons, and TRPV1 that lead to its chemosensory action are unclear. The cell membrane is a complex, fluid structure composed of various components including phospholipids, proteins, and organic molecules that protect cells by maintaining the delicate balance between the intra- and extracellular domains. Isolation of specific interactions in this complex environment are difficult to obtain by conventional experimental methods, especially at the resolution of molecular processes. Molecular simulations are useful for studying these interactions in model environments. A combination of experiments and simulations is the best approach to obtain insight into the complex interactions of cells and their environment. This is especially true to expand our understanding of the chemosensory action of capsaicin.

The ability of TRPV1 to sense both chemical and thermal stimuli has made it a model system in the study of the pain pathway and somatosensations [2]. The study presented here will address a small but essential subsection of the chemical activation of TRPV1 by capsaicin, namely, its initial interaction with the plasma membrane that encloses the receptor. Molecular dynamics simulations are used to obtain structural and dynamic properties of model cell membranes, modeled as phospholipid bilayers, in the presence of

capsaicin. The study will provide insight into selected aspects of the chemosensory effects of capsaicin and will describe the change on biological membranes induced by capsaicin.

1.2 Organization of the Thesis

This thesis is organized as follows. Chapter 2 provides an overview of the literature that pertains to this study. Background information of early studies, recent experimental studies, and molecular simulations of small molecules in lipid bilayers are discussed.

Chapter 3 describes the molecular simulation method used in this study. The theory of the method and the development of computational algorithms employed here are briefly mentioned.

Chapter 4 discusses the study of an 1-octanol/water system to assess force fields for capsaicin. The force fields are evaluated by their ability to represent capsaicin, both quantitatively and qualitatively. Structural properties of capsaicin in an amphiphilic aqueous environment are determined using simulations.

Chapter 5 details simulations performed for capsaicin and model cell membranes consisting of dipalmioylphosphatidylcholine and dipalmioylphosphatidylethanolamine, two of the most commonly found lipids. Simulations investigate capsaicin in the aqueous and lipid phases. The results provide insight into the changes to the lipid bilayers caused by capsaicin.

Chapter 6 summarizes the study contained in this dissertation and elaborates on possible future studies. A complete list of references cited is also provided as well as appendices with supplemental information for Chapter 3.

Chapter 2

Literature Review

2.1 Introduction

This chapter reviews the relevant literature as background for the study presented in this dissertation. The chapter is divided into two main sections. The first section will address experimental studies of capsaicin and its effects on model cell membranes. The reader is referred elsewhere for general reviews of the pharmacokinetics of capsaicin [5, 6] and its interactions with its receptor [1, 4, 7]. The second section will address the use of molecular dynamics simulations in the modeling of phospholipid bilayers, in particular in the presence of small organic molecules. There are a large number of publications on capsaicin and molecular simulations of phospholipid bilayers, as separate subjects, and this review will only address the literature that is most pertinent to this dissertation.

2.2 Background

Capsaicin is a member of the capsaicinoid family of chemosensory molecules found in *Capsicum* fruits. All capsaicinoids are vanillylamides of fatty acids that differ in the length of

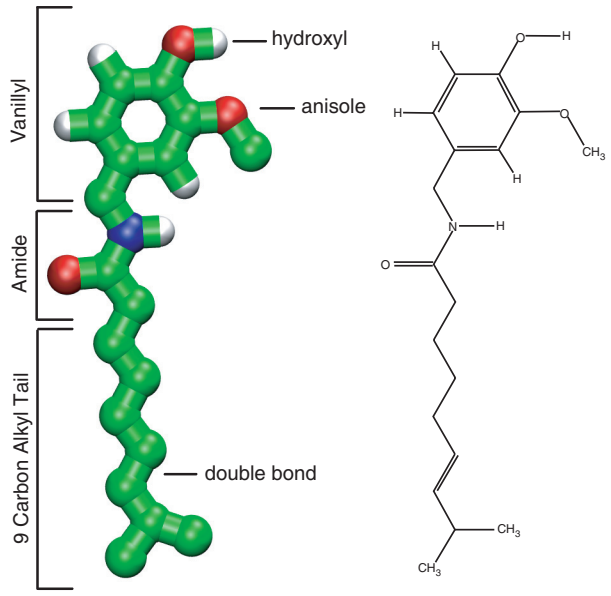

Figure 2.1: Chemical structure of capsaicin ((6*E*)-*N*-(4-hydroxy-3-methoxybenzyl)-8-methylnon-6-enamide).

their aliphatic side chain [8]. The capsaicin hydrocarbon group consists of a 7-methyl-8-octene hydrocarbon moiety that exists purely in the *trans* configuration about the double bond, as shown in Figure 2.1 [8, 9]. Capsaicin is one of the most commonly found capsaicinoids and is also the most pungent. The effects of capsaicin have intrigued scientists since it was first isolated by Thresh in 1846 [10]. The most famous research concerning capsaicin was the development of the "Organoleptic Test" by Wilbur Scoville in 1912, which was used to quantify the pungency of chili peppers in what is now known as Scoville units [11]. The Scoville unit measures the degree of "hotness," indicating that the effect of capsaicin was initially related to the perception of noxious temperatures.

Other applications of capsaicin are found in non-culinary avenues, including pepper sprays, analgesic medicines, and bird seed additives. The effectiveness of pepper sprays is attributed to capsaicin acting as an irritant to the mucus membranes and ocular cavities. Capsaicin has found widespread clinical use as an analgesic in topical creams and by intravenous instillation because of its seemingly paradoxical ability to desensitize sensory neurons

after prolonged exposure [5]. Recently, the medicinal use of capsaicin has been expanded because of its ability to target cancer cells without damaging healthy cells [12], and its ability to have chemoprotective activity against some carcinogens [13]. The use of capsaicin in bird seed is beneficial because of the species specific sensitivity to capsaicin, which is exhibited by the indifference of birds to its effects [14]. These diverse applications can all be attributed to a phenomenon that occurs at the molecular level between capsaicin and sensory neurons.

The cell membrane is a fluid mosaic of lipids, proteins, and other organic molecules that serve as a protective barrier by facilitating transport into and out of cells [15]. The cell membrane of sensory neurons, in particular, maintains a chemical potential in the form of an ion gradient between the intra and extracellular domains. Disturbances in this chemical potential activate a signaling process in the central nervous system that corresponds to the perception of various stimuli. As a result of the chemosensory and physiological effects of capsaicin, it is evident that capsaicin affects this chemical potential. This indicates that the action of capsaicin is localized in the vicinity of sensory neurons. Further evidence for a site specific interaction of capsaicin was gathered by the cloning of the capsaicin receptor, TRPV1 [4]. This transmembrane protein is naturally expressed in thinly myelineated Aδ-neurons and unmyelineated C-neurons [1], and it is believed to be the binding site for capsaicin interaction. The expression of this protein in the cell membrane also indicates that the action of capsaicin occurs in the local environment of the cell membrane, as depicted in Figure 2.2.

The focus of this dissertation will be on the interactions of capsaicin with the cell membrane of sensory neurons. These specific interactions are strongly coupled to those occurring between capsaicin and TRPV1, and they likely have an influence on the chemosensory effects of capsaicin. Experiments suggest that capsaicin can cause substantial changes in the structure and fluidity of biological membranes, which are represented as phospholipid bilayers [16–19]. Moreover, structural changes in the bilayer are known to affect the conformation of embedded membrane proteins [16, 20], which in turn can lead to changes in the chemical potential of ions in sensory neurons.

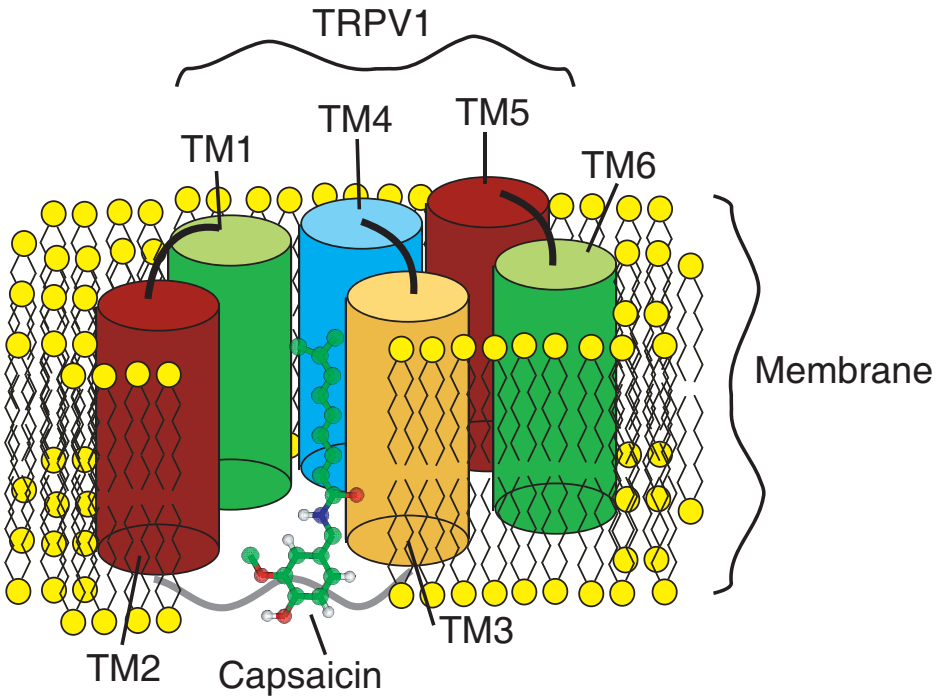

Figure 2.2: Suggested alignment of capsaicin in the cell membrane that leads to its specific interactions with the transmembrane protein TRPV1.

Molecular dynamics simulations are a valuable tool for studying molecular interactions, providing insight into the behavior and properties observed at the macroscopic level. Simulations are particularly useful in the study of phospholipid bilayers since their complex structure can be difficult to study by conventional experimental methods. Therefore, we use molecular dynamics simulations to determine the structural and dynamic properties of capsaicin in phospholipid bilayers.

2.3 Experimental Studies of Capsaicin

Initial interests in capsaicin originated from its pharmacokinetic responses after exposure [11]. Studies have focused on the interactions of capsaicin with cells at the molecular level, and the possible mechanisms of sensory activity. These two avenues of research detailed the effects of capsaicin on biological membranes and led to the discovery of TRPV1.

A detailed review by Buck and Burk [6] was the first to suggest that the mechanism of capsaicin action may be the result of intrinsic interactions with lipid membranes. After reviewing previous experimental studies, the authors suggested that the lipophilic nature of capsaicin can lead to an accumulation of capsaicin in lipid membranes, and the subsequent effects on membrane fluidity may induce the formation of ion channels or increase ion permeability [6]. Meddings *et al.* were the first to test this hypothesis by studying the changes in membrane fluidity caused by capsaicin on different types of cells [16]. The study used steady-state fluorescence polarization of two different probes on platelets, β-Lymphocytes, peritoneal mast cells, red blood cells, and erythrocytes. The different probes were chosen to differentiate localizations in the cell membrane: 1-(4-(trimethylamonium)phenyl)-6-phenyl-1,3,5-hexatriene (TMA-DPH) for regions near the phospholipid headgroups and 1,6-diphenyl-1,3,5-hexatriene (DPH) for regions in the core of the bilayer. The affect on the cells was studied for various concentrations of capsaicin, indicating that capsaicin increases the fluidity of platelets and does not affect the fluidity of β-Lymphocytes or erythrocytes. The results

for the peritoneal mast cells and red blood cells are the most applicable to the study here since they share similar characteristics to sensory neurons and model cell membranes. For these cells, the affect of capsaicin was found to be biphasic, that is, at low concentrations of capsaicin, cell membranes became more fluid and at high concentrations the opposite effect was observed [16]. The authors attempted to duplicate the results for liposomes prepared from dimyristoylphosphatidylcholine (DMPC) and cholesterol at a 60:40 weight ratio; however, they were unable to observe any change in the fluidity using a DPH probe. It was speculated that the affect of capsaicin is cell specific and likely requires non-lipid, extractable components [16]. The results of those experiments were inconclusive, but they indicated that capsaicin changes the membrane fluidity as a function of the concentration.

Subsequent experiments by Aranda *et al.* studied the specific interactions of capsaicin with model cell membranes in a more controlled setting [17]. Meddings *et al.* were unable to distinguish the action of capsaicin on inner or outer membranes, which are known to have different lipid compositions. Aranda *et al.* studied the effect of capsaicin on dipalmitoylphosphatidylcholine (DPPC) and dielaidoylphosphatidylethanolamine (DEPE) membranes by using differential scanning calorimetry (DSC) and fluorescence spectroscopy with TMA-DPH, DPH, and 2-AS (a fatty acid with an anthroyloxy group that resides near the lipid/water interface) probes. For the DPPC systems, capsaicin decreased the gel to liquid-crystalline phase transition temperature (T_c) with increasing concentration. This change was attributed to the preferential alignment of capsaicin within the membrane, where the polar hydroxyl and amide groups locate near the lipid/water interface, and the alkyl chain aligns with the lipid acyl tails [17]. The changes were less pronounced in the more ordered DEPE membranes. The fluorescence spectroscopy analysis was inconclusive for TMA-DPH and DPH probes, but 2-AS indicated that both membranes became more rigid with capsaicin mole fractions above 0.20 (water-free mole fraction based on the molar ratio of capsaicin and lipids). This phenomenon was attributed to the formation of capsaicin rich domains that increase the order of the lipid acyl tails. It was speculated that the formation of these domains could facilitate the activity of capsaicin at low concentrations by modifying the

structure of the membrane.

Analogous experiments were conducted by Feigin *et al.* examining the effects of capsaicin and other vanilloids on the conductance across cell membranes [19]. Feigin *et al.* studied the membrane potential across 1,2-dioleoyl-*sn*-glycero-3-phosphoethanolamine (POPE) and 1,2-dioleoyl-*sn*-glycero-3-phosphocholine (POPC) bilayers, and concluded that vanilloids increase the permeability of non-specific cations. Furthermore, the increased permeability of the membranes to ions was directly correlated to their pungency [19]. This result is particularly interesting because of its implications in the physiological basis of capsaicin sensitivity, which is attributed to a change in the chemical potential across sensory neurons [4, 5].

More recently, Tsuchiya performed fluorescence spectroscopy on pure and cholesterol containing POPC, DPPC, and DMPC liposomes in the presence of capsaicin [18]. As concluded by Meddings [16], Tsuchiya determined that capsaicin induces a biphasic structure on cholesterol-free liposomes (low concentrations make the membrane more fluid and high concentrations less fluid). This biphasic behavior was attributed to the free volume present in the hydrophobic region of the membrane. At low concentrations, the lipid acyl tails can bend cooperatively to fill the free volume created by the capsaicin polar groups that align near the interface. This cooperative bending of the lipid tails results in an increase in the fluidity of the membrane. At higher concentrations, the author speculated that interdigitation of the lipid acyl tails fills the free volume, making the membrane less fluid [18].

The ability of capsaicin to change the fluidity of cell membranes could be partially responsible for its chemosensory activity according to a recent study by Lundbæk *et al.* [21]. These authors investigated the regulation of membrane protein functions by altering the elastic properties of the host lipid bilayer. Gramicidin A, a mixture of three polypeptides that form a membrane spanning channel, was used as a molecular force transducer to measure alterations in the bilayer, and voltage-dependent sodium channels monitored the potential across the membrane. After application of capsaicin, the bilayer stiffness increased and the

voltage-dependent sodium channels were deactivated. These results indicated that structural changes to the host bilayer are sufficient to regulate membrane protein function. The authors speculated that similar changes could be responsible for the regulation of TRPV1. There is also experimental evidence suggesting that endogenous lipids can modulate the function of TRPV1, but it is unclear whether these effects are allosteric or if they result from direct interactions with the active site [22]. The physical properties of the bilayer are highly dependent on the lipid composition, and the addition of certain endogenous lipids may induce changes in the bilayer elasticity. These results are speculative, nevertheless they indicate the importance of the interactions of capsaicin with biological membranes.

The changes in structural properties of cell membranes caused by capsaicin was the subject of a recent study by Kogure *et al.* [23], in which the authors investigated the mechanism for the potent antiperoxidative effect of capsaicin by measuring its ability to scavenge free radicals in a membrane environment. The authors hypothesized that the antiperoxidative effect of capsaicin results from scavenging free radicals by the phenolic hydroxyl group (this group is known to be a potent antiperoxidative agent) [23]. However, their experiments concluded that this group did not participate in free radical scavenging because of the intramolecular hydrogen bond formed between the hydroxyl and neighboring anisole group (Figure 2.1). Conversely, the carbon atom linking the aromatic vanillyl and amide groups did scavenge free radicals near the lipid/water interface. This result was also supported by Aranda *et al.*, in that the polar groups in capsaicin aligned with the lipids in the membrane [17].

All of the experimental studies suggest that capsaicin affects the structure of membranes, despite disagreement as to the specific interaction sites. Meddings *et al.* concluded that an extractable non-lipid component is required. The results obtained by Aranda *et al.* and Tsuchiya indicated that pure lipid membranes are affected. It is also unclear whether the changes caused by capsaicin are biphasic [16, 18] or if capsaicin only serves to rigidify membranes [17]. A detailed molecular analysis is needed to resolve these issues and to provide insight into the specific interactions of capsaicin with cell membranes. One goal

of this dissertation is to perform a molecular dynamics study to understand the structural and dynamic changes in cell membranes in the presence of capsaicin. In the next section, relevant molecular dynamics studies will be reviewed to provide a background for the studies presented in Chapters 4 and 5.

2.4 Molecular Dynamics Simulations

The details of molecular dynamics simulations are discussed in Chapter 3. This section will focus on the development of force fields and algorithms that are used to characterize the systems studied here.

1-Octanol

The main component of cell membranes is lipid molecules, which are characterized as amphiphiles, that is, they are composed of lipophilic and hydrophilic domains. The membrane interface, composed of the hydrophilic groups, can occupy up to 40% of the membrane volume, and it is thus instrumental in the function of these systems [24]. The large interface also makes cell membranes very complex and difficult systems to model accurately. As a result, analgous compounds have been used to characterize the behavior of cell membranes, while retaining the basic hydrophilic and lipophilic properties. The most common compound that serves that function is 1-octanol, as it has the essential characteristics to represent lipids. 1-Octanol is widely used as a model system to predict the solubility of drugs in membranes in the pharmaceutical industry [25]. It is also often used in simulation studies of cell membranes because of the vast knowledge of octanol/water partition coefficients from experiments.

The optimized potentials for liquid simulations (OPLS) force field was one of the first force fields developed with transferable atomic parameters for organic liquids [26–31]. There are no specific OPLS parameters for capsaicin; however, one can use OPLS parameters of the functional groups of similar molecules to construct one for capsaicin. This

process requires validation of the assembled force field to ensure that the physical properties predicted are consistent with known measured values. The comparison of these force fields is described in detail in Chapter 4, where the properties of capsaicin are determined in an 1-octanol/water system. Capsaicin is first characterized in the 1-octanol/water system to validate the use of the OPLS parameters, and then followed by studies of the interactions of capsaicin with model cell membranes. The OPLS parameters for 1-octanol were based on the modifications proposed by Debolt and Kollman [25]. This in-depth analysis used molecular dynamics to study the structural, dynamic, and energetic properties of the 1-octanol/water system. These parameters were used for the united-atom representation of 1-octanol in Chapter 4.

One of the goals of studying the properties of capsaicin in an 1-octanol/water system is to determine the partitioning of capsaicin in an amphiphilic system. To accomplish this, two liquid phases need to be represented. The presence of two phases also implies the presence of an interface, which is an important structure in cell membranes, as described previously. In previous simulations of octanol and water, only pure and water saturated octanol systems were investigated [25, 32–35]. Consequently, the two-phase system implemented in Chapter 4 must be systematically characterized before introducing capsaicin. Experimental work by Steel *et al.* indicates that the 1-octanol/water interface is characterized by a strong association with a region of reduced polarity between the bulk water and hydrocarbon phases [36]. This region is attributed to the alignment of alcohol molecules along the interface, which creates a region without polar groups (hydrocarbon tails). Molecular dynamics simulations have been used to verify the interfacial structure of the 1-octanol/water interface by computing the electron absorption spectra of a point dipole chromophore embedded at different locations along the interface [37]. These simulations quantitatively accounted for the experimental observation of Steel *et al.* by showing that interfacial, hydrogen bonded octanol molecules align perpendicular to the interface [37]. The author concluded that octanol molecules have a higher affinity for forming hydrogen bonds with water and are less stable when forming hydrogen bonds with other octanol molecules.

Properties of the bulk octanol phase in an 1-octanol/water system can be inferred from computational studies on water saturated octanol systems. A number of studies agree that a hydrogen bond network is formed in pure octanol, and that this network is extended by the addition of water [25, 32, 35, 38]. The structure of these networks is described as "overlapping elongated inverse micelles" [35] because of the clustering of alcohol and water molecules that assume an oval shape, and the corresponding interdigitation of the alkyl chains. This localized formation of hydrophilic clusters makes the bulk octanol phase less hydrophobic than the region of reduced polarity near the 1-octanol/water interface described previously. In light of these experimental and computational results, we expect the 1-octanol/water system to form two bulk phases with an interface that has different physical properties than either bulk phase. The interface is expected to have a high degree of ordering, and the mole fraction of water in the bulk octanol phase should be similar to the saturation value of 0.255 at 298K and 1 bar [25].

Lipid Bilayers

The 1-octanol/water system is acceptable for predicting the general behavior of solutes in cell membranes, but it cannot provide molecular detail of specific interactions pertaining to cell membranes. To address the specific effects that capsaicin has on the structure and dynamics of cell membranes, these interactions need to be studied explicitly. One of the first computer simulations of a fully hydrated cell membrane in the biologically relevant liquid-crystalline phase was performed for a binary system of dipalmitoylphosphatidylcholine (DPPC) and water by Egberts *et al.* [24]. The DPPC force field developed by Egberts *et al.* was slightly modified by Berger *et al.* [39] to improve the accuracy of the predicted experimental volume per lipid and density. To improve the atomic representation of the lipid tails, OPLS van der Waals parameters were modified for pentadecane to reproduce the experimental density and heat of vaporization. The partial atomic charges for the lipid headgroup were also modified by using values obtained from quantum mechanical *ab initio* calculations.

By experimenting with different charge groups (sub-groups of partially charged atoms), the authors determined that neutral groups were more accurate than groups with partial charges [40]. This representation of DPPC is well characterized and has been used as a foundation for studying the interactions of DPPC bilayers with proteins and small molecules. These parameters are used to represent DPPC in Chapter 5.

Chapter 5 details the interactions of capsaicin with pure DPPC bilayers and mixed bilayers at a 3:1 molar ratio of DPPC to DPPE (dipalmitoylphosphatidylethanolamine) (see Figure 2.3). The molecular representation of DPPE was taken from Leekumjorn and Sum [41], where a detailed analysis of various mixtures of these lipids is given. Due to their similarity, DPPC was used as a model for the atomic representation of DPPE by changing the masses of the CH_3 choline groups in DPPC to represent the atomic mass of hydrogen found in the ethanolamine group of DPPE. The charges and intramolecular interactions were changed to reflect those of hydrogens. The major difference between DPPC and DPPE is the hydration of the lipid headgroups. DPPE has the ability to form intermolecular and intramolecular hydrogen bonds which decreases the area per lipid. Since DPPC does not form hydrogen bonds, water molecules form a shell around the headgroup that increases the hydration and area per lipid. The effect of decreasing the area per lipid is extended to the lipid acyl tails by a corresponding increase in the lipid tail order parameter.

2.5 Small Molecules and Lipid Bilayers

The development of a molecular model for lipid bilayers is the foundation to study the interactions of small molecules with cell membranes. Lipid bilayers are a barrier to diffusion (passive and active) into and out of the cell, and as such they maintain a non-equilibrium state across the cell membrane that is necessary for the viability of the cell [42]. The cell membrane represents the first layer of contact between the cell and cellular compounds, including nutrients, ligands, drugs, and so on [43]. Many types of interactions can occur

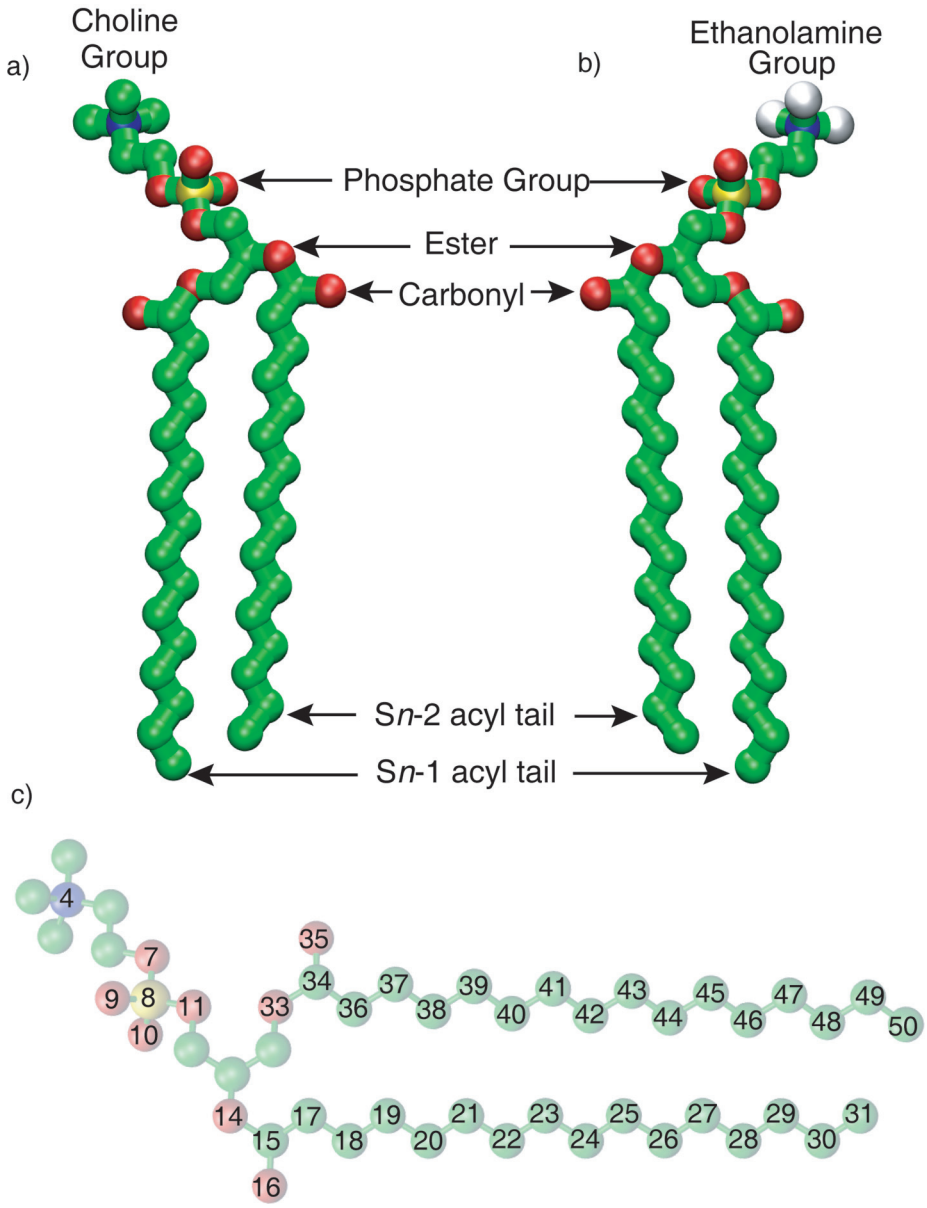

Figure 2.3: Molecular structure of a) DPPC and b) DPPE with c) their corresponding atom numbering. The phosphate, ester, carbonyl, Sn-1, and Sn-2 groups are also labeled for each lipid. Carbon atoms are shown in green, oxygen in red, nitrogen in blue, phosphorus in yellow, and hydrogen in white.

between these compounds and the membrane, including passive diffusion through the bilayer, accumulation in the bilayer core, and prolonged interactions of the interface. All of these interactions can change structural properties of the membrane and it is important to know how these changes are imposed.

Previous simulations of small molecules with lipid bilayers are an important predecessor to this study since they provide a foundation for the evaluation of our simulations. Agreement of simulation results and experimental data is the best validation of the method. There are several studies that investigated the partitioning of small molecules into the membrane. Some of the compounds considered include: benzene [44–46], alcohols, sugars, and dimethylsulfoxide [43]. The permeability and structural changes of these molecules are experimentally known, and the similarities between simulations and experiments not only validate the simulations, but they also provide valuable insight into the molecular interactions that are manifested in experiments. A detailed review of these simulations is not addressed here as excellent reviews exist in the literature [43, 47]. This section will focus on recent simulations of larger molecules, comparable to capsaicin, and their interactions with lipid bilayers.

Valproic acid is an amphiphilic molecule that has distinct polar and non-polar groups, as shown in Figure 2.4a. Molecular dynamics simulations were performed by Ulander and Haymet to study the properties of valproic acid in a DPPC bilayer by constraining the molecule at different depths within the lipid bilayer [48]. The authors determined that in crossing the lipid/water interface, the van der Waals forces created a large energy barrier that was countered by favorable electrostatic interactions. Consequently, crossing the interface was found to be the rate limiting step for permeation into the bilayer. After entering the bilayer, the authors determined that the most favorable location for valproic acid is beneath the lipid headgroups, approximately 1.3 nm from the bilayer center. At this depth, the carbonyl group can form hydrogen bonds with interfacial water, and the hydrocarbon chains are stabilized by lipophilic interactions with the lipid acyl tails, which increases the order of the bilayer. These authors also observed the formation of hydrating water columns into the center of the bilayer when valproic acid was constrained there [48]. However, this could be

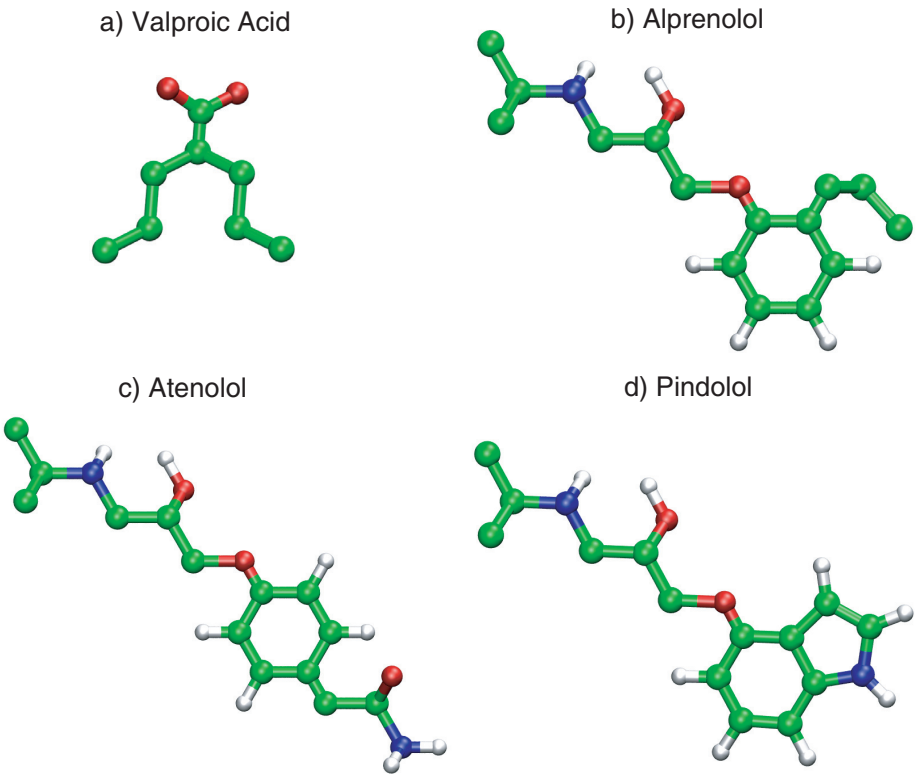

Figure 2.4: Molecular structure of a) valproic acid and three different β-blockers: b) alprenolol, c) atenolol, and d) pindolol. Carbon atoms are shown in green, oxygen in red, nitrogen in blue, and hydrogen in white.

an artifact of the simulation because of the unrealistic constraints that are used to hold the molecule at an unfavored location in the bilayer.

Similar simulations were performed for various small molecules and large drugs by Bemporad *et al.* [47, 49, 50]. Constrained molecular dynamics were used to study the properties of three β-blockers in a fully hydrated DPPC bilayer. Each β-blocker has the same base structure with differing side groups from the aromatic ring, as shown in Figures 2.4b,c,d. The side groups were varied in their chemical composition to determine the effects of hydrogen bonding and molecular volume on the order of the bilayer and the orientation of the drug in the bilayer at different depths. The authors determined that nitrogen-containing functional groups form more hydrogen bonds than oxygen-containing groups despite the

strong polarization of the O-H bond [47]. This preferential binding results in the drug solutes orienting in the bilayer, parallel to the bilayer normal, to maximize the number of hydrogen bonds. The authors suggest that hydrogen bonding possibilities are as important as steric constraints in determining solute behavior in the membrane [47].

These simulations constrained amphiphilic molecules in the bilayer to study their properties. Molecular dynamics simulations using unconstrained solutes allows them to diffuse freely in lipid/water systems. The dynamics of these systems requires the use of substantially longer time scales; however, recent advances in computational power compensate for this cost. Molecules like trehelose and dimethylsulfoxide have been widely studied by molecular dynamics without constraining the solute [51–53].

In Chapter 5, molecular dynamics were used to study the properties of unconstrained capsaicin in model cell membranes. However, as mentioned previously, the atomic representation of capsaicin must first be validated. The work described in Chapter 4 analyzes the properties of capsaicin in an 1-octanol/water system using both OPLS-UA and OPLS-AA force field representations.

Chapter 3

Simulation and Analysis Methods

3.1 Introduction

This chapter will discuss the methods used in Chapters 4 and 5 and their implementation by GROMACS [54, 55], namely energy minimization and molecular dynamics (MD). These methods describe complex molecular systems from empirical force fields, and predict macroscopic properties from detailed interactions on the molecular level. GROMACS is an extremely high performance package for both energy minimization and MD. By using optimized algorithms in a user-friendly command line interface, GROMACS efficiently implements a number of methods and utilities to perform and analyze simulations. GROMACS is also an open-source software under the GNU Free Public License with community based user support. It is also easily adapted to parallel environments using standard MPI communication. These benefits make it an excellent choice for performing large-scale molecular simulations.

3.2 Calculating the Forces

The mathematical model used to describe the interactions between atoms in a system is composed of an array of parameters that are either calculated from *ab initio* methods or empirically derived from experimental properties. These parameters are chosen to approximate interactions at the atomic level and are collectively referred to as force fields. A force field describes the intermolecular and intramolecular interactions for all the particles in a system. Intramolecular forces are accounted for by bond stretching, angle bending, and torsion potentials, while van der Waals and electrostatic forces are part of both intermolecular and intramolecular interactions. The potential energy contribution $U(\mathbf{r}^N)$ for molecules experiencing these forces are

$$U(\mathbf{r}^N) = U_{\text{bond}} + U_{\text{angle}} + U_{\text{torsion}} + U_{\text{LJ}} + U_{\text{elec.}} \tag{3.1}$$

where the contributing potentials are defined by

$$U_{\text{bond}} = \sum_{i=1}^{N} \frac{k_i}{2}(l_i - l_{i,o}) \tag{3.2}$$

$$U_{\text{angle}} = \sum_{i=1}^{N} \frac{c_i}{2}(\theta_i - \theta_{i,o}) \tag{3.3}$$

$$U_{\text{torsion}} = \sum_{i=1}^{N} \sum_{j=0}^{5} C_j (cos(1 - \phi_i))^j \tag{3.4}$$

$$U_{\text{LJ}} = \sum_{i,j>i}^{N} 4\epsilon_{i,j} \left[\left(\frac{\sigma_{i,j}}{r_{i,j}} \right)^{12} - \left(\frac{\sigma_{i,j}}{r_{i,j}} \right)^{6} \right] \tag{3.5}$$

$$U_{\text{elec.}} = \sum_{i,j>i}^{N} \frac{q_i q_j}{4\pi\epsilon_o r_{i,j}} \tag{3.6}$$

Here $U(\mathbf{r}^N)$ denotes the potential energy, which is a function of the positions ($\mathbf{r}$) of N

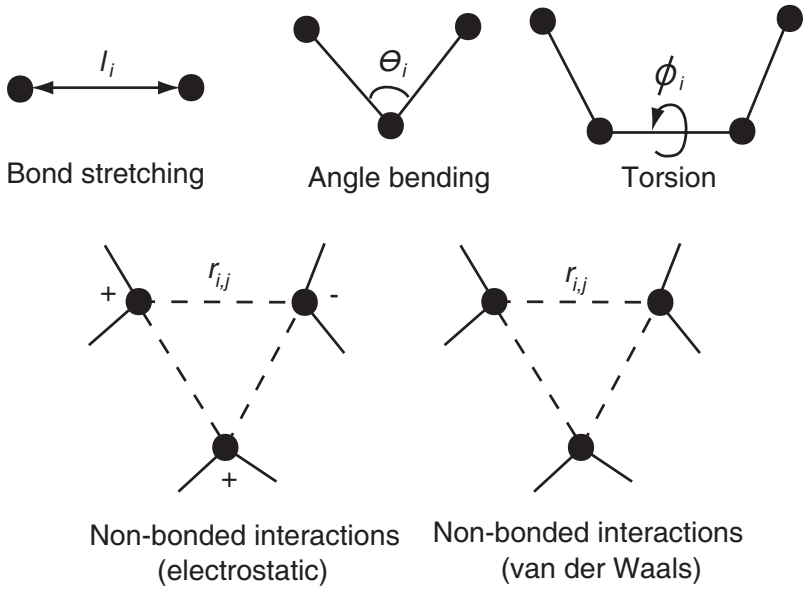

Figure 3.1: Schematic representation of the potential energy contributions defined in Equation 3.1.

particles [42]. The vector **r** is defined from the Cartesian x, y, and z coordinates. The Lennard Jones (LJ) potential is used to represent the van der Waals interactions. The contributions of bond stretching, angle bending, torsion potentials, non-bonded electrostatics, and Lennard Jones interactions to the potential energy are defined separately where k, c, C, ϵ, σ, and q are all defined parameters of the force field. The values k, c, and C are force constants that define the strength of the bond stretching, angle bending, and torsion potentials, respectively. The Lennard Jones potential has σ and ϵ to define the location of the potential energy minimum and "well depth," respectively, and q is the partial atomic charge of an atom. A schematic representation of the contributions to the potential energy function is depicted in Figure 3.1 [42].

Equation 3.1 defines the potential energy as a function of the atomic positions. Given a set of atomic coordinates, the forces $\mathbf{F}_N$ acting on N atoms can be computed from

the gradient of the potential $U(\mathbf{r}^N)$ with respect to the positions $\mathbf{r}$,

$$\mathbf{F}_i = -\frac{\delta U}{\delta \mathbf{r}_i} \tag{3.7}$$

As a result, the parameters used in the potential energy function define the forces in the system, hence the name force field. Calculating the forces in a system is the first step for both energy minimization and MD. Energy minimization is used to relax the forces in a system to a corresponding energy minimum, and MD uses the forces between atoms to advance the system in position and time.

The OPLS all-atom and united-atom parameters [26–31, 56] were used for the molecular representation of capsaicin and 1-octanol. These parameters are listed in Appendix A where a sample parameter file suitable for GROMACS is also given. The parameters for DPPC [39], DPPE [39, 41] and SPC water [57] are also defined in Appendix A.

3.3 Energy Minimization

In this study, the steepest descent method is used to find the local energy minimum of a configuration based on the intermolecular forces. This method works by taking a step in the direction of the negative energy gradient, which corresponds to a decrease in the forces. After calculating the initial forces, the atomic positions are shifted to $\mathbf{r}_{n+1}$ where

$$\mathbf{r}_{n+1} = \mathbf{r}_n + \frac{\mathbf{F}_n}{\max(|\mathbf{F}_\mathrm{n}|)} h_n \tag{3.8}$$

Here h_n and $\max(|\mathbf{F}_n|)$ are the maximum displacement and largest absolute value of the force components, respectively, and are defined by the user. The maximum displacement is increased ($h_{n+1} = 1.2h_n$) if the step is accepted and decreased ($h_n = 0.2h_n$) if rejected. This robust method is easily implemented and quickly moves toward a local minimum, but it converges very slowly. As a precursor to MD simulations, this is acceptable, as we are only

concerned with obtaining an initial configuration with realistic forces. Appendix B contains a sample input file for GROMACS that details these input parameters.

3.4 Molecular Dynamics

MD simulations solve the classical mechanics equation of motion to describe the interactions and dynamics of model systems. Equilibrium and transport properties can be determined by calculating the evolution of a model system over time. Using molecular mechanics, the forces between all atoms in a system can be calculated from a classical theory, and from these forces, one can integrate the equation of motion for all particles to determine their future position. As a result, the dynamics of a system can be determined in discrete time steps.

GROMACS uses the leap-frog algorithm [58] to integrate the equation of motion. For a system of N interacting atoms, Newton's equation of motion is defined as

$$\mathbf{F}_N = m_N \frac{d^2}{dt^2} \left(\mathbf{r}_N(t) \right) = m_N \frac{d}{dt} \left(\boldsymbol{v}_N(t) \right) \tag{3.9}$$

where m_N is the atomic mass of atom N. The leap-frog integration algorithm uses the positions $\mathbf{r}$ at each time step Δt, and the velocities $\boldsymbol{v}$ which are calculated from the previous step at $t - \frac{\Delta t}{2}$. The future positions at $t + \Delta t$ and the velocities at $t + \frac{\Delta t}{2}$ can be calculated from the forces using the following expressions

$$\mathbf{r}\left(t + \Delta t\right) = \mathbf{r}(t) + \boldsymbol{v}\left(t + \frac{\Delta t}{2}\right) \Delta t \tag{3.10}$$

$$\boldsymbol{v}\left(t + \frac{\Delta t}{2}\right) = \boldsymbol{v}\left(t - \frac{\Delta t}{2}\right) + \frac{\mathbf{F}(t)}{m} \Delta t \tag{3.11}$$

The term *leap-frog* reflects the positions being evaluated at t and the velocities at $(t \pm \frac{\Delta t}{2})$ [58].

To begin MD, three components are required: the potential $U(\mathbf{r}^N)$ as a function of atomic positions, the positions $\mathbf{r}$ of all atoms, and the velocities $\boldsymbol{v}$ of all atoms in the system. Since the leap-frog algorithm requires velocities at $(t - \frac{\Delta t}{2})$, these values must be generated to start a simulation if not available. In GROMACS, a Maxwell type velocity distribution is initially calculated based on a user supplied random seed and temperature [58]. After the velocity distribution is generated, the center of mass motion of the simulation box is set to zero, and the future positions are predicted.

For each discrete MD step, the forces are computed, the future positions are determined, and the trajectory is updated. The forces are computed based on bonded and non-bonded interactions, and external constraints or forces that are imposed on the system. Common constraints are thermodynamic variables that can be controlled in physical experiments such as constant temperature, pressure, volume, and energy. After the forces are calculated and the equation of motion is integrated, the configuration and trajectory are updated. Using these methods, a MD protocol can be implemented. However, to compare simulations and experiments, one needs methods to control and measure thermodynamic properties. The following section details the methods used in this study.

3.5 Methodological Procedures

3.5.1 Long Range Non-bonded Interactions

The Lennard Jones potential is proportional to $(1/r^6)$ and $(1/r^{12})$ and quickly diminishes to zero after about 3σ. In MD simulations, this potential is truncated as it approaches zero. This distance is referred to as the van der Waals cut-off distance. The electrostatic interactions are proportional to $(1/r)$ and a simple truncation of this potential may introduce artifacts into the simulation [59]. In our simulations, a twin cut-off and the Particle Mesh Ewald (PME) [60] methods are used to treat long range electrostatics. In the twin cut-off

method, both the LJ and electrostatic potentials are truncated at a relatively large distance. The PME method discretizes the simulation box and its periodic image into a grid with spacing defined by the user. The potential is calculated at each grid node using a cardinal B-spline interpolation with an order that is user defined [60]. This method splits the coulombic interactions into real and reciprocal spaces. The boundary between these spaces is defined by the user as a cut-off distance. The interactions in real space are computed normally, and in reciprocal space, the grid assigned charges are used [60].

3.5.2 Temperature Control

The temperature is calculated from the atomic velocities and is controlled by the Berendsen weak coupling technique [61]. In the Berendsen weak coupling algorithm, temperature is controlled by coupling the system to an external heat bath. In MD, this corresponds to scaling atomic velocities that drift from a characteristic distribution of the set temperature, which is defined by

$$k_B T = \left\langle m_i \boldsymbol{v}_i^2 \right\rangle \tag{3.12}$$

where k_B is Boltzman's constant, and m and $\boldsymbol{v}$ are the mass and velocity of particle i [62]. The angle brackets denote the ensemble average over all atoms in the system. Coupling the system to an external heat bath corresponds to adding frictional terms to the equation of motion such that

$$m_i \frac{d}{dt} \boldsymbol{v}_i = \mathbf{F}_i + \frac{m_i}{2\tau_T} \left(\frac{T_o}{T} - 1 \right) \boldsymbol{v}_i \tag{3.13}$$

where τ_T is the coupling time constant that determines the strength of coupling and T_o is the set temperature [61]. By choosing different values of τ_T, the strength of the coupling can be made weak to minimize the disturbance to the system, or it can be varied depending on the application. This method also has an advantage of maintaining a Maxwell type velocity distribution. The values required for this method are readily accessible from the leap-frog algorithm.

In GROMACS, the imposed temperature can be static or dynamic. Dynamic temperatures are controlled by simulated annealing, where the temperature is linearly changed between two set points over a specified period of time. This method is useful for mixing at high temperatures followed by a slow cooling process that allows the system to relax gradually.

3.5.3 Pressure Control

The pressure is controlled in a similar manner by the Berendsen weak coupling technique [61]. Pressure is directly related to the forces between atoms in the system, and as a result, controlling the pressure implies scaling the atomic coordinates and box vectors at every time step [58]. The change in the equation of motion is characterized by a change in the derivative of particle positions

$$\frac{d}{dt}\mathbf{r}_N(t) = \boldsymbol{v}_N(t) - \frac{\beta\left(P_o - P\right)}{3\tau_P}\mathbf{r}_N(t) \tag{3.14}$$

where $\mathbf{r}$ is defined by the coordinates, β is the isothermal compressibility of the system, P_o is the set pressure, and τ_P is the coupling time constant [58, 61]. The latter three variables are user defined.

Three pressure coupling schemes were used in this dissertation: isotropic, semi-isotropic, and anisotropic. In isotropic coupling, all three box vectors are proportionally scaled. This coupling of the box vectors ensures that a box remains square. In semi-isotropic pressure coupling, two dimensions are coupled and the third scales independently. For interfacial systems, this is beneficial because the surface area of the interface remains proportional. In anisotropic coupling, all of the box vectors scale independently, and as such, it imposes the least amount of constraint on the system.

3.5.4 Thermodynamic Ensembles

To compare simulations and physical experiments, the same thermodynamic variables must be controlled. In physical experiments the temperature (T), pressure (P), volume (V), and number of moles (N) are controlled as independent variables to measure static and dynamic physical properties. In simulations, these same variables can also be controlled. Controlling T and P was previously mentioned, and V and N are easily controlled in MD. Maintaining constant V is accomplished by fixing the volume of the simulation box, and classical MD does not consider chemical reactions, so maintaining constant N is trivial. In this dissertation both NVT and NPT ensembles are employed.

3.5.5 Inserting Capsaicin

In Chapters 4 and 5, capsaicin is introduced into the systems by overlaying two coordinate files and then deleting overlapping molecules. Any molecule that has an atom within 0.13 nm of an inserted capsaicin molecule is deleted. The configuration is then minimized before performing MD. Appendix C contains a perl script that was written to perform this task.

3.6 Simulation Analysis Protocols

3.6.1 Order Parameter

The order parameter of the lipid tails is often used to determine the fluidity of the membrane and the thermodynamic phase of the system. This value is readily available from both experiments and simulations, which makes it a valuable tool for determining the accuracy of a force field. The order parameter is represented as a tensor ($\mathbf{S}$) with elements

$$\mathbf{S}_{i,j} = \frac{1}{2} \langle 3 \cos\theta_i \cos\theta_j - \delta_{ij} \rangle \tag{3.15}$$

where θ_i denotes the angle formed between the ith direction and the outward pointing normal of the bilayer. A common representation of the order parameter for lipid systems is the deuterium order parameter, which is determined from the order tensor $\mathbf{S}$ by

$$-S_{CD} = \frac{2}{3}\mathbf{S}_{xx} + \frac{1}{3}\mathbf{S}_{yy} \tag{3.16}$$

This value can be determined for every C-C bond along each lipid acyl tail from their positions in simulations and from selectively placed deuterium atoms in experiments. The order parameter is also indirectly related to the dihedral conformation of the lipid acyl tails. It is generally accepted that as the order parameter increases, the percentage of gauche transitions decreases [63].

3.6.2 Hydrogen Bonding

The criteria for hydrogen bonding was defined according to the method of Brady and Schmidt [64]. A hydrogen bond exists if the maximum distance between a donor and acceptor is less than 0.35 nm and the angle (donor-hydrogen-acceptor) is greater than 120 degrees. Figure 3.2 shows a diagram of the distance and angle requirements for this method. The angle requirement was used for all hydrogen bonds, and the distance of 0.35 nm was used unless noted otherwise (some distances were evaluated by the first minimum in the radial distribution function).

3.6.3 Diffusion Coefficient

The diffusion coefficient (D) was calculated using Einstein's relation based on the mean-squared displacement of the molecules over the course of the simulation, given by

$$D = \lim_{t\to\infty} \frac{\left\langle [\mathbf{r}(t) - \mathbf{r}(0)]^2 \right\rangle}{2dt} \tag{3.17}$$

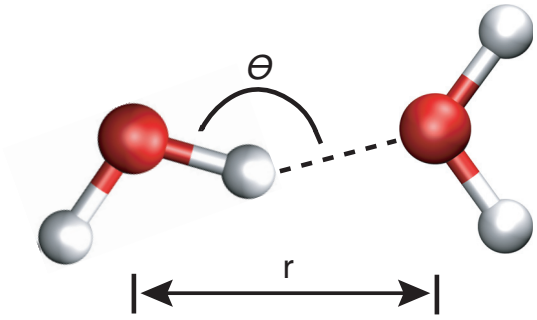

Figure 3.2: Schematic representation of the distance and angle requirements for hydrogen bonding. A minimum angle (θ) of 120 degrees was imposed and a maximum distance of 0.35 nm was used unless stated otherwise.

where $r(t)$ is the position at time t relative to the position $r(0)$ at $t = 0$, and d is a dimensionality constant ($d = 2$ for lateral diffusion in two dimensions and $d = 3$ for three dimensional diffusion). The diffusion coefficient is determined by linearizing Equation 3.17. The linear form is given by

$$\log_{10} \left\langle [\mathbf{r}(t) - \mathbf{r}(0)]^2 \right\rangle = \log_{10} t + \log_{10}(2dD) \tag{3.18}$$

and by plotting $\log_{10} \left\langle [\mathbf{r}(t) - \mathbf{r}(0)]^2 \right\rangle$ versus $\log_{10} t$, the diffusion coefficient can be determined from the y-intercept of the tangent to the function where the slope equals one (a slope of one defines the diffusive regime).

Chapter 4

Molecular Dynamics Study of the Properties of Capsaicin in an 1-Octanol/Water System

4.1 Abstract

Molecular dynamic simulations were performed to study the behavior of capsaicin in an 1-octanol/water system at 298 K and 1 bar. Capsaicin is the pungent chemical found in chili pepper that stimulates our sensory system resulting in a burning pain sensation. In the first step to investigate the activity of capsaicin, we have used two molecular representations for capsaicin based on the OPLS force field: all-atom (AA) and united-atom (UA) models. The octanol/water mixture was selected as a model system to determine the hydrophobic and hydrophilic properties of capsaicin by analyzing equilibrium, structural, and dynamic properties from the simulations. Our simulations showed that capsaicin preferentially partitions to the octanol phase, with its hydrocarbon segment oriented with that in octanol, while the polar part remains exposed to the aqueous phase. The AA and UA models simulations gave

similar results.

4.2 Introduction

Capsaicin is the active compound in chili pepper that causes the hot and burning sensation that is usually associated with the perception of noxious temperatures. Capsaicin acts as a noxious stimulant to the sensory neurons, and as such it has been central in the studies of sensory stimuli and the response of the central nervous system. Some implications of capsaicin to the sensory system have already been discussed in Chapters 1 and 2, and the reader is referred elsewhere [2, 5, 6, 65] for detailed reviews of the the diverse research concerning capsaicin and its chemosensory effects. One particular application of capsaicin that has found wide-spread use is in topical ointments for pain relief. Since capsaicin causes a noxious stimulation of the sensory neurons, it has been applied as analgesic [5]. Capsaicin has also been shown to have chemoprotective activity against some chemical carcinogens [13]. More recently, capsaicin was demonstrated to target cancer cells without causing damage to healthy cells [12]. The biological processes that are involved in the action of capsaicin occur at the cellular level where capsaicin interacts with the membrane environment, as well as specific receptors [4]. The underlying mechanism of the biological activity of capsaicin remains elusive, and this study is the first step toward broadening our understanding of the properties of capsaicin and their implications in biological systems.

Capsaicin is an amphiphilic compound and as such it can associate with both hydrophobic and hydrophilic groups. The octanol/water system is widely accepted as a standard reference for predicting the partitioning of a solute between hydrophilic and hydrophobic environments [25]. Capsaicin is sparsely soluble in water, 60 mg/l [66], thus it is expected to show little affinity for an aqueous phase. Octanol and water form a two-phase system, with the interface between the two liquid phases forming an anisotropic environment with strong ordering of the polar groups [36, 37]. The interfacial region is chemically distinct

from either of the bulk phases [37]. A region of reduced polarity has been shown to exist within the interface as a result of tight packing among the octanol hydrocarbon tails [36, 37].

To the best of our knowledge, this study is the first to investigate the behavior of capsaicin from a molecular stand point. In order to obtain a proper molecular description of capsaicin for simulation studies, we will evaluate the appropriateness of the OPLS force field. The OPLS force field has been refined by several efforts to adequately reproduce thermodynamic data of various organic systems [26–31, 56]. The all-atom and united-atom models differ in their treatment of hydrogens bound to carbon atoms. The AA model explicitly accounts for hydrogen atoms while the united-atom model treats carbons and the hydrogens bound to them as a single unit. Both the all-atom and united-atom models of the OPLS force field have been investigated in this study in order to determine the most appropriate representation of capsaicin. The properties of capsaicin are described with respect to its behavior in an octanol/water system.

4.3 Simulation Details

Simulations were performed for pure octanol, octanol/water, and capsaicin/octanol/water systems, each represented by both an AA and UA models. The pure octanol systems were composed of 500 octanol molecules initially placed on evenly spaced lattice points (Figure 4.1a). The octanol/water systems contained 500 octanol molecules and a large number of water molecules (4106 and 4615 for the all-atom and united-atom configurations, respectively). The initial configurations of the octanol/water systems were developed by stacking a box of water molecules on top of the equilibrated simulation boxes of pure octanol (obtained from pure octanol simulations, Figure 4.1c). The equilibrated octanol/water systems were used to characterize the interactions of capsaicin in both hydrophobic and hydrophilic environments. The capsaicin/octanol/water configurations were created by inserting 8 capsaicin molecules into the water phase of each equilibrated octanol/water configuration and

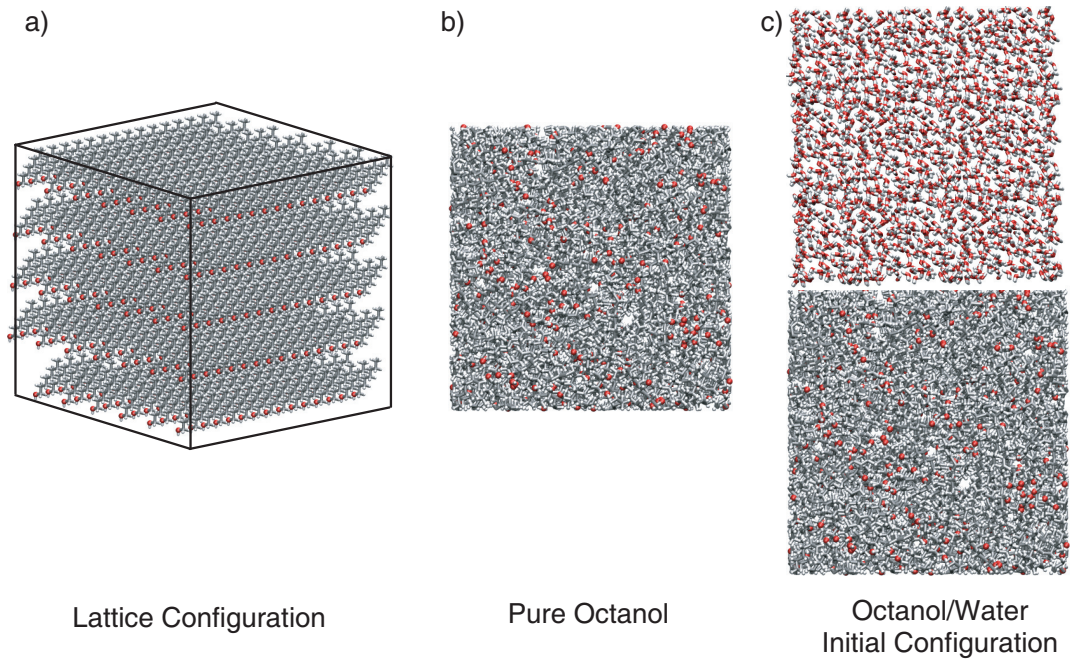

Figure 4.1: Snapshots of the all-atom model simulation boxes for a) the initial lattice configuration of octanol, b) the final configuration from the pure octanol simulation, and c) the initial configuration of the octanol/water simulation. These snap shots are also representative of the united-atom configurations. Differences in the two configurations only appeared when octanol and water were mixed.

then removing all unfavorable contacts by deleting overlapping water molecules. The final configurations contained 8 capsaicin, 500 octanol, and 3984 (all-atom) / 4525 (united-atom) water molecules. Figures 4.2 and 4.3 show the configuration of the simulations boxes for the AA and UA models, respectively. Table 4.1 summarizes the concentrations for capsaicin in the octanol/water systems. The OPLS all-atom [56] and OPLS united-atom [26–31, 56] models were used for octanol and capsaicin. The united-atom model for octanol includes the modifications suggested by Debolt and Kollman [25]. In the united-atom model for capsaicin, only polar and aromatic hydrogens were explicitly included. The SPC model was used for water [57].

Molecular dynamics simulations were performed with the leap-frog integration with a time-step of 2 fs. Non-bonded (van der Waals and electrostatics) interactions were

cut off beyond 1.0 nm. Particle mesh Ewald (PME) [60] was used to account for long-range electrostatic interactions with 0.12 nm grid-size and sixth-order spline interpolation. For the simulations with pure octanol, a twin-cutoff (1.0 nm for van der Waals and 1.4 nm for electrostatics) was also applied in order to compare its accuracy to the PME method. Constant temperature and pressure simulations were controlled using the Berendsen weak coupling technique [61] with $\tau_T = 0.2$ ps and $\tau_P = 2.0$ ps for the temperature and pressure, respectively. For pure octanol, NPT simulations were performed for 1.5 ns at 298 K and 101.3 kPa (isotropic pressure control with $\kappa = 7.64 \times 10^{-6}$ kPa^{-1}, obtained from [67]) after the systems were compressed from their initial lattice configuration. For the octanol/water systems, the combined octanol and water boxes were mixed at 598 K and then annealed to 298 K at constant volume over a 3 ns simulation. At that point, the simulations were set to NPT for an additional 1.5 ns with a pressure of 101.3 kPa (anisotropic pressure control with $\kappa = 4.6 \times 10^{-6}$ kPa^{-1}, obtained from [67]). In the process of annealing the systems, a phase separation occurred, creating aqueous and octanol-rich phases (see Figures 4.2 and 4.3). After the introduction of capsaicin into the equilibrated octanol/water systems, an energy minimization was initially performed, followed by NPT simulations at 298 K and 101.3 kPa. The dynamics of the systems were accumulated for a total of 15 and 20 ns for the all-atom and united-atom configurations, respectively. The simulation times reflect the time required for the capsaicin molecules to partition to the octanol-rich phase. All simulations were performed with the the GROMACS 3.3-beta software package [54, 55] (single-precision mode) in parallel (about 2.0 ns/day in 8 nodes and 3.6 ns/day in 8 nodes for AA and UA configurations, respectively) using Virginia Tech's System X cluster (dual 2.3 GHz Apple Xserve G5).

4.4 Results and Discussion

The main goal of this work is to study the properties of capsaicin in an octanol/water system. In order to have a complete and consistent representation of capsaicin in octanol/water, we

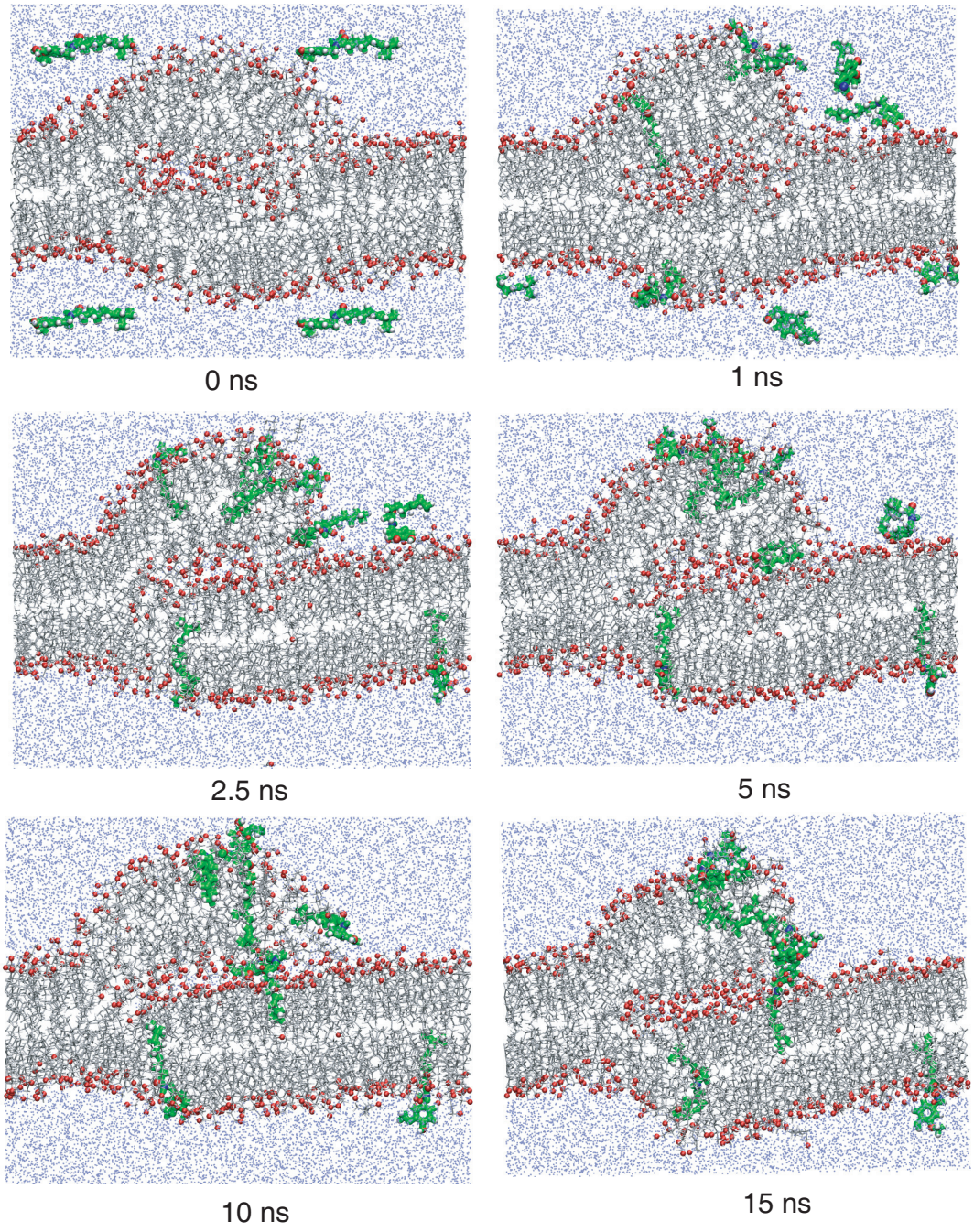

Figure 4.2: Snapshots of the all-atom model simulation boxes of capsaicin in an octanol/water system. Initially, all capsaicin molecules were placed in the aqueous phase. Capsaicin molecules are shown in green, octanol in gray (hydroxyl oxygen highlighted by red spheres), and water by blue dots.

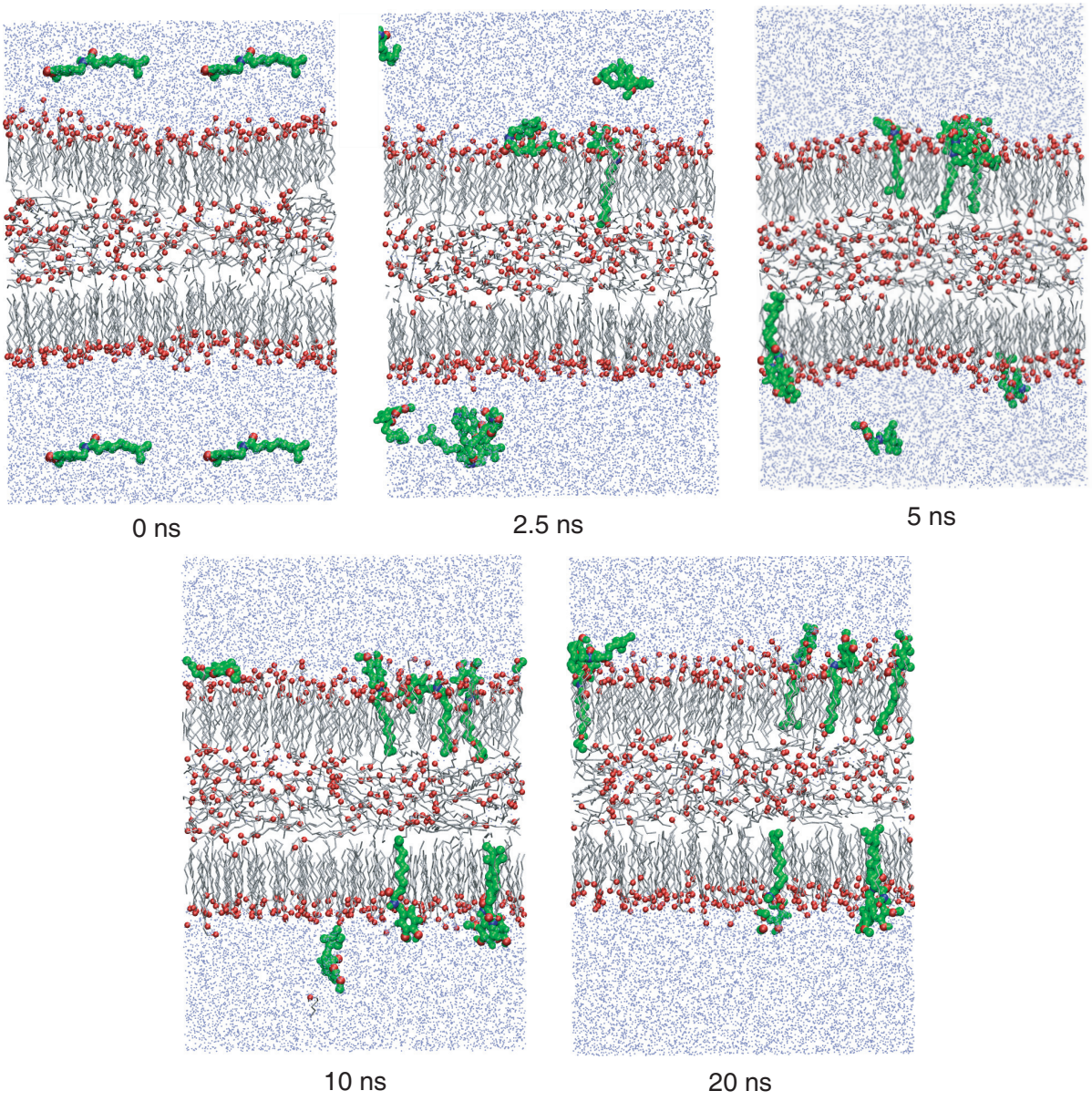

Figure 4.3: Snapshots of the united-atom model simulation boxes of capsaicin in an octanol/water system. Initially, all capsaicin molecules were placed in the aqueous phase. Capsaicin molecules are shown in green, octanol in gray (hydroxyl oxygen highlighted by red spheres), and water by blue dots.

Table 4.1: Composition of capsaicin in the octanol/water systems considered in this work. Values correspond to concentration in each phase for all-atom and united-atom models, respectively.

	Weight%	Mole%
Water	3.29 / 2.91	0.20 / 0.18
Octanol	3.62 / 3.62	1.57 / 1.57

have systematically characterized the pure octanol and octanol/water systems separately.

4.4.1 Pure Octanol

Equilibrium, structural, and dynamic properties were analyzed for the pure octanol systems based on the AA and UA models. In the simulations of pure octanol, we considered two methods to treat long-range electrostatics, namely twin-cutoff and PME. Because octanol, and subsequently water and capsaicin, is a polar molecule, it is important to account for long-range corrections. The computations with PME often add a factor of two to the computational time, however, it overcomes many of the artifacts usually encountered with a simple truncation of the potential. The density obtained with the AA and UA representations of octanol are 832.1 and 849.7 kg/m^3, respectively, with the PME method, and accordingly 811.0 and 816.9 kg/m^3 with the twin-cutoff method. The experimental value for the density at 298 K and 1 bar is 826.3 kg/m^3 [68]. Previous simulations studies have reported density values of 823.9 kg/m^3 for the OPLS-AA force field [35] and 807.6 kg/m^3 [35], 816 kg/m^3 [25], and 810 kg/m^3 [33] for the UA representations. Our values for the density deviate from the experimental ones by about 0.7% and 2.8% for the AA and UA models with PME, respectively, and 1.9% (AA) and 1.1% (UA) with twin-cutoff. The results with the PME method overestimate the density, whereas those with the twin-cutoff underestimate. The values reported here for the density are slightly higher than previous simulations since we used PME, and others have used reaction-field dielectric [25] and twin-cutoff [33] to account for long-range electrostatics interactions, both of which are less accurate and known

to introduce artifacts [59].

For the structural properties, we analyzed the radial distribution functions (RDF) between the octanol oxygen atoms (Figure 4.4) for the AA and UA models with PME. The shape and location of the first peak in the RDFs suggest the formation of hydrogen bonds between octanol hydroxyl groups. The first maximum in the RDFs occurs at 0.279 and 0.273 nm for the AA and UA models, respectively. These numbers compared well with previous simulation results from both MacCallum and Tieleman [35] and Debolt and Kollman [25] that predicted the location of the first peak to be approximately 0.275 nm. Integration of the RDFs yields the number of coordinating molecules, which in this case are 1.89 and 1.98 for the AA and UA models. As expected, each octanol molecule is associated with about two others through possible hydrogen bonding, with the hydroxyl group serving as both hydrogen-donor and hydrogen-acceptor. The hydrogen bonding network formed by octanol is also reflected in the RDFs in Figure 4.4 by the well-defined second peak at about 0.471 nm and 0.465 nm for the AA and UA models, respectively. A similar structure was observed by Debolt and Kollman [25] and MacCallum and Tieleman [35]. The differences in the RDFs between the AA and UA models can be attributed to the steric repulsions caused by the explicit hydrogen atoms in the AA model (large distance for the second maximum).

Figure 4.5 depicts a typical hydrogen bond network observed in the simulations for the UA configuration of octanol. The extent of the hydrogen bond networks varied, but the majority of octanol molecules in both simulations participated in donor-acceptor interactions. The hydrogen bond networks formed mostly long, thin, polymeric-type chains, although some dense aggregates of hydroxyl headgroups were also observed. MacCallum and Tieleman observed similar long chain networks for pure octanol, but they noticed a shift toward high density clusters with increasing water concentration [35].

The number of actual hydrogen bonds formed between octanol hydroxyl groups was also calculated for each simulation. Hydrogen bonding was determined by testing potential donors and acceptors found within a hydrating radius (evaluated to the first minimum of

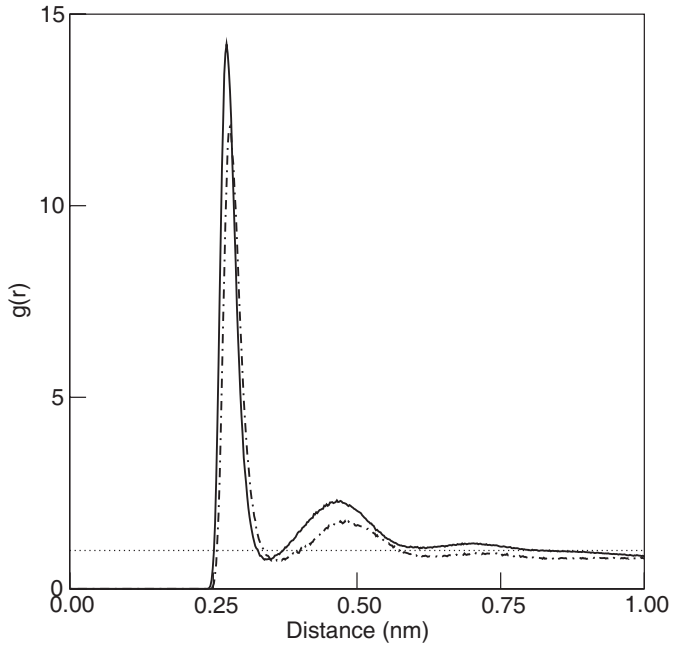

Figure 4.4: Radial distribution functions for oxygen-oxygen in pure octanol for the all-atom (solid line) and united-atom (dashed line) models.

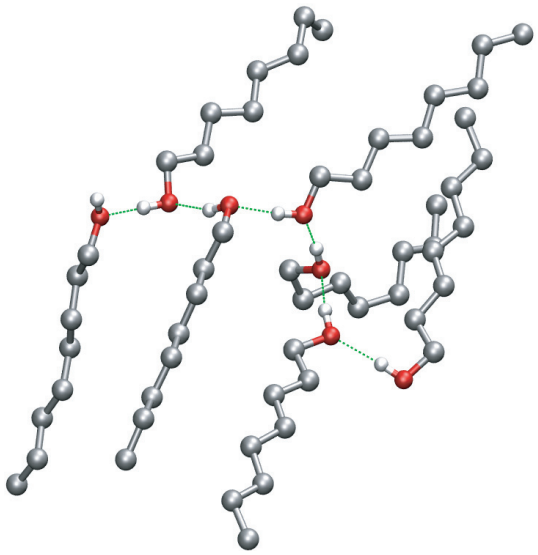

Figure 4.5: Representative snap shot from the united-atom pure octanol simulation illustrating a typical hydrogen bond network formed among octanol hydroxyl groups. Hydrogen bonds are shown by green lines.

a given radial distribution function) for angle and distance requirements. It was determined that 0.92 ± 0.01 and 0.97 ± 0.01 hydrogen bonds formed for the AA and UA systems with octanol oxygen being the donor and acceptor. This result indicates that each octanol oxygen donates its hydrogen to another oxygen molecule; therefore, it is likely that each octanol is participating in two hydrogen bonds. Debolt and Kollman also report this finding [25].

The self-diffusion coefficient (D) of octanol was calculated using the Einstein relation based on the mean-squared displacement of the molecules over the course of the simulation as shown by

$$D = \lim_{t\to\infty} \frac{\left\langle [r(t) - r(0)]^2 \right\rangle}{2dt} \tag{4.1}$$

where $r(t)$ is the position at time t relative to the position $r(0)$ at $t = 0$, and d is a dimensionality constant. Diffusion coefficients for the AA and UA models were $D_{\mathrm{AA}} = 1.67 \pm 0.44 \times 10^{-6}$ cm^2/s and $D_{\mathrm{UA}} = 0.83 \pm 0.20 \times 10^{-6}$ cm^2/s, respectively, both in good agreement with the experimental value of $D = 1.8 \times 10^{-6}$ cm^2/s [69].

4.4.2 Octanol and Water

As described under Simulation Details, the octanol/water systems were first mixed at a high temperature and then annealed to 298 K and 1 bar. In that process, two phases were formed, resulting in an aqueous (water only) and an octanol-rich phases. The final configurations of the simulation boxes are shown in Figure 4.2 and 4.3 for the AA and UA models, respectively (configurations at $t = 0$ without the capsaicin molecules). As seen in those figures, a clear interface was formed between octanol and water, consistent with experimental observations. One can also see that the obtained configurations show ordering of the octanol molecules along the interface. The structures formed by octanol are "bilayer-like," with the hydroxyl groups (hydrophilic part) exposed to the aqueous phase and the hydrocarbon chain (hydrophobic part) aligned away from the aqueous phase. The interface for the AA configuration (Figure 4.2) is not as smooth and well-defined as in the UA

configuration (Figure 4.3). Part of the difference is the octanol and water molecules trapped in the bulk octanol-rich phase. In the AA case, octanol and water molecules form a small pocket inside the octanol-rich phase, whereas in the UA case, a mixed layer of octanol and water is evenly distributed between the two octanol layers. The octanol molecules trapped in the bulk octanol-rich phase are unhindered to diffuse, whereas those aligning with the interface are more constrained due to the ordering in the layers. We should emphasize that the configurations obtained were not imposed in the simulations, but simply resulted as a consequence of the mixing and annealing process leading to the desired conditions.

The concentration of water in the octanol-rich phase is not easily computed since it is unclear how to define an interface and determine which molecules should be considered as part of the bulk phase. The interface is commonly defined as the region where the bulk solvent concentration decreases from 90 to 10%. By examining the UA configuration, the 90 and 10% values can be determined in relation to the most probable location of the interfacial octanol oxygen atoms. By assuming that the two systems are similar, the 90 and 10% interface distances from the UA model can be used to approximate the AA distances. Using this relationship, the mole fraction of water in the octanol-rich phase is 0.5491 and 0.0842 at the 90 and 10% limits, respectively.

In the UA configuration, *if only* the octanol and water molecules enclosed by the two octanol layers is considered the bulk phase, the water mole fraction is 0.248, in good agreement with the experimental value. At the conditions considered, experimental measurements of the equilibrium concentrations report an aqueous phase with negligible amounts of octanol, and an octanol-rich phase containing 0.255 mole fraction water [25]. Using the the 90 and 10% limits to calculate the concentration in the octanol-rich phase, we obtain the water mole fraction to be 0.554 and 0.126. Since the experimental value for the concentration lies in between these numbers, we are confident in our representation of the octanol/water system for both models.

Previous simulations of octanol/water mixtures [25, 34, 35] have not considered

the explicit formation of the two phases, instead, an octanol-rich phase saturated with water (based on the experimental concentration) was often assumed. Experimental studies by Steel *et al.* support our findings of a highly ordered interface with an "alkane-like" region of low polarity [36]. This region has properties unlike either bulk phase and partially represents the lipophilic core of cell membranes. Although this region is not as thick as the membrane core, the chemical properties of the hydrocarbon chain of octanol are similar to lipid acyl tails. Molecular dynamics simulations of the 1-octanol/water interface by I. Benjamin agree with our findings as well. During these simulations, a well defined interface was formed with a high degree of order among interfacial octanol hydrocarbon chains [37].

Figure 4.6 shows the RDF between the oxygen atoms in octanol (solid-line) and octanol oxygen and water (dashed-line) for both AA and UA models. It should be noted that the RDFs in the figure correspond to only those octanol molecules associated with the interface (octanol and water molecules trapped in the bulk octanol-rich phase were not included in this calculation). The location of the first maximum for the octanol oxygen RDF is 0.275 and 0.279 for the AA and UA models, respectively, which are similar to those determined in the pure octanol systems. Integration of the RDFs to obtain the number of coordinating molecules surrounding a central one gives 0.83 and 0.81 for the AA and UA models, respectively. These numbers are about half of those in pure octanol, the reason being that octanol molecules now also share hydrogen bonds with water molecules. This is supported by analyzing the RDFs between octanol and water. The coordination number of water molecules around the oxygen in octanol is about 1.52 and 1.6 for the AA and UA models, respectively. These results suggest that octanol is preferentially binding with water molecules.

Analysis of the hydrogen bonds formed between octanol molecules and octanol and water support this finding also. It was determined that the number of hydrogen bonds between octanol molecules decreased in comparison to the pure octanol systems to average values of 0.383 ± 0.02 and 0.387 ± 0.02. The number of hydrogen bonds formed by octanol and water with octanol as the donor group was determined to be 0.541 ± 0.02 and 0.589 ± 0.02 for

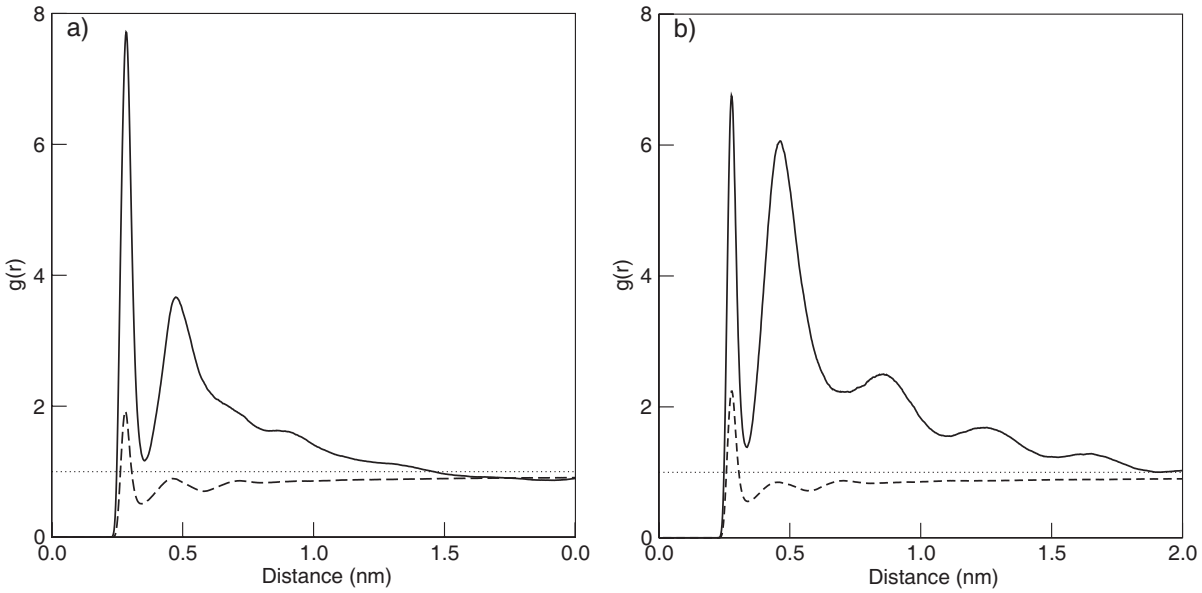

Figure 4.6: Radial distribution functions for oxygen-oxygen in octanol (solid line) and octanol oxygen-water (dashed line) in the a) all-atom and b) united-atom models in the octanol/water simulations.

the AA and UA systems, and with water as the donor values of 0.862 ± 0.02 and 0.791 ± 0.02 were determined. The total number of hydrogen bonds formed by octanol acting as a donor are 0.924 ± 0.04 and 0.976 ± 0.04 for each system, which compares to the numbers found in the pure octanol systems.

We also investigated the dynamic properties of the octanol/water system. The calculated diffusion coefficients of octanol in the octanol/water systems were similar to those obtained in the pure octanol. The diffusion coefficients of octanol are $D_{\mathrm{AA}} = 0.70 \pm 0.24 \times 10^{-6}$ cm^2/s and $D_{\mathrm{UA}} = 1.01 \pm 0.15 \times 10^{-6}$ cm^2/s for the AA and UA models, respectively. For water, the calculated values are $D = 2.14 \pm 0.27 \times 10^{-5}$ cm^2/s and $D = 2.65 \pm 0.29 \times 10^{-5}$ cm^2/s in the AA and UA configurations, respectively, which are in good agreement with the experimental value at 298 K of $D_{\mathrm{exp}} = 2.3 \times 10^{-5}$ cm^2/s [70].

The results show that the AA and UA models of octanol in the octanol/water system are very similar and both provide a good description of equilibrium, structural, and

dynamic properties. This gives us confidence and a solid basis for the discussion in the next section that includes the behavior of capsaicin in an octanol/water system.

4.4.3 Capsaicin, Octanol, and Water

The equilibrated configurations obtained from the octanol/water systems were used as the starting point for the simulations including capsaicin. As described in Simulation Details, 8 capsaicin molecules were inserted in the aqueous phase of their corresponding AA and UA configurations. One of the goals of these calculations was to determine the partition of capsaicin between the aqueous and octanol-rich phase. Since capsaicin is an amphiphilic molecule, it is expected that its hydrophilic part will interact favorably with water or the polar part of octanol, while the hydrophobic part will preferentially interact with the hydrocarbon chain of octanol. This behavior is indeed observed in our simulations. Figures 4.2 and 4.3 show snapshots of the simulations boxes at different times along the simulation. The capsaicin molecules were initially placed in the middle of the aqueous phase and soon after the simulation started, the molecules either aggregate or diffuse to the interfacial region. In the AA simulation, the first capsaicin molecule penetrated the the octanol-rich phase after 750 ps and the last one after 12 ns. Each molecule entered the octanol-rich phase in a similar manner. Molecules directly diffused from the bulk aqueous phase to the interface where the hydrophilic (polar) part of capsaicin associated with water and the hydroxyl groups in octanol for a prolonged period of time before actually penetrating into the octanol-rich phase. The hydrophobic part of capsaicin was always inserted first into the region below the interface associated with the hydrocarbon chains. For the UA system, the first capsaicin molecule penetrated the octanol-rich phase at about 700 ps from the start of the simulation. After about 5 ns, all except one of the capsaicin molecules were dissolved in the octanol-rich phase. One capsaicin molecule never actually penetrated into the octanol-rich phase, but it remained bound to the interface for long periods of time (see last frame at 20 ns in Figure 4.3). Just as in the AA case, all the capsaicin molecules entered the octanol-rich phase

with the hydrophobic part first. As also seen from the snapshots, the capsaicin molecules are aligned with the interfacial octanol molecules. Another common behavior observed with both AA and UA models is the aggregation of capsaicin molecules in the aqueous phase. Before penetrating the octanol-rich phase, a small aggregate formed with few of the capsaicin molecules (see frame at 1 ns and 2.5 ns in Figures 4.2 and 4.3, respectively), which is mainly due to the hydrophobic interaction of their hydrocarbon segment. Our results are consistent with our daily experience when eating chili pepper. We know that drinking water does not soothe the burning pain from spicy food since water will simply disperse even more capsaicin. Drinking or ingesting some "fatty" food (e.g., milk or yogurt) alleviates the pain much quicker because they can absorb capsaicin.

Since the octanol molecules in the obtained configurations formed a "bilayer-like" structure, we wanted to obtain some measure of the ordering of the hydrocarbon chains and whether capsaicin had any effect in that ordering. For lipid bilayer structures, the ordering and alignment of the aliphatic tails of the lipids are quantified with the deuterium order parameter, as described in Chapter 2. We applied the same formalism for the hydrocarbon chains in octanol (only those associated with the interface). Figure 4.7 shows the order parameter of the hydrocarbon chains for the AA and UA models in the configurations with and without capsaicin. As seen in the figure, the penetration and alignment of capsaicin into the octanol-rich phase increases the ordering of the octanol molecules. If one can translate these observations to a lipid bilayer, then we would also expect that capsaicin would greatly influence the structure of (and possibly the dynamics) of lipid bilayers (discussed in detail in Chapter 4). The changes induced by capsaicin are the first step in understanding its biological function from a molecular perspective.

A closer look at the position of the capsaicin molecule in the octanol-rich phase reveals that the aromatic (polar) part of the molecule is exposed to the aqueous phase, while the hydrocarbon tails of capsaicin and octanol align with each other. Figure 4.8 illustrates a capsaicin molecule surrounded by octanol molecules from the AA simulation (analogous results are observed in the UA simulations). The position and orientation of capsaicin is such

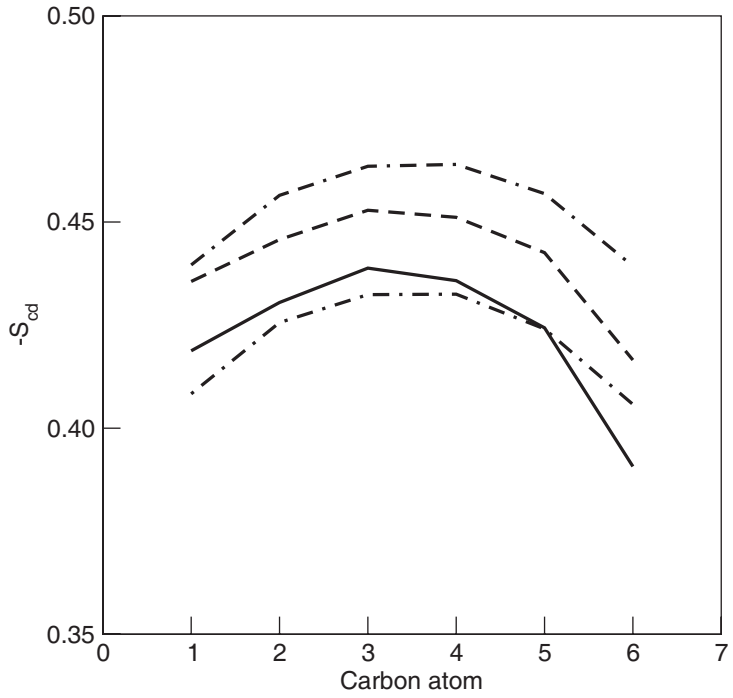

Figure 4.7: Deuterium order parameters for the hydrocarbon tail of octanol. Only those molecules aligned along the interface were considered in the calculation. Atom 0 is the carbon attached to the hydroxyl group and atom 7 is the methyl group. The different lines correspond to the following systems: all-atom octanol/water (solid line), all-atom capsaicin/octanol/water (dashed line), united-atom octanol/water (dot-dashed line), and united-atom capsaicin/octanol/water (dot-dash-dashed line).

that the hydrophilic and hydrophobic interactions are optimized. The insertion of capsaicin in the octanol-rich phase disrupts the hydrogen bond network between octanol/octanol and octanol/water molecules. Capsaicin in turn can also interact with octanol and water through hydrogen bonds with the amide nitrogen (H-donor) and amide oxygen (H-acceptor) groups. Analysis of the various RDFs of capsaicin with octanol and water, Figures 4.9 and 4.10, provides insight into the interactions of capsaicin at the interface. As seen in the RDFs (Figures 4.9a,b and 4.10a,b), the amide group is essentially surrounded by octanol molecules. There is little water binding either with the amide nitrogen or oxygen atoms. The amide oxygen (carbonyl oxygen) is the main site for hydrogen bonding between capsaicin and octanol, seen by the well-defined peak at about 0.35 nm in Figures 4.9b and 4.10b. On the other hand, the amide nitrogen only forms a small number of hydrogen bonds with octanol (shoulder in Figures 4.9a and 4.10a) because of it is unfavorable orientation and the preference for hydrogen bonding between octanol and the carbonyl oxygen. The octanol molecules found in the vicinity of the amide nitrogen are simply "solvating" that group. There are few octanol or water molecules actually hydrogen bonding to the anisole group (Figures 4.9d and 4.10d). Part of the reason is the intramolecular hydrogen bond formed between the hydroxyl group (H-donor) and anisole (H-acceptor) which occurs during these simulations.

For the hydroxyl group in the aromatic ring of capsaicin, hydrogen bonds were formed with both octanol and water in the AA model, whereas in the UA model, hydrogen bonds are predominantly with water molecules (Figures 4.9c and 4.10c). This difference is attributed to the different configurations of the octanol rich phase. In the AA representation, one interface is not uniform. This exposes capsaicin molecules to octanol molecules in the pockets, as shown in Figure 4.2 at t = 2.5, 5, 10, and 15 ns. The other interface in the AA configuration is approximately planar (lower interface in Figure 4.2). An analysis of the RDF for the hydroxyl group of capsaicin molecules in this lower interface is similar to that of the UA hydroxyl group RDF, as shown in Figure 4.11. The similarity in the RDFs validates the consistency of the representations for capsaicin. In terms of the structure and binding

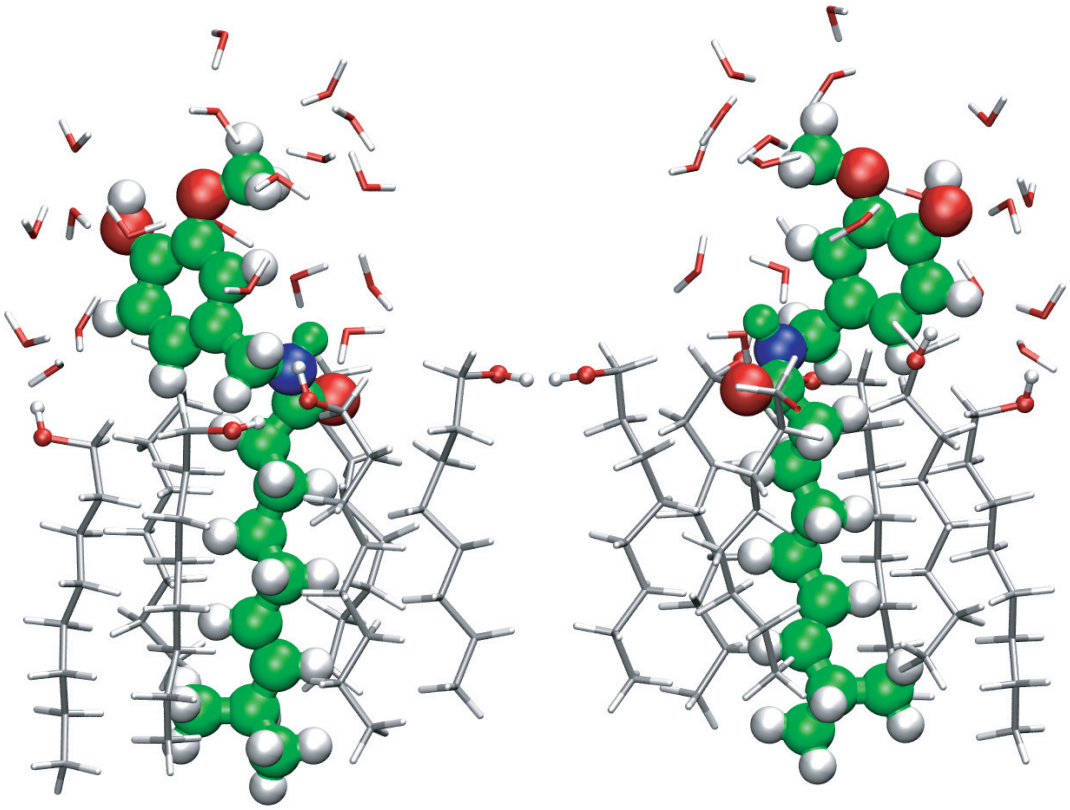

Figure 4.8: Sample all-atom model of capsaicin surrounded by octanol molecules. The amide group in capsaicin is shown preferentially aligning with the hydroxyl groups of octanol. Note the alignment of the hydrophobic part of capsaicin with the hydrocarbon tail of octanol. The aromatic segment is exposed to the aqueous phase.

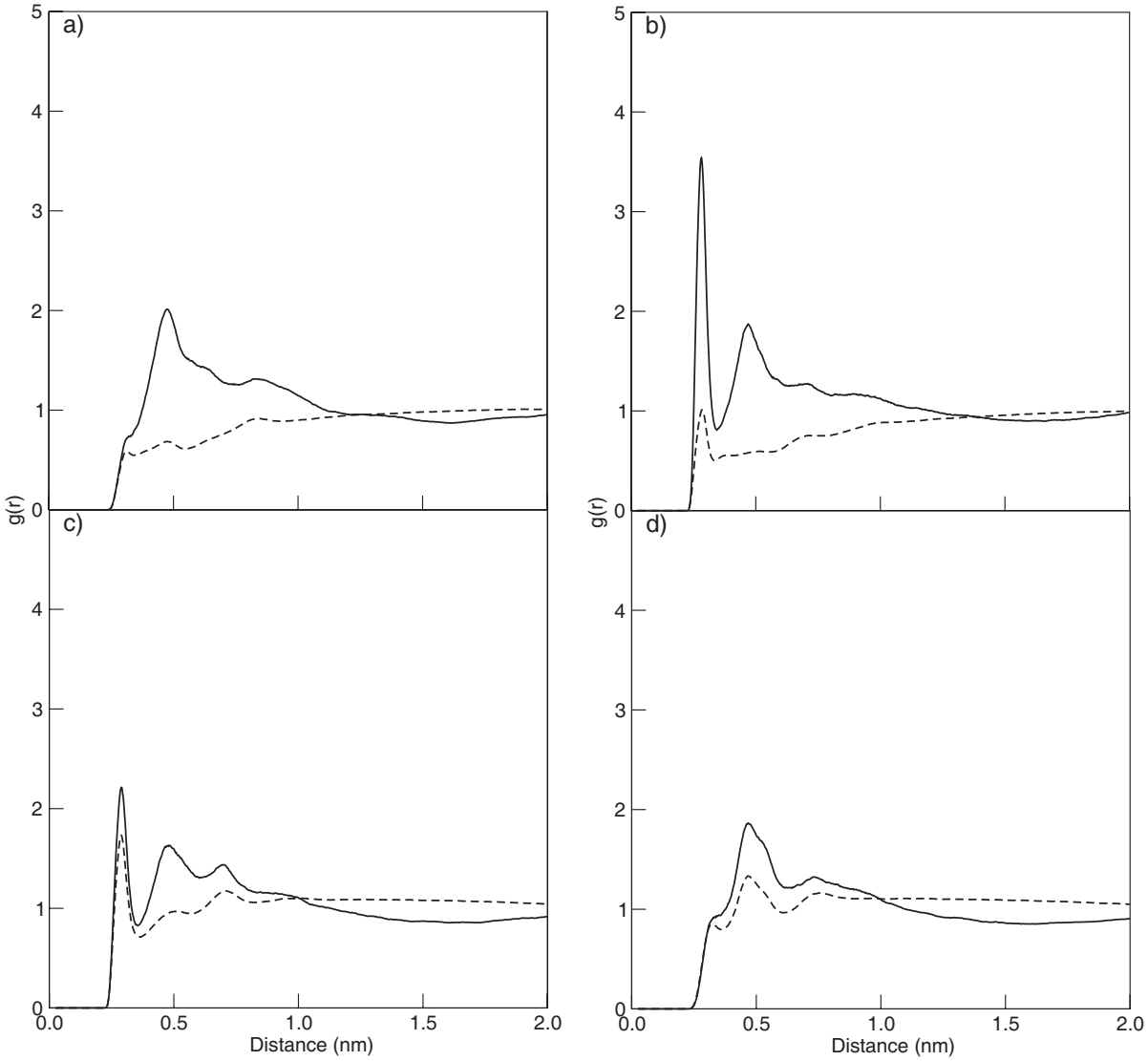

Figure 4.9: Radial distribution functions from the all-atom model simulation between capsaicin groups and octanol oxygen (solid line) and water (dashed line). The graphs correspond to the following groups in capsaicin: a) amide nitrogen, b) amide oxygen, c) hydroxyl oxygen, and d) anisole oxygen.

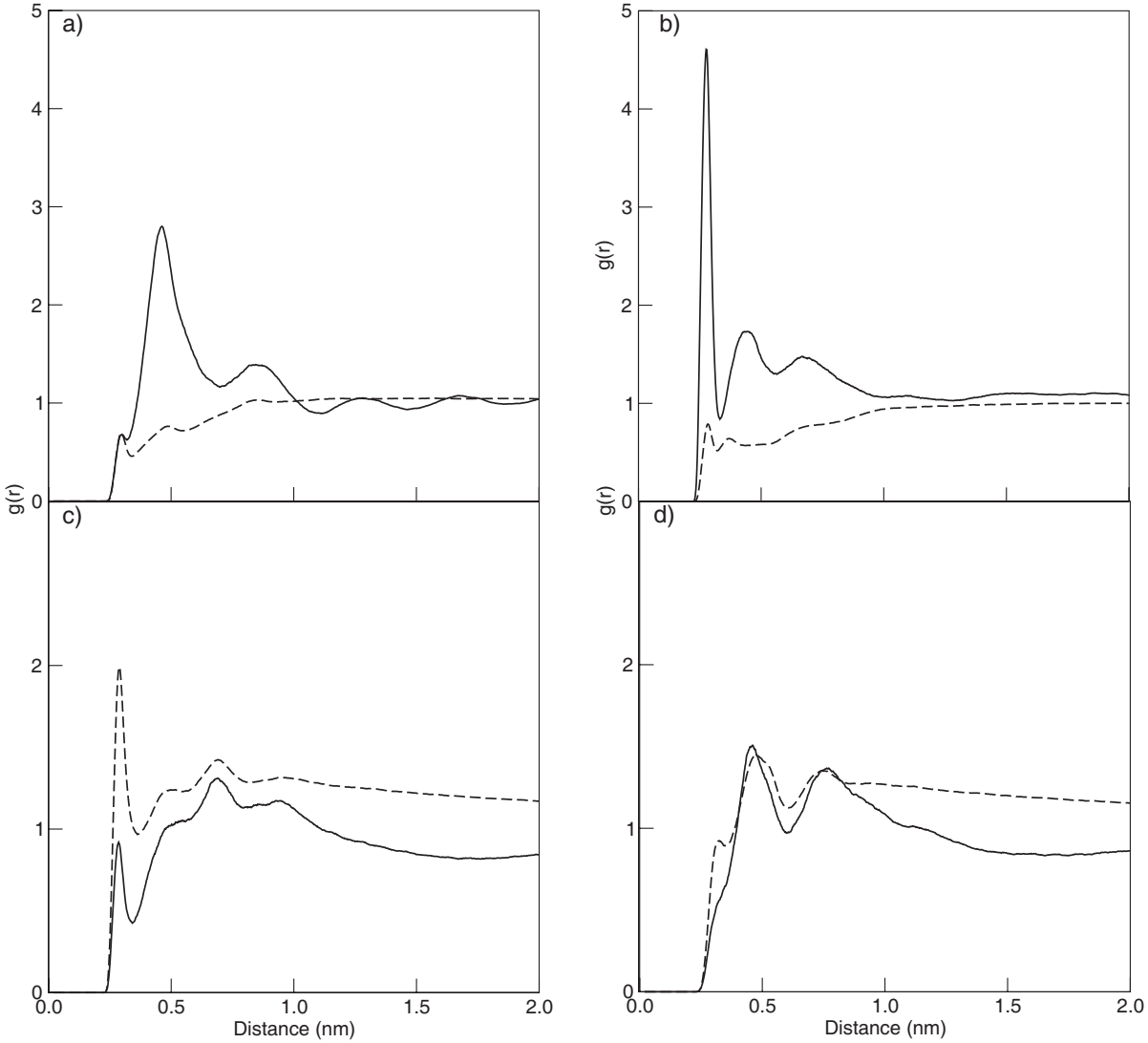

Figure 4.10: Radial distribution functions from the united-atom model simulation between capsaicin groups and octanol oxygen (solid line) and water (dashed line). The graphs correspond to the following groups in capsaicin: a) amide nitrogen, b) amide oxygen, c) hydroxyl oxygen, and d) anisole oxygen.

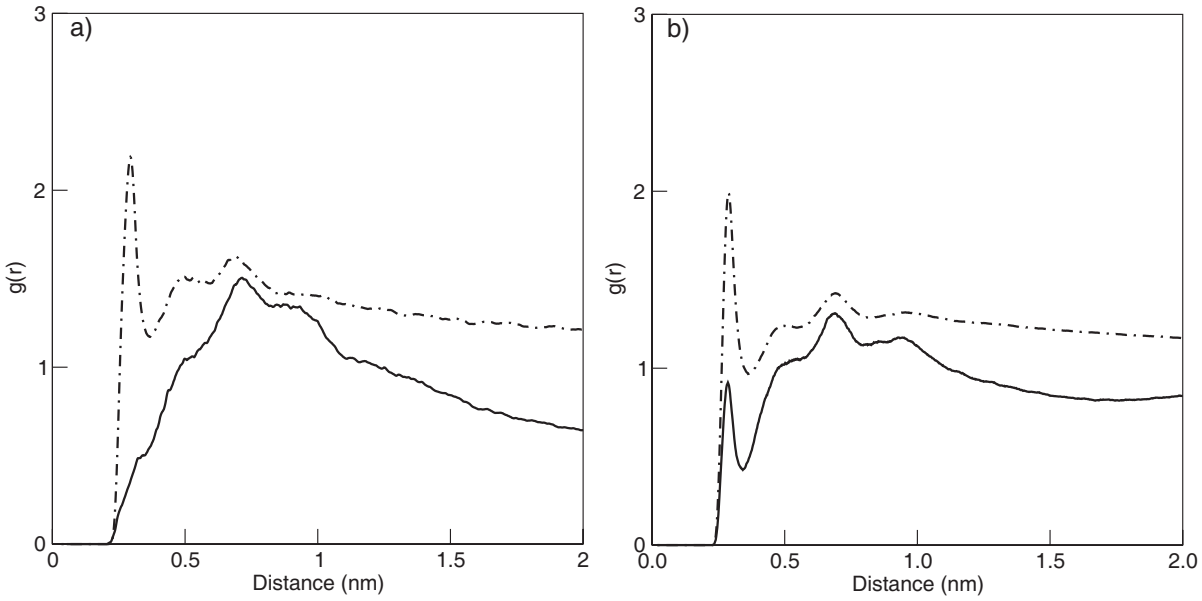

Figure 4.11: Radial distribution functions between a) the hydroxyl group of capsaicin in the lower interface of the all-atom configuration and b) the hydroxyl group of all capsaicin molecules from the united-atom configuration and octanol oxygen (solid line) and water (dot-dash line).

of the molecules, there are no major differences between the AA and UA models employed in the simulations.

The dynamic properties of capsaicin in the octanol/water systems were also analyzed by calculating the diffusion coefficient. We determined two sets of diffusion coefficients, one for unbound capsaicin in the aqueous phase (D_{aq}), and one for capsaicin incorporated into the octanol-rich phase (D_{or}). As noted earlier, once the octanol molecules penetrated the octanol-rich phase, it remained there for the remainder of the simulation, thus significantly reducing its mobility. This is indeed what was found. In the AA simulations, the diffusion coefficient of capsaicin decreased from $D_{\mathrm{aq}} = 1.95 \pm 0.16 \times 10^{-6}$ cm^2/s in the aqueous phase to $D_{\mathrm{or}} = 0.145 \pm 1.33 \times 10^{-6}$ cm^2/s once dissolved into the octanol-rich phase. And for the UA simulations, it decreases from $D_{\mathrm{aq}} = 1.96 \pm 0.14 \times 10^{-6}$ cm^2/s to $D_{\mathrm{or}} = 0.264 \pm 0.39 \times 10^{-6}$ cm^2/s. As seen, the motion of capsaicin is highly restrained in the octanol-rich phase, decreasing the diffusion coefficient by one order of magnitude.

The mobility of capsaicin in the octanol-rich phase is largely restricted by the dynamics of the octanol molecules. Since the octanol molecules self-assembled and formed a bilayer-like structure, the motion of one molecule is directly coupled to all the others. And the same applies to capsaicin once incorporated among the octanol molecules. This is seen from the diffusion coefficient of the octanol molecules, $D_{\mathrm{AA}} = 0.328 \pm 0.22 \times 10^{-6}$ cm^2/s and $D_{\mathrm{UA}} = 0.300 \pm 0.15 \times 10^{-6}$ cm^2/s, which are the same as those for capsaicin, within statistical uncertainty.

4.5 Conclusions

We presented here a study of the properties of capsaicin in an octanol/water system. To that end, an evaluation was performed for two molecular representations of capsaicin and octanol, an all-atom and a united-atom model based on the OPLS force field. Equilibrium, structural, and dynamic properties were calculated with molecular dynamics simulations, and compared with available experimental data and previous simulation studies of octanol and water. The octanol/water simulations resulted in an inhomogeneous system with two phases formed, an aqueous and an octanol-rich phase. The octanol molecules assembled in a bilayer-like structure forming a clear interface with the hydroxyl groups exposed to the aqueous phase. Capsaicin molecules, initially dissolved in the aqueous phase, were incorporated into the octanol-rich phase. The hydrophobic part of capsaicin aligned with the octanol hydrocarbon chains, and the polar part was exposed to the aqueous phase. Both octanol and water bind to the capsaicin molecules, forming hydrogen bonds with the amide oxygen and hydroxyl groups. Both the all-atom and united-atom models gave comparable results and adequately represent the behavior of capsaicin at the atomic level. Our simulations consider only a small number of capsaicin molecules, thus the extra number of sites in the all-atom model compared to the united-atom model was not significant. The study performed here is the initial stage of a more extensive study on capsaicin aimed at studying its behavior in biological systems, specifically the role of capsaicin in the interactions at the cellular level. These interactions are

described in detail in Chapter 5 where the properties of capsaicin in model cell membranes are investigated.

Chapter 5

Molecular Dynamics Study on the Properties of Capsaicin in Lipid Bilayers of DPPC and DPPE

5.1 Introduction

Capsaicin is the pungent chemical found in chili peppers that causes a burning sensation usually associated with noxious temperatures. This chemosensory action affects sensory neurons [5] and is attributed to the activation of the vanilloid receptor TRPV1 [4]. Dose dependent studies suggest that capsaicin can induce inflammatory response, desensitize sensory neurons, and cause neuronal toxicity with increasing concentrations [4]. The ability of capsaicin to desensitize sensory neurons to various stimuli has resulted in its use in clinical analgesic applications for topical creams and intravenous instillation [71]. As such, capsaicin is an attractive therapeutic agent because it is naturally occurring, non-toxic (in moderate doses), and non-steroidal. Because the vanilloid receptor TRPV1 is activated by noxious temperatures and vanilloids, it has been used as a model system for understanding the pain pathway

[2]. The interactions of capsaicin with sensory neurons are an integral aspect of this phenomena. Chapter 2 provided a detailed review of the chemosensory properties of capsaicin. This chapter presents our studies of the properties of capsaicin in biological membranes.

There are two main objectives of this study: to characterize the permeation of capsaicin through membranes and to determine the effects of capsaicin on the properties of the membrane. Capsaicin, a lipophilic molecule, is sparsely soluble in water [66]. In the study presented in Chapter 4, capsaicin partitioned into an 1-octanol phase [72]. The octanol/water system is a good approximation of lipophilic systems [47, 50]; however, the molecular interactions of solute molecules may differ for membranes. Simulations by Bemporad *et al.* showed that 1-octanol/water systems slightly overestimate the partitioning of solutes in membranes [49, 50]. Lipid composition and solute size also affect the permeability of solutes in membranes. The lipid composition determines the spacing between headgroups in the interface [41], and the perturbation of the interface is proportional to the solute molecular volume. These variables are not well represented by simple bulk solvents.

The chemosensory action of capsaicin is materialized by changing the chemical potential across sensory neurons. Whether this action is the result of allosteric binding to TRPV1 or perturbations in the membrane, the interactions of capsaicin and the bilayer are an integral aspect of this phenomena. Experimental studies have shown that capsaicin also affects various non-neural cells. Meddings *et al.* observed a biphasic influence of capsaicin on the membrane fluidity of peritoneal mast cells and red blood cells by using fluorescent probes TMA-DPH and DPH [16]. Their results concluded that low concentrations of capsaicin increased membrane fluidity and high concentrations decreased fluidity [16]. These findings were dependent on the cell type, as erythrocytes and β-Lymphocytes were unaffected. That study suggested that capsaicin action requires an extractable, non-lipid component, that may not be the result of intrinsic interactions with membrane lipids [16]. Similar studies of pure and cholesterol containing 1-palmitoyl-2-oleoylphosphatidylcholine (POPC) and dipalmitoylphosphatidylcholine (DPPC) liposomes by Tsuchiya also showed a biphasic response [18]. Adding cholesterol made the bilayer more rigid and reduced this effect at low

concentrations. The results of Meddings *et al.* and Tsuchiya indicate that the composition of the membranes affects the action of capsaicin. In another study, Aranda *et al.* observed that, in the presence of capsaicin, the structure of both DPPC and dielaidoylphosphatidylethanolamine (DEPE) bilayers was modified, indicating that the membrane fluidity was reduced at mole fractions above 0.20 for DPPC membranes [17]. Their study did not indicate a biphasic response. All three studies investigated membrane fluidity using fluorescence spectroscopy with TMA-DPH and DPH probes. Tsuchiya [18] and Aranda *et al.* [17] also used N-phenyl-1-napthylamine (PNA) and 2-anthroyloxystearic acid (2-AS) as additional fluorescent probes, respectively. Since each probe partitions to a different region of the bilayer, the range of results suggest that capsaicin may interact with a specific region of the bilayer.

Feigin *et al.* observed that capsaicin induces non-specific ion channels in an equimolar bilayer of 1,2-dioleoyl-*sn*-glycero-3-phosphocholine (DOPC) and 1,2-dioleoyl-*sn*-glycero-3-phospho-ethanolamine (DOPE) at an "active concentration" of 10 μM [19]. This result showed the chemosensory action of capsaicin resulting from changes in the potential across sensory neurons. Aranda *et al.* suggested that the effect of capsaicin at low concentrations is facilitated by a lateral phase separation that could greatly affect the functional behavior of the membrane [17]. Lundbæk *et al.* showed that capsaicin altered the bilayer fluidity and regulated voltage dependent sodium channels (VDSC) at concentrations of 30 μM [21]. The authors concluded that capsaicin can induce changes in the bilayer that alter the conformation of an embedded membrane protein. These results establish the importance of the interactions of capsaicin with the membrane as an essential component of its chemosensory action.

Aranda *et al.* studied the effects of capsaicin on the phase transition of DPPC and DEPE using differential scanning calorimetry (DSC) [17]. They determined that the gel to liquid-crystalline phase transition temperature of DPPC decreased with increasing capsaicin concentration; this effect was less pronounced in DEPE. It was concluded that capsaicin had a preferential alignment in the lipid bilayer, in which the alkyl chain aligned with the lipid tails

and the polar amide and vanillyl groups with the headgroups along the lipid/water interface [17]. Experimental studies and quantum chemical calculations performed by Kogure *et al.* also supported this conclusion [23]. Their study observed the scavenging of free radicals by capsaicin at different depths within a rat liver mitochondrial membrane. The phenolic hydroxyl group in capsaicin was ineffective in scavenging free radicals since it forms an intramolecular hydrogen bond with the neighboring anisole group [23]. This intramolecular hydrogen bond reduces the polarity of the vanillyl aromatic group, thus preventing it from scavenging free radicals [23]. Free radical scavenging by the carbon atom between the vanillyl and amide groups occurred near the lipid/water interface, indicating that the amide group in capsaicin is also near the interface. Recent simulations by Bemporad *et al.* give further support for the interaction of capsaicin with lipid bilayers [47]. Their study determined that nitrogen containing functional groups are more favorable for forming hydrogen bonds than oxygen based groups. From the experimental and computational results, we expect capsaicin to preferentially align within the lipid bilayer, with the alkyl chain oriented with the lipid tails and the amide group near the lipid/water interface. This orientation is similar to the observed alignment of cholesterol in DPPC bilayers from recent molecular simulations [73, 74].

Here we will characterize the partitioning of capsaicin between an aqueous phase and a phospholipid bilayer, the structural effects induced by capsaicin on the bilayer, and the properties of capsaicin in the bilayer. To the best of our knowledge, this is the first computational study at the molecular level detailing the interactions of capsaicin and biological membranes, modeled as a phospholipid bilayer. Pure DPPC bilayers have been well characterized [75–77] (most abundant lipid in eukaryotic membranes) and they have been commonly used to study the partitioning and binding interactions of small molecules with lipid bilayers [43, 44, 47, 51]. We are also interested in the specific interactions of capsaicin with sensory neurons. These membranes are complex and contain a diverse array of lipid headgroups and fatty acid chains. The most predominant headgroups in neurons are the phosphatidylcholine (PC) and phosphatidylethanolamine (PE) at an average ratio of 2:1,

and for fatty acids, eighteen carbon saturated (18:0) and monounsaturated (18:1) chains are most abundant [78–82]. Here we will use a mixed bilayer with a 3:1 molar ratio of DPPC to DPPE (dipalmitoylphosphatidylethanolamine). Molecular dynamics simulations will be used to describe the properties of capsaicin and its behavior in lipid bilayers.

5.2 Simulation Details

Pure DPPC bilayers and mixed bilayers with a 3:1 molar ratio of DPPC to DPPE were used as model cell membranes. The molecular representation of DPPC is based on the model developed by Berger *et al.* [39], and that of DPPE according to modifications employed by Leekumjorn and Sum [41] (choline methyl groups were replaced by hydrogens). As shown and discussed in Chapter 4, capsaicin was modeled with the OPLS UA force field [26–31, 56]. Two sets of studies are used to characterize the properties of capsaicin with the bilayer systems: one examined the penetration of capsaicin into the bilayer, and the other the structural and dynamic properties of capsaicin and the bilayer. In total, eighteen simulations were performed representing 785 ns of simulation time. The systems considered are summarized in Table 5.1, where the naming scheme reflects the composition of the bilayer (LipidP for the DPPC bilayer and LipidM for the mixed bilayer) and the number of capsaicin molecules. All lipid systems contained 256 lipid molecules. All LipidM systems contained a 3:1 molar ratio of DPPC to DPPE in each leaflet.

Molecular dynamics simulations were performed using the leap-frog integration algorithm with a time-step of 2 fs. Non-bonded (van der Waals and electrostatics) interactions were cut off beyond 0.9 nm. The Particle Mesh Ewald (PME) method [60] was used to account for long-range electrostatic interactions with a 0.12 nm grid-size and a fourth-order spline interpolation. Dispersion corrections for the energy and pressure were included to improve the accuracy of the PME method. The linear constraint solver (LINCS) algorithm was used to constrain all bonds of the lipid and capsaicin molecules [83], and the SETTLE

Table 5.1: Composition of the lipid bilayer systems. Each system contains 256 lipid molecules, and each leaflet has an identical composition. The naming scheme represents the composition of the bilayer (LipidP for the DPPC bilayer and LipidM for the mixed bilayer) and the number of capsaicin molecules (A-H).

System	Water	DPPC	DPPE	Capsaicin	Time (ns)
LipidP-A	7680	256	—	—	40
LipidP-B	15360	256	—	4[a,b]	35
LipidP-C	15360	256	—	8[a]	30
LipidP-D	10392	256	—	12	50
LipidP-E	10392	256	—	16	50
LipidP-F	10392	256	—	20	50
LipidP-G	10392	256	—	24	50
LipidP-H	10392	256	—	40	50
LipidM-A	7680	192	64	—	40
LipidM-B	15360	192	64	4[a,c,d]	40/30
LipidM-C	15360	192	64	8[a,c]	40/30
LipidM-D	9549	192	64	12	50
LipidM-E	9549	192	64	16	50
LipidM-F	9549	192	64	20	50
LipidM-G	9549	192	64	24	50
LipidM-H	9549	192	64	40	50

[a] capsaicin molecules were inserted into the aqueous phase.

[b] four additional capsaicin molecules were added after the initial four penetrated into the bilayer.

[c] simulations were also performed at 350 K.

[d] four additional capsaicin molecules were added for the system simulated at 350 K.

algorithm for water molecules [84]. Constant temperature and pressure simulations were controlled using the Berendsen weak coupling technique [61] with $\tau_T = 0.2$ ps and $\tau_P = 2.0$ ps for the temperature and pressure, respectively. All LipidP and LipidM systems were simulated at 323 K and 1 bar with a compressibility of 4.63×10^{-5} bar^{-1}. Additional simulations were performed for LipidM-B,C at 350 K and 1 bar. The temperature of each component was coupled separately, and the anisotropic pressure control allowed the dimensions of the box to fluctuate. For LipidP systems, anisotropic pressure coupling was used, and for LipidM systems D-H, semi-isotropic pressure coupling was applied (box vectors in the x and y Cartesian directions were coupled and the box vector in the Cartesian z direction scaled independently). This pressure coupling scheme was introduced to prohibit artificial ordering that was observed for selected LipidM systems when using anisotropic pressure coupling. All simulations were performed with the GROMACS 3.3 software package (single-precision mode) [55] in parallel (about 4.2 ns/day on 12 processors) using Virginia Tech's System X (dual 2.3 GHz Apple Xserve G5). Trajectories were saved every 5 ps for lipid systems A and D-H, and every 2.5 ps for lipid systems B-C.

For lipid systems B and C, capsaicin molecules were initially inserted into the aqueous phase, as shown in Figure 5.1. The aqueous phase for these systems contained a large number of water molecules in order to create a layer approximately 6 nm thick (this ensured that the interactions of capsaicin were with a single bilayer leaflet at any given time). For lipid systems D-H, the number of waters per lipid is sufficient for an aqueous phase of approximately 3 nm. Fully extended, evenly spaced capsaicin molecules were inserted into pre-equilibrated bilayers, such that the aromatic vanillyl group was aligned with the lipid headgroups and the nine carbon alkyl chain was aligned with the lipid acyl tails along the bilayer normal (Figure 5.2). Capsaicin was inserted by superimposing molecules onto the system and then systematically deleting overlapping lipid and water molecules. Overlapping molecules were defined as those having any atom within 0.13 nm of the inserted capsaicin molecules. For LipidP-B and LipidM-B at 350 K, all initially inserted capsaicin molecules dissolved into the bilayer. Additional molecules were inserted following the same procedure,

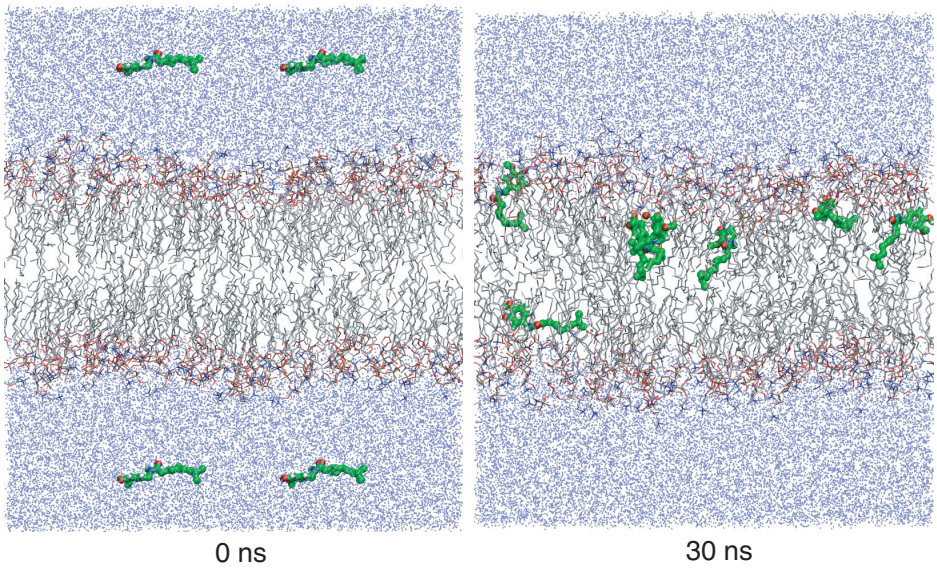

Figure 5.1: Initial and final configurations of LipidM-B at 350 K. Capsaicin molecules were initially inserted into the aqueous phase, and at the conclusion of the simulation, all eight molecules penetrated the bilayer at a 7:1 leaflet ratio. Capsaicin molecules are shown as the space-fill representation.

then the simulation was resumed with a new set of velocities. This method mimics biological conditions where capsaicin is not administered instantaneously but rather intravenously. After inserting capsaicin in systems D-H, an 1 ns NVT simulation was performed at 400 K to relax the system using the same simulation protocol previously described.

5.3 Results and Discussion

The objective of this study is to characterize the properties of capsaicin in a pure DPPC bilayer and a mixed bilayer with a 3:1 molar ratio of DPPC to DPPE. These bilayer systems were systematically characterized at 323 K and 1 bar before adding capsaicin to establish a representation that is consistent with experiments and simulations.

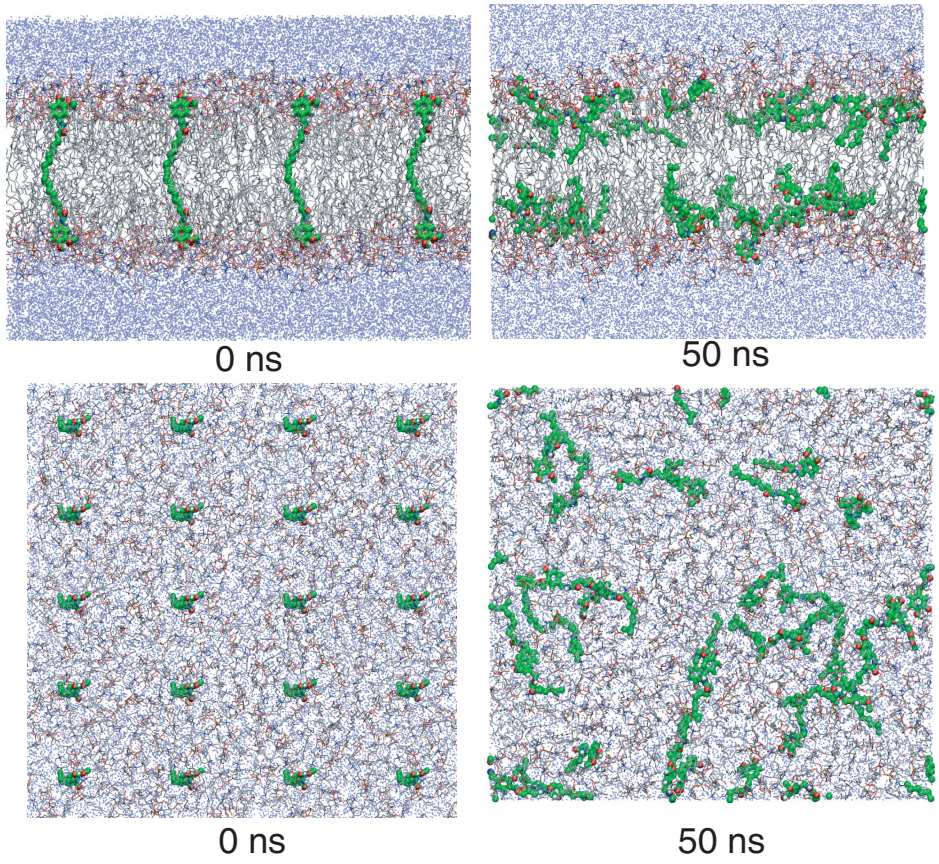

Figure 5.2: Initial and final configurations of LipidP-H at 323 K containing 40 capsaicin molecules. The top figures are a side-view of the simulation box and the lower figures are the top-view. Capsaicin molecules are shown as the space-fill representation.

5.3.1 Pure Lipid Bilayers

Pure lipid systems (LipidP-A and LipidM-A) were simulated for 40 ns at 323 K and 1 bar to establish a control for measuring the effects of capsaicin on the structure and dynamics of each bilayer system. The stability and convergence of the simulations was measured with the area per lipid, which was calculated from the cross-sectional area of the simulation box along the bilayer surface, divided by the number of lipids per leaflet (128 in this case). As shown in Figure 5.3, the area per lipid of each system converged after about 10 ns to the equilibrium values of 0.65 ± 0.01 nm^2 and 0.60 ± 0.01 nm^2 for LipidP-A and LipidM-A, respectively. The value for LipidP-A is within an acceptable range of the experimental value of 0.62 nm^2 at 323 K and 1 bar [75]. For LipidM-A, the predicted value is similar to the experimental result for pure DPPE at 342 K of 0.60 nm^2 [85] and pure DPPC at 323 K of 0.62 nm^2 [75]. Previous simulations for LipidP-A obtained values of 0.63 nm^2 [86, 87] and 0.61 nm^2 [39] at 323 K, and for LipidP-A and LipidM-A at 350 K and 1 bar values of 0.69 nm^2 and 0.65 nm^2, respectively [41]. Based on the area per lipid, equilibrium, structural and dynamic properties were calculated over the last 20 ns for each system.

The density profiles for LipidP-A and LipidM-A are shown in Figure 5.4. The intermembrane region is about 3 nm and is predominantly occupied by lipid acyl tails. The interface is represented by the highest density region of the system ($|1.5 - 2.5|$ nm from the center of the bilayer) and is characterized by the lipid headgroups and water [88, 89]. The aqueous phase is the region with a density of approximately 970 kg/m^3 ($|2.5 - 4|$ nm from the bilayer center). The interfacial density of each system was compared by evaluating the maximum interfacial density (the maximum density is calculated by averaging the maximum interfacial density of each leaflet). This analysis shows that the interfacial density of LipidM-A (1310 kg/m^3) is slightly higher than that of LipidP-A (1283 kg/m^3) at 323 K and 1 bar. This trend agrees with the previously calculated area per lipid (Figure 5.3), as a decrease in the area per lipid corresponds to a tighter packing of the lipid headgroups. The affects of temperature and lipid composition are best represented by the thickness of the bilayer,

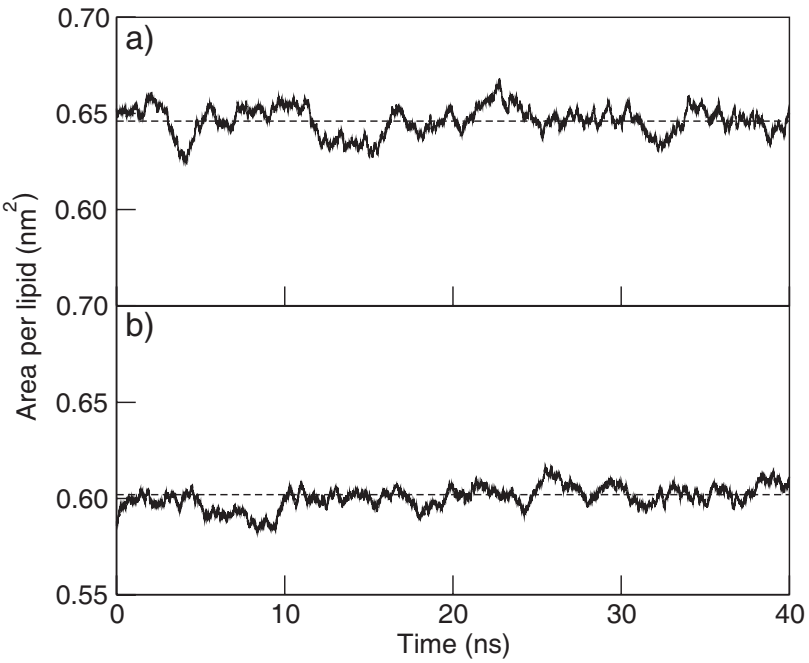

Figure 5.3: Area per lipid for a) LipidP-A and b) LipidM-A at 323K and 1 bar. Dash lines show the average area per lipid.

which is measured by the average distance between phosphorus atoms of opposing leaflets (P-P distance). Using this correlation, the P-P distances of LipidP-A and LipidM-A are 3.72 ± 0.03 nm and 3.89 ± 0.05 nm, which are larger than previously reported values of 3.59 ± 0.01 nm and 3.66 ± 0.01 nm at 350 K, respectively [41]. Adding DPPE increases the bilayer thickness and increasing the temperature has the opposite effect.

Figure 5.5 shows the deuterium order parameters (-S_{CD}) averaged over both acyl tails for LipidP-A and LipidM-A at 323 K and 1 bar. The carbon atoms considered are depicted in Figure 2.3: C34, C36-C50 and C15, C17-C31 for the lipid Sn-1 and Sn-2 acyl tails, respectively, where atoms C34 and C15 correspond to atom 0 and atoms C50 and C31 to atom 15 in Figure 5.5. The calculated values for LipidP-A agree with experimental results [85, 90] and previous simulations [39]. The -S_{CD} values for LipidM-A are similar to previous simulations at 350 K [41]. Adding DPPE increases the order of the lipid acyl tails by approximately 9%. This agrees with the area per lipid decrease (Figure 5.3), and the

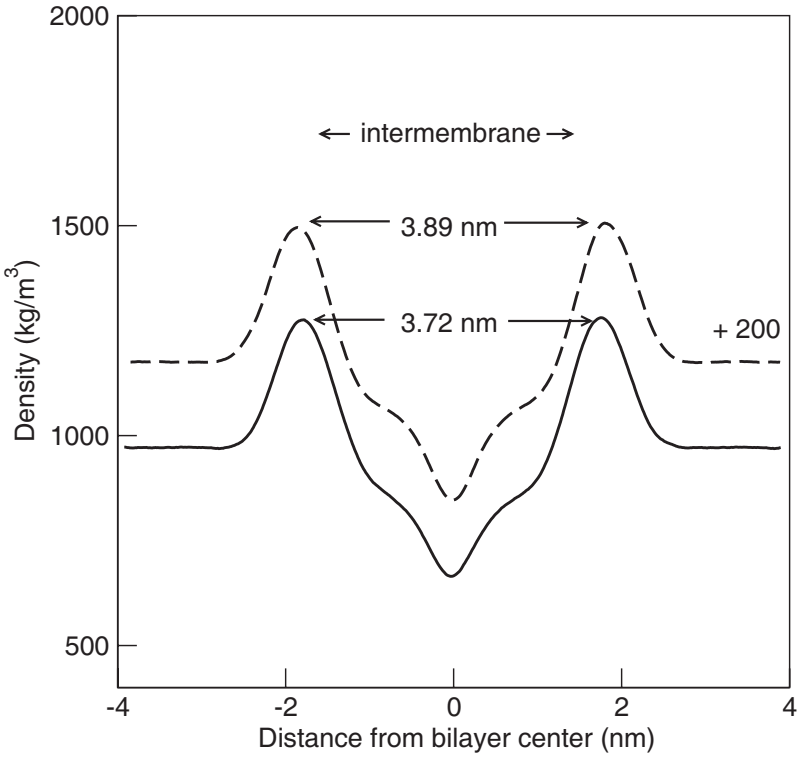

Figure 5.4: Density profiles for LipidP-A (solid line) and LipidM-A (dashed line) at 323 K and 1 bar. The bilayer thickness, measured by the average distance between phosphorus atoms, is also shown for each system.

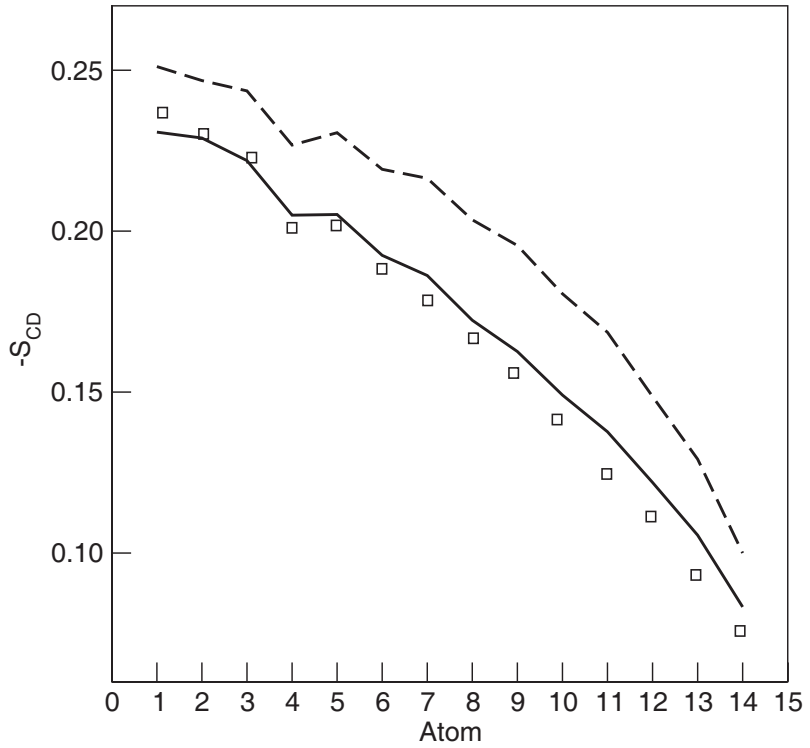

Figure 5.5: Deuterium order parameters (-S_{CD}) for LipidP-A (solid line) and LipidM-A (dashed line) at 323 K and 1 bar averaged for all lipid acyl tails in each system over the last 20 ns. Previous simulation results of LipidM-A at 350 K are shown by the open squares [41].

increase in the P-P distance and interfacial density (Figure 5.4).

The dynamics of each system are represented by the lateral 2D diffusion coefficient of the lipids along the plane of the bilayer. This parameter is calculated by the mean-squared displacement (MSD) shown in Equation 3.17, where *r(t)* is evaluated along the x and y directions only and the dimensionality constant (d) is equal to 2. The 2D diffusion coefficient was affected by temperature but not lipid composition. The calculated 2D diffusion coefficients averaged over all lipids in LipidP-A and LipidM-A at 323 K and 1 bar are $D_{\mathrm{P-A}} = 0.194 \pm 0.018 \times 10^{-6}$ cm^2/s and $D_{\mathrm{M-A}} = 0.163 \pm 0.050 \times 10^{-6}$ cm^2/s, respectively. These values are in good agreement with previous simulations of LipidP-A at 323 K ($0.127 \pm 0.005 \times 10^{-6}$ cm^2/s) [91] and at 350 K ($0.282 \pm 0.018 \times 10^{-6}$ cm^2/s) [53].

The area per lipid, density profile, -S_{CD}, and diffusion coefficients of LipidP-A

and LipidM-A are consistent with experimental and previous simulations. These properties indicate that both systems are in the biologically relevant liquid-crystalline phase. Addition of DPPE decreases the area per lipid, which corresponds to an increase in the interfacial density and the order of the lipid acyl tails. Comparison of these results with previous simulations at 350 K and 1 bar indicate that higher temperature increases the area per lipid and decreases the order of the lipid acyl tails [41].

5.3.2 Capsaicin Inserted Into the Aqueous Phase

As described in the Simulation Details section, singly dispersed capsaicin molecules were inserted into the aqueous phase of LipidP-B,C and LipidM-B,C. A visual representation of the initial configuration for LipidM-B is shown in Figure 5.1. The dynamics of LipidP at 323 K and LipidM at 323 K and 350 K are shown in Figures 5.6 and 5.7 for systems B and C, respectively. In these figures the center of mass of capsaicin is used to show its instantaneous position in the system over the course of the simulation. The average position of lipid phosphorus atoms are also shown to denote the interface ($|2|$ nm from the bilayer center); an additional periodic image of a bilayer leaflet is also shown for clarity ($|7.5 - 8|$ nm from the bilayer center). Individual capsaicin molecules are depicted by colored lines, where each color represents a separate molecule. In LipidP-B and LipidM-B at 350 K, four additional capsaicin molecules were inserted after 25 ns and 20 ns, respectively, as shown in Figure 5.6.

In LipidP-B, all four capsaicin molecules initially inserted into the aqueous phase penetrated the bilayer (three in one leaflet and one in the other). The three capsaicin molecules that penetrated the lower leaflet entered the bilayer as an aggregate, that is, as a unit at the same time (Figure 5.6a). After four additional capsaicin molecules were introduced in the aqueous phase at 25 ns, only one of them penetrated the bilayer in the additional 10 ns of simulation. For LipidM-B at 323 K (Figure 5.6b), one capsaicin molecule penetrated the bilayer after approximately 22 ns of simulation time. Of the remaining

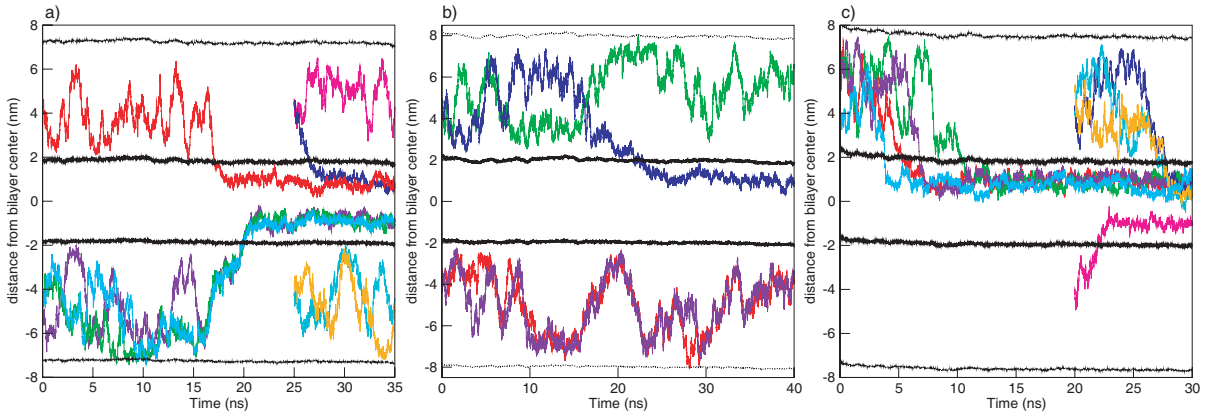

Figure 5.6: Center of mass position of capsaicin molecules inserted into the aqueous phase over the course of the simulation for a) LipidP-B, b) LipidM-B at 323 K, and c) LipidM-B at 350 K. In each figure, the average location of all phosphorus atoms are shown (bold, black lines), as well as the nearest periodic image of the bilayer (thin, black, dotted lines). Individual capsaicin molecules are shown by colored lines. After 25 ns and 20 ns of simulated time, four additional capsaicin molecules were inserted into LipidP-B and LipidM-B at 350 K.

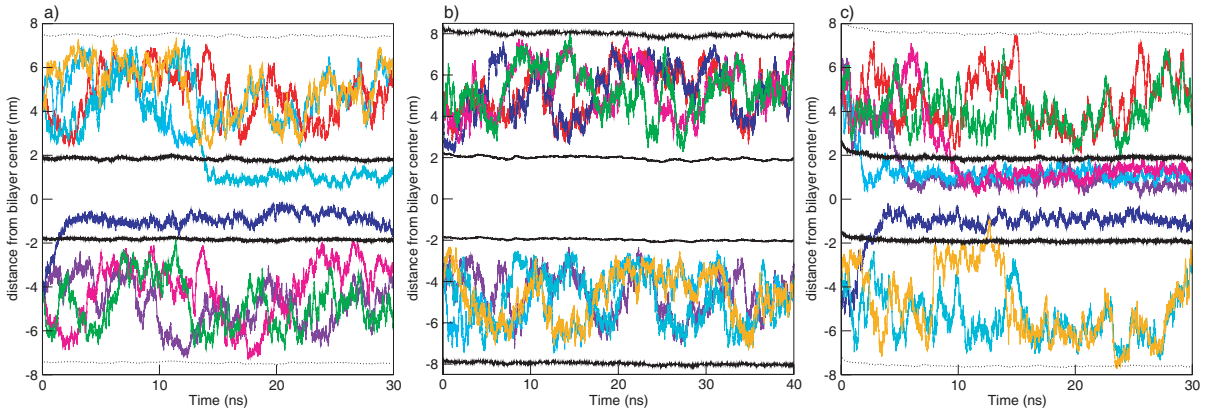

Figure 5.7: Center of mass position of capsaicin molecules inserted into the aqueous phase over the course of the simulation for a) LipidP-C, b) LipidM-C at 323 K, and c) LipidM-C at 350 K. In each figure, the average location of all phosphorus atoms are shown (bold, black lines), as well as the nearest periodic image of the bilayer (thin, black, dotted lines). Individual capsaicin molecules are shown by colored lines.

three molecules in the aqueous phase, two formed a loose aggregate, which is shown by the overlapping lines in Figure 5.6b, and the other remained singly dispersed in the aqueous phase (a loose aggregate is defined as a group of molecules that are able to aggregate or disperse). At 350 K, LipidM-B had a higher permeability than at 323 K. In this simulation, all four capsaicin molecules initially in the aqueous phase penetrated the same leaflet. Three of these molecules entered the bilayer at different locations. The fourth molecule penetrated the bilayer in the immediate proximity of another capsaicin molecule in the bilayer (Figure 5.8d). After four additional capsaicin molecules were introduced at 20 ns, three penetrated the bilayer as an aggregate, and the other by itself. The final configuration contained eight capsaicin molecules in the bilayer (seven in one leaflet and one in the other), as shown in Figure 5.1. In Figure 5.1, the three capsaicin molecules in the center of the top leaflet entered the bilayer as an aggregate, and at the end of the simulation, they dispersed in the bilayer. For LipidP-C (Figure 5.7a), two capsaicin molecules penetrated the bilayer, while the remaining six molecules periodically formed loose aggregates in the aqueous phase. For LipidM-C at 323 K (Figure 5.7b), all molecules remained in the aqueous phase over the course of the simulation, forming two loose aggregates of four molecules each. At 350 K, four capsaicin molecules penetrated the bilayer at a leaflet ratio of 3:1 (Figure 5.7c).

Figure 5.8 illustrates four different configurations observed for capsaicin penetrating the bilayer: nine carbon alkyl chain first, aromatic vanillyl group first, folded, and by interacting with another capsaicin molecule already in the bilayer. All capsaicin molecules that penetrated the bilayer in each simulation are represented by one of these configurations. Those that penetrated the bilayer with the vanillyl group or carbon chain first generally dissolved into the bilayer faster than those entering folded. The folded configuration is representative of molecules that penetrated the bilayer after prolonged association with the interface.

Bilayers containing DPPE are less permeable to capsaicin. This is seen from the simulations at 323 K and 1 bar, in which only one capsaicin molecule dissolved into LipidM-B, whereas seven dissolved into LipidP. The structural differences between the bilayer

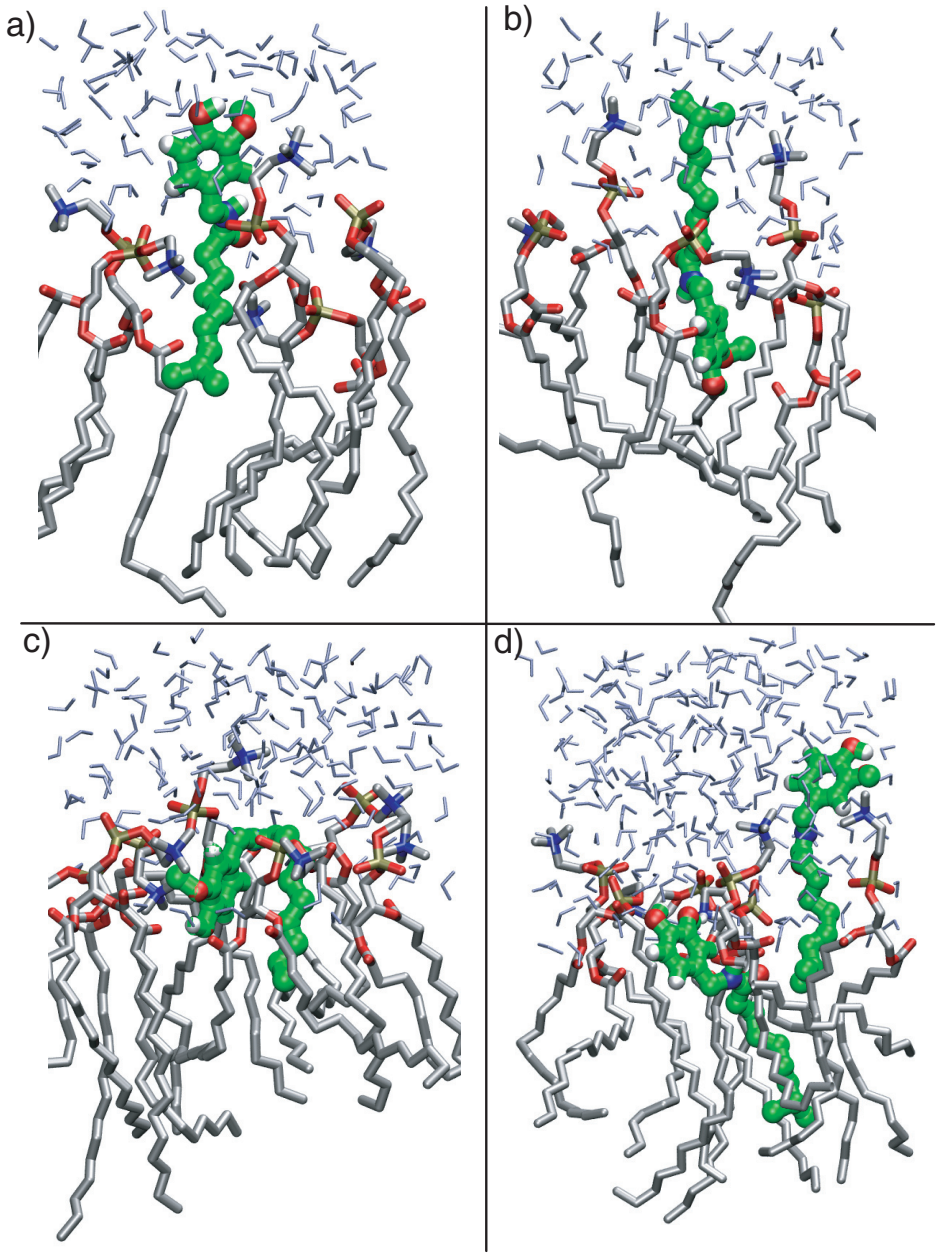

Figure 5.8: Representative snapshots for different configurations of capsaicin penetrating the bilayer: a) nine carbon alkyl chain first, b) vanillyl aromatic group first, c) folded, and d) interacting with a capsaicin molecule already in the bilayer.

systems suggest that crossing the interface is the rate limiting step to penetrate the bilayer. The activation energy of translocating an amphiphilic solute across the bilayer has been attributed to the steric barrier of colliding lipid headgroups in the interface [48, 92]. The interfacial density of LipidM-A is larger than LipidP-A at 323 K and 1 bar, suggesting that the lipid headgroups are closer together (also reflected in the area per headgroup - see Figure 5.3). As a result, the steric barrier created by the dynamic movements of the headgroups is increased [48, 92]. The differences in the structure of the bilayer are also reflected in the radial distribution functions (RDF) for the phosphorus atoms. Figure 5.9 shows the RDFs for phosphorus atoms in LipidP-A and LipidM-A at 323 K and 1 bar. The first maximum in the RDFs occur at 0.590 and 0.565 nm for LipidP-A and LipidM-A, respectively. The first peak height of LipidM-A is also larger, which agrees with the larger interfacial density. Increasing the temperature has the opposite effect on bilayers containing DPPE, that is, the interfacial density of LipidM decreases and the permeability increases [41].

To penetrate the bilayer, capsaicin must momentarily displace water molecules from the interface and disrupt the local structure of the lipid headgroups. The amount of water displaced from the interface can be approximated by comparing the molecular volumes of capsaicin and water. Assuming that a simple mass balance holds for the interface, the volume entered equals to the volume displaced, if the density remains constant. The molecular volume of capsaicin and water are 0.433 nm^3 and 0.022 nm^3, respectively, indicating that capsaicin must displace approximately 20 water molecules.

The momentary disruption of lipid structure at the interface was quantified by calculating the distance between lipid phosphorus atoms in the vicinity of the site at which capsaicin penetrated the interface of the bilayer. This process is illustrated based on visual inspection of two trajectories from the simulations, one with an aggregate of capsaicin and another for a single capsaicin. For these two cases, there were nine and eight lipids, respectively, around the penetration site. By isolating these lipids and calculating the distances between all pairs of phosphorus atoms (36 pairs for aggregates and 27 for a single capsaicin),

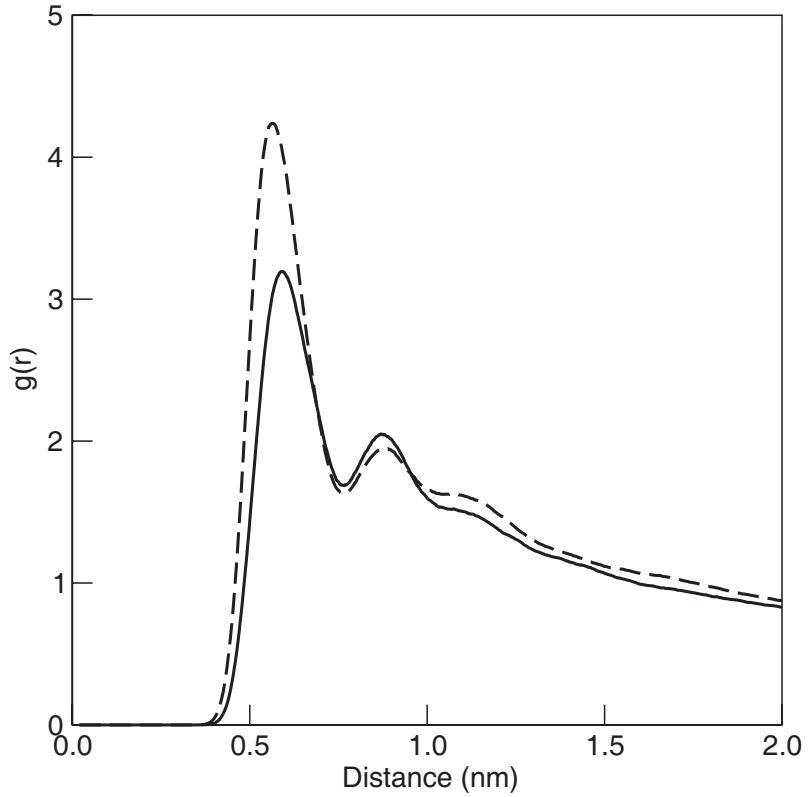

Figure 5.9: Radial distribution functions for phosphorus atoms in LipidP-A (solid line) and LipidM-A (dash line) at 323 K and 1 bar.

insightful results were obtained. Figure 5.10 summarizes the instantaneous local lipid behavior at the site of the three aggregated capsaicin molecules penetrating the bilayer from LipidP-B (Figure 5.6a. The positions of the local phosphorus atoms at a) 18.6 ns, b) 19.7 ns, and c) 22 ns are shown with the corresponding snapshots of the aggregate and its position relative to the lipids. Figure 5.10 also shows the instantaneous distance between select phosphorus atoms from 18.4 to 22 ns. The colored lines in Figures 5.10a,b,c correspond to the atom pairs depicted in Figure 5.10d. The initial displacement of the lipid headgroups occurred at approximately 19.4 ns when the aggregate first entered the interface. Most lipids were displaced, some closer, some farther from one another, to accommodate the additional molecular volume of capsaicin in the interface, as shown in Figure 5.10d. The initial displacement of the lipids is relatively fast compared to the slow relaxation once the aggregate enters the bilayer: the displacement occurs over a period of about 0.5 ns, and the relaxation to the initial configuration about 1.5 ns. The approximate location of the aggregate is shown by the shaded gray area in Figures 5.10b,c. The largest displacement was observed for pairs that spanned the penetration site (green and magenta lines in Figure 5.10d). These pairs were displaced by about 2 nm, whereas pairs around the perimeter of the penetration site were displaced by 0.5 nm. Perimeter pairs are located at an average distance of 0.6 nm, which is similar to the first maximum of the phosphorus atom RDFs of 0.590 and 0.565 nm for LipidP-A and LipidM-A, respectively.

The lipid headgroups were also affected when single capsaicin molecules penetrated the bilayer, but the displacement was less pronounced. Figure 5.11 shows the instantaneous local lipid behavior for the penetration of a single capsaicin in the bilayer in LipidM-B at 350 K. The notation in this figure is consistent with Figure 5.10. Capsaicin penetrated the bilayer with the vanillyl group first at about 5.4 ns (Figure 5.11d). Lipid pairs represented by the red and magenta lines were separated by the additional molecular volume of capsaicin in the bilayer, whereas other pairs around the perimeter of the penetration site were only momentarily displaced (Figure 5.11d). Similar trends were observed for other capsaicin molecules crossing the bilayer, with the most affected pairs of phosphorus

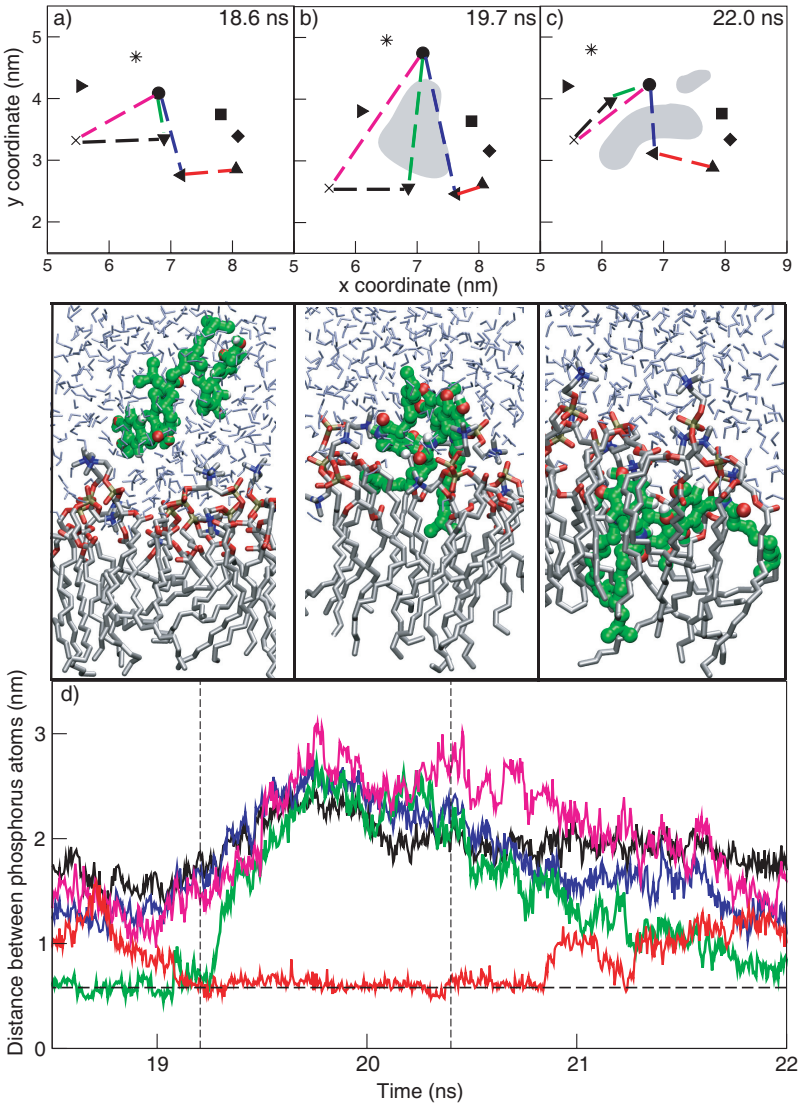

Figure 5.10: Position of nine phosphorus atoms local to the site of capsaicin penetrating the bilayer for LipidP-B at a) 18.6 ns, b) 19.7 ns, and c) 22 ns. Each phosphorus atom is depicted by a different symbol (circle, square, diamond, triangle up, triangle right, triangle down, triangle left, star, and ×) and the colored lines correspond to the distances between phosphorus atoms that are depicted in d). The shaded regions are the approximate location of the aggregate. Snapshots showing the relative position of capsaicin (green) as it approaches the bilayer (gray) are shown for the same times below a), b), and c). d) shows the instantaneous distance between pairs of phosphorus atoms from 18.6 to 22 ns. The vertical dashed lines show the times when the center of mass enters and leaves the interface, and the horizontal dashed line show the location of the first maximum in the radial distribution function between lipid phosphorus atoms (0.590 nm).

atoms near the penetration site. The changes caused by capsaicin penetrating the bilayer with the alkyl tail first and in the folded configuration were similar to the dynamics shown in Figure 5.11, and for molecules that entered the bilayer by interacting with capsaicin in the bilayer, displacement of the lipid headgroups was not as significant.

Experimental studies on the thermodynamics of amphiphilic solute diffusion into POPC bilayers suggest that solute diffusion into the bilayer is not driven by the traditional hydrophobic effect [93], which is entropic in nature, but it is rather the result of favorable enthalpic interactions, that is, van der Waals interactions between the hydrophobic portion of the solute and the bilayer core [94]. This "bilayer effect" is driven by the optimal packing of amphiphilic solutes in the bilayer [63, 94]. After penetrating the bilayer, capsaicin preferentially aligns beneath the interface in a region where the hydrophilic vanillyl and amide groups can interact with both water and polar lipid groups, and the hydrophobic, carbon chain aligns with the lipid acyl tails. Previous simulations of pentachlorophenol (PCP) in POPC and POPE bilayers indicate that this amphiphilic molecule assumes a similar orientation in the bilayer where both hydrophilic and hydrophobic groups can be accommodated by favorable enthalpic, van der Waals interactions [63]. Other simulations of β-blockers in a DPPC bilayer show that that this region is the most favorable location for these amphiphilic molecules as well [47].

A common structure in simulations of solute partitioning into bilayers is the formation of water columns that hydrate solutes in the core of the bilayer [47, 48]. These "water fingers" were not observed in the simulations here as capsaicin molecules that penetrated the bilayer were not solvated within the bilayer core. The capsaicin vanillyl group lost hydrating waters for times up to 1.5 ns after penetrating the bilayer. The associated desolvation energy is expected to be less for this group than the amide group because of the intermolecular hydrogen bond formed between the hydroxyl and neighboring anisole group [23]. Desolvation of the amide group was only observed for time periods of 0.5 ns during the reorientation of capsaicin within the bilayer after crossing the interface. The energy associated with desolvation of the polar groups is countered by the hydrophobic interactions

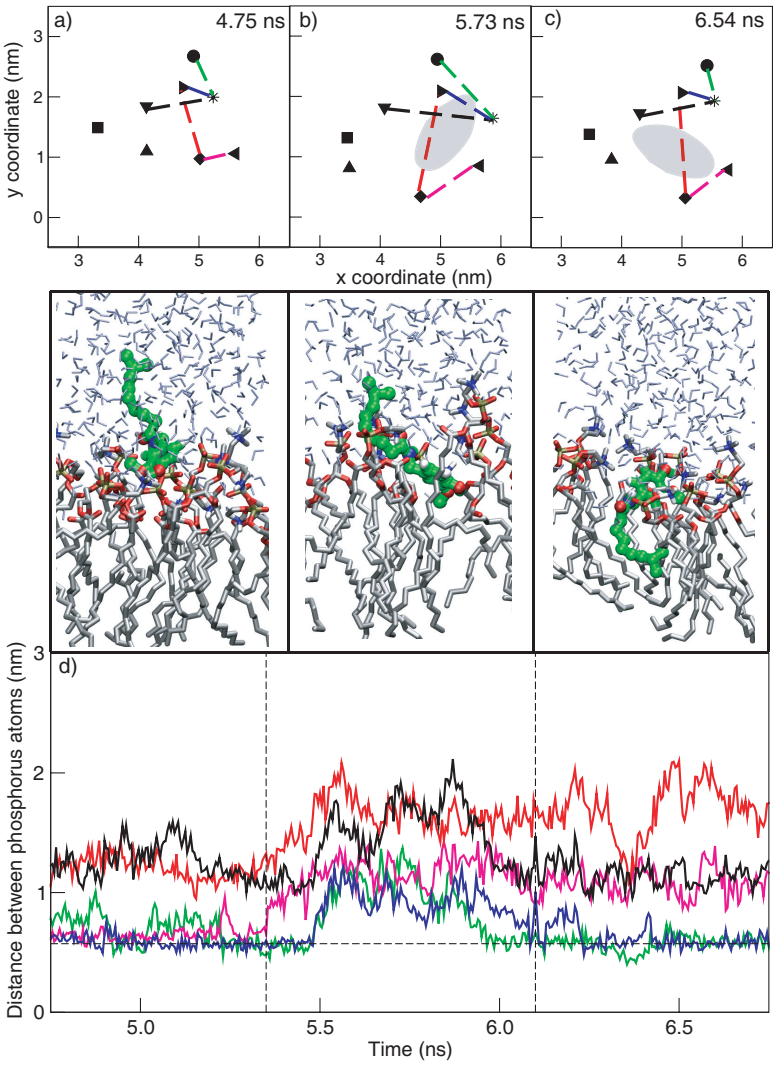

Figure 5.11: Position of eight phosphorus atoms local to the site of capsaicin penetrating the bilayer for LipidM-B at a) 4.75 ns, b) 5.73 ns, and c) 6.54 ns. Each phosphorus atom is depicted by a different symbol (circle, square, diamond, triangle up, triangle right, triangle down, triangle left, and star) and the colored lines correspond to the distances between phosphorus atoms that are depicted in d). The shaded region shows the approximate location of capsaicin. Snapshots showing the relative position of capsaicin (green) as it approaches the bilayer (gray) are shown for the same times below a), b), and c). d) shows the instantaneous distance between pairs of phosphorus atoms from 4.75 to 6.75 ns. The vertical dashed lines show the times when the center of mass enters and leaves the interface, and the horizontal dashed line show the location of the first maximum in the radial distribution function between lipid phosphorus atoms (0.565 nm).

between the alkyl chain of capsaicin and the lipid acyl tails [93].

Capsaicin molecules remaining in the aqueous phase formed loose aggregates of two to four molecules. These aggregates preferentially diffused toward the interface, but they did not interact with the lipid headgroups. Figure 5.12 shows the density profile of LipidM-C at 323 K averaged over 40 ns of simulation time. The partial density of capsaicin is magnified by 50 times to show the preferential distribution near the bilayer interface. The binding of capsaicin with the lipids was determined by the formation of hydrogen bonds. For molecules remaining in the aqueous phase, hydrogen bonds were not formed with the lipids. Hydrogen bonds were only formed with the lipids after capsaicin crossed the interface. It appears that capsaicin is attempting to dissolve into the bilayer, but the steric barrier created by the dynamic motions of the lipid headgroups in the interface is too large. This effect is most pronounced in LipidM-B,C at 323 K. Previously, this system was shown to have a smaller area per headgroup (Figure 5.3) and a higher interfacial density (Figure 5.4). As a result, fewer capsaicin molecules were dissolved into the bilayer. Our results are consistent with previous simulations by Ulander *et al.*, who determined that the rate limiting step for valproic acid to dissolve into the bilayer is the diffusion through the interface [48].

The probability of a capsaicin molecule to penetrate the bilayer is also affected by the local headgroup density of the interface of the bilayer. Visual inspection of the simulation trajectories indicates that if there is a high headgroup density, then the favorable, non-bonded interactions between the alkyl chain of capsaicin and the lipid tails will be shielded by the steric barrier of the interface. If the headgroup density is relatively low, then capsaicin can penetrate further into the interface, having a higher probability for favorable lipophilic interactions.

From these simulations, it is evident that capsaicin will enter both lipid bilayer systems considered; however, the slow dynamics of penetration into the bilayer does not permit a detailed study of the concentration dependent effects of capsaicin on the structure and dynamics of these systems. To compensate for this, capsaicin was introduced directly

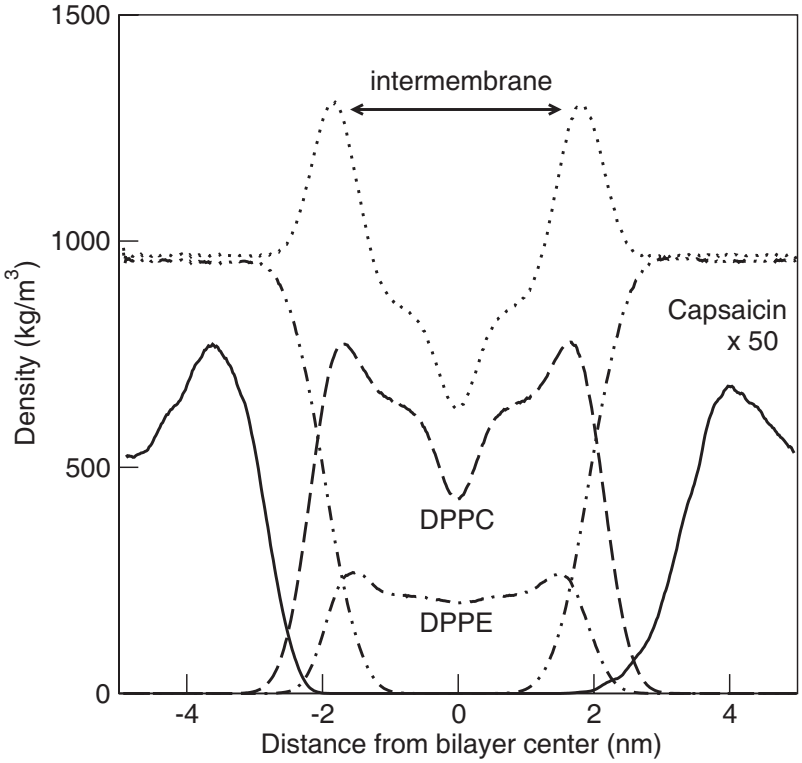

Figure 5.12: Density profile for LipidM-C at 323 K averaged over 40 ns (dotted line). Partial contributions to the density profile are shown for DPPC (dash line), DPPE (dot dash line), water (dot dot dash line), and capsaicin (solid line).

into the bilayer at various compositions (Table 5.1), as described in Simulation Details. Based on our previously mentioned results and experimental evidence describing the probable alignment of capsaicin within the bilayer [17, 23], we have confidence to proceed using the previously described initial configuration where fully extended capsaicin molecules were incorporated into the bilayer. The orientation of capsaicin in the final configuration for LipidM-B at 350 K, where seven capsaicin molecules penetrated the bilayer, and the initial configuration for LipidP-H are compared in Figures 5.1 and 5.2, respectively.

5.3.3 Capsaicin Inserted Into the Lipid Bilayer

The area per molecule was used to determine the convergence of simulations D-H. The area per molecule is calculated from the cross-sectional area of the bilayer divided by the number of molecules per leaflet. This property converged to an equilibrium value for all systems after about 10 ns, as shown in Figures 5.13 and 5.14. The final 20 ns were used to analyze the structure and dynamics of all systems, except for LipidM-F, in which the last 30 ns were used due to large fluctuations in the area per molecule in the last 10 ns (Figure 5.14c). The initial sharp decrease in the area per molecule occurred because of the initial relaxation of the system after insertion of capsaicin in the bilayers. The largest difference between anisotropic and semi-isotropic pressure coupling is observed during this initial lipid relaxation. For LipidP simulations with anisotropic pressure coupling, the area per molecule converges slightly faster than LipidM simulations with semi-isotropic pressure coupling. Both pressure coupling methods allow lateral scaling of the simulation box vectors with similar fluctuations in the area per molecule (0.01 nm^2). Semi-isotropic pressure coupling is beneficial because a square simulation box is maintained. Anisotropic pressure coupling allows the Cartesian x and y box vectors to vary independently, which in some cases led to divergence for select LipidM systems. This artifact is attributed to numerical inaccuracy, causing the simulation to diverge, and it is not a deficiency of the force field. Similar behavior was observed for LipidP systems, but to a lesser degree. For LipidP systems the Cartesian x and y

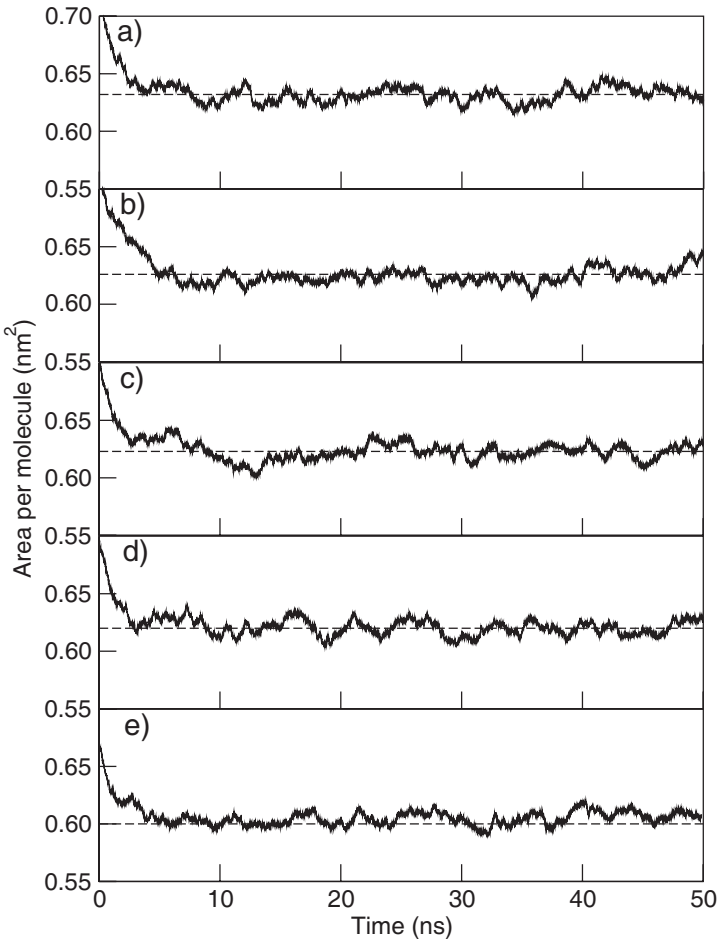

Figure 5.13: Area per molecule for LipidP systems over the course of the simulations for a) LipidP-D, b) LipidP-E, c) LipidP-F, d) LipidP-G, and e) LipidP-H. Dash lines show the average area per molecule.

box vectors did not drift more than 2.5 nm apart, causing the system to have a rectangular shape instead of square.

The equilibrium values for the area per molecule of each system are listed in Table 5.2. Each leaflet of systems D-H is a heterogeneous mixture of lipids and capsaicin. Special considerations need to be addressed when comparing the area per lipid of heterogeneous and homogeneous systems. Recently, Edholm and Nagle derived a method to partition the total area per molecule into two components by implementing a canonical definition of the molecular area [77]. In this method, the area per lipid $a_{\mathrm{lipid}}(x)$ is defined as a function of the

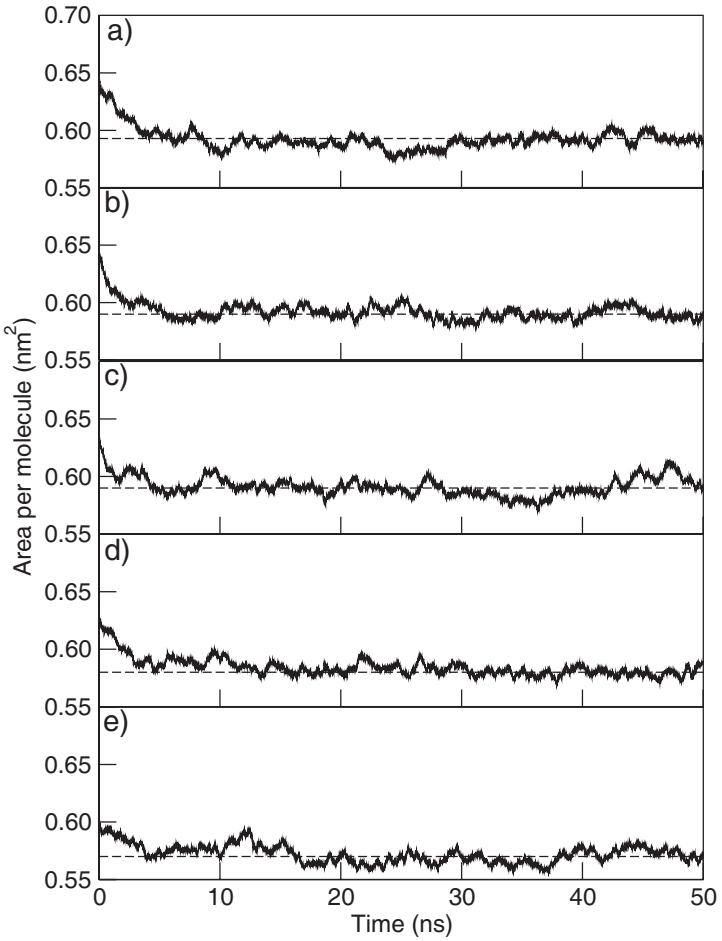

Figure 5.14: Area per molecule for LipidM systems over the course of the simulation for a) LipidM-D, b) LipidM-E, c) LipidM-F, d) LipidM-G, and e) LipidM-H. Dash lines show the average area per molecule.

mole fraction of capsaicin,

$$x_{\text{caps}} = \frac{N_{\text{caps}}}{(N_{\text{lipid}} + N_{\text{caps}})} \tag{5.1}$$

where N_{caps} and N_{lipid} are the moles of each component. Since the area per molecule is an additive property, the total molecular area $A_{\text{total}}(x_{\text{caps}})$ can be divided into contributing parts, namely $a_{\text{lipid}}(x)$ and $a_{\text{caps}}(x_{\text{caps}})$ using the linear relation

$$\frac{A_{\text{total}}(x_{\text{caps}})}{N_{\text{lipid}} + N_{\text{caps}}} = (1 - x_{\text{caps}})a_{\text{lipid}} + x_{\text{caps}}a_{\text{caps}} \tag{5.2}$$

The partial specific area $a_i(x)$ of a bilayer containing $i = 1,..,\ m$ different molecules is defined by the partial derivative of $A_{\text{total}}(x)$ with respect to each component mole fraction of a given leaflet, or

$$a_i(X) = \left(\frac{\delta A(N_1, ..., N_m)}{\delta N_i}\right)_{N_{i\neq j}} \tag{5.3}$$

where X is the sum of all partial mole fractions. Since A_{total} is a homogeneous function of each component, then its value is the sum of each partial contribution. Based on Equation 5.3, multiple mole fractions are needed to define the partial molecular area of each component. By rewriting Equation 5.2 as

$$\frac{A_{\text{total}}(x_{\text{caps}})}{N_{\text{lipid}}} = a_{\text{lipid}}(x_{\text{caps}}) + \frac{x_{\text{caps}}}{(1 - x_{\text{caps}})}a_{\text{caps}}(x_{\text{caps}}) \tag{5.4}$$

and plotting $A_{\text{total}}(x_{\text{caps}})/N_{\text{lipid}}$ versus $x_{\text{caps}}/(1-x_{\text{caps}})$, a_{lipid} and a_{caps} can be determined from the y-intercept and slope, respectively. This plot is shown in Figure 5.15 for both bilayer systems. The linear dependence in $x_{\text{caps}}/(1 - x_{\text{caps}})$ indicates that the area per lipid is not affected by mole fractions of capsaicin up to 0.156. The y-intercepts for LipidP and LipidM systems are 0.645 nm^2 and 0.604 nm^2, respectively, which are the same as the previously calculated area per lipid values of 0.646 ± 0.007 nm^2 and 0.602 ± 0.005 nm^2 for LipidP-A and LipidM-A, respectively. The area per capsaicin was calculated as 0.35 nm^2 and 0.36 nm^3 for LipidP and LipidM, respectively, indicating that capsaicin has similar molecular areas in both systems.

Table 5.2: Equilibrium values for the area per molecule. Equilibrium values are averaged over the last 20 ns of all simulations, except for LipidM-C, which the last 30 ns were used. All values are reported at 323 K and 1 bar.

	Area per molecule (nm^2)		Area per molecule (nm^2)
LipidP-A	0.646 ± 0.007	LipidM-A	0.602 ± 0.005
LipidP-D	0.632 ± 0.007	LipidM-D	0.593 ± 0.004
LipidP-E	0.626 ± 0.008	LipidM-E	0.590 ± 0.005
LipidP-F	0.623 ± 0.006	LipidM-F	0.590 ± 0.009
LipidP-G	0.620 ± 0.006	LipidM-G	0.580 ± 0.004
LipidP-H	0.600 ± 0.007	LipidM-H	0.570 ± 0.007

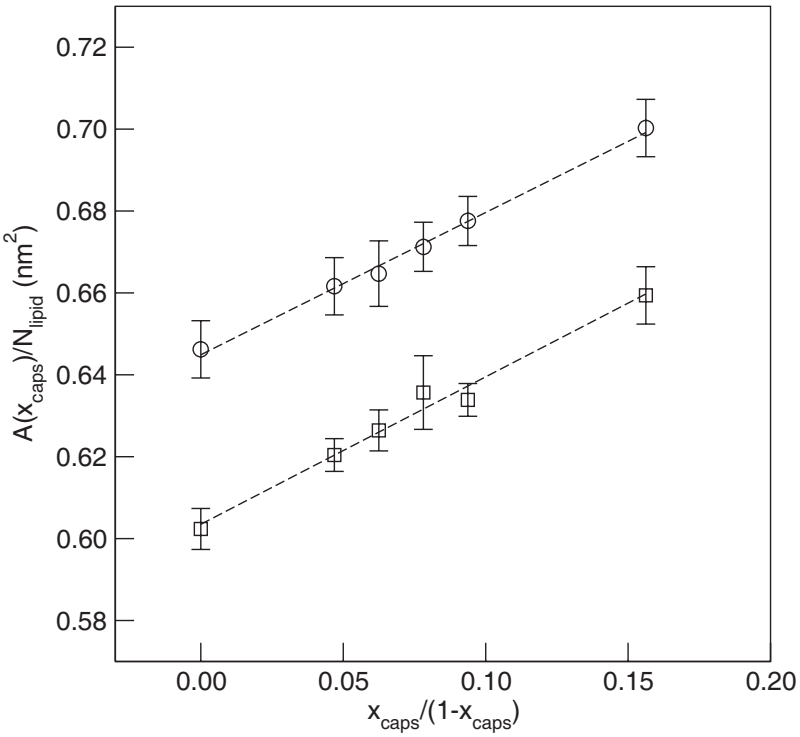

Figure 5.15: Total molecular area $A_{\text{total}}(x)$ divided by the number of lipids plotted as a function of $x_{\text{caps}}/(1 - x_{\text{caps}})$, where x_{caps} is the water-free mole fraction of capsaicin. LipidP D-H are represented by circles and LipidM D-H are represented by squares. Linear fits to the data are shown as dash lines.

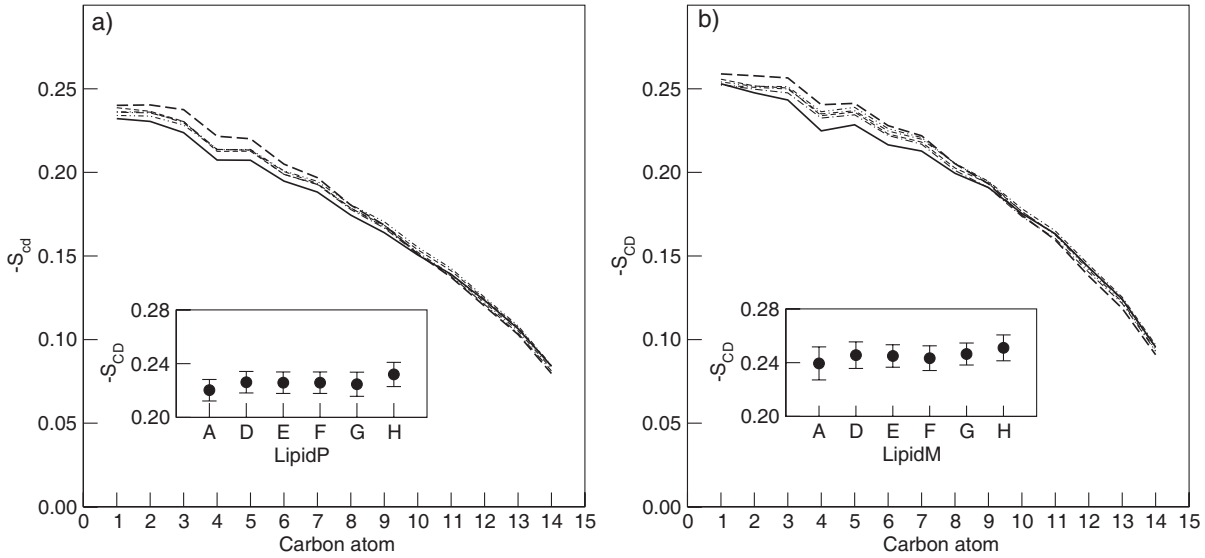

Figure 5.16: Deuterium order parameters (-S_{CD}) at 323 K and 1 bar for a) LipidP and b) LipidM. The line annotations for each system are as follows: A (bold solid), D (short dash), E (dot-short-dash), F (dot-long-dash), G (dot-dot-dash), and H (long-dash). The insets show the average -S_{CD} value for the first five carbon atoms of each system.

Figures 5.16a,b show the order parameter of the lipid tails averaged over both acyl tails for systems D-H in LipidP and LipidM, respectively. The insets in Figure 5.16 show the average value of -S_{CD} for the first five carbon atoms. Significant changes in -S_{CD} were not observed for systems D-G, and a small increase occurs for system H in both LipidP and LipidM. The similarity of the order parameters agrees with the area per lipid remaining relatively constant.

The P-P distances for each system also reflect that capsaicin is not changing the internal structure of the bilayer for the compositions studied. Table 5.3 lists the average P-P distances calculated for each lipid component. For LipidP systems there are negligible changes in the PC-PC distance. For LipidM systems, a slight decrease of 0.1 nm is observed in the PC-PC distance, and the PE-PE distance remains constant within statistical uncertainty. The difference between the P-P distance of DPPC and DPPE in LipidM is attributed to the structure of the lipid headgroups [41]. The choline group of DPPC cannot form intramolecular hydrogen bonds by acting as a donor, and it extends into the aqueous

Table 5.3: Equilibrium values for the P-P distance. Equilibrium values are averaged over the last 20 ns of all simulations, except for LipidM-C, which the last 30 ns were used. All values are reported at 323 K and 1 bar. PC-PC and PE-PE denote the average distance between DPPC and DPPE phosphorus atoms in opposing leaflets, respectively.

	PC-PC (nm)		PC-PC (nm)	PE-PE (nm)
LipidP-A	3.72 ± 0.03	LipidM-A	3.96 ± 0.03	3.66 ± 0.07
LipidP-D	3.72 ± 0.04	LipidM-D	3.93 ± 0.03	3.63 ± 0.05
LipidP-E	3.72 ± 0.04	LipidM-E	3.91 ± 0.03	3.66 ± 0.06
LipidP-F	3.72 ± 0.03	LipidM-F	3.88 ± 0.05	3.62 ± 0.07
LipidP-G	3.70 ± 0.03	LipidM-G	3.90 ± 0.03	3.60 ± 0.06
LipidP-H	3.68 ± 0.03	LipidM-H	3.86 ± 0.05	3.60 ± 0.08

phase, whereas the ethanolamine group of DPPE can, and bends toward the core of the bilayer. The main intramolecular binding site of the ethanolamine group is the O7 phosphate oxygen (see Figure 2.3), which causes the ethanolamine group to point toward the center of the bilayer [41]. This intramolecular structure and the thickness of the bilayer were not substantially changed by capsaicin. This agrees with the result of Lundbæk *et al.*, who did not observe a change in bilayer thickness in the presence of capsaicin [21].

The partial density profiles of capsaicin and the lipid headgroups, represented by phosphorus and nitrogen atoms, are shown in Figure 5.17. Figure 5.17a shows that the relative position of the headgroups and the distribution of capsaicin are not affected by increased capsaicin concentrations. The maximum peak of the capsaicin partial density profile occurs at about |1| nm from the center of the bilayer. The distance between this peak and the phosphorus atom peak is 0.8 nm indicating that capsaicin is closer to the interface than to the center of the bilayer. This region of the bilayer is characterized as having a high lipid tail density [88, 89] and has previously been described as a favorable position for amphiphilic molecules [48, 63]. In this region, capsaicin can bind to both lipids and water molecules in the interface, and its alkyl chain can interact favorably with the lipid acyl tails. A similar alignment was observed for capsaicin molecules that dissolved into the bilayer from the aqueous phase (see Figure 5.1). In Figure 5.17b, capsaicin has a similar distribution in

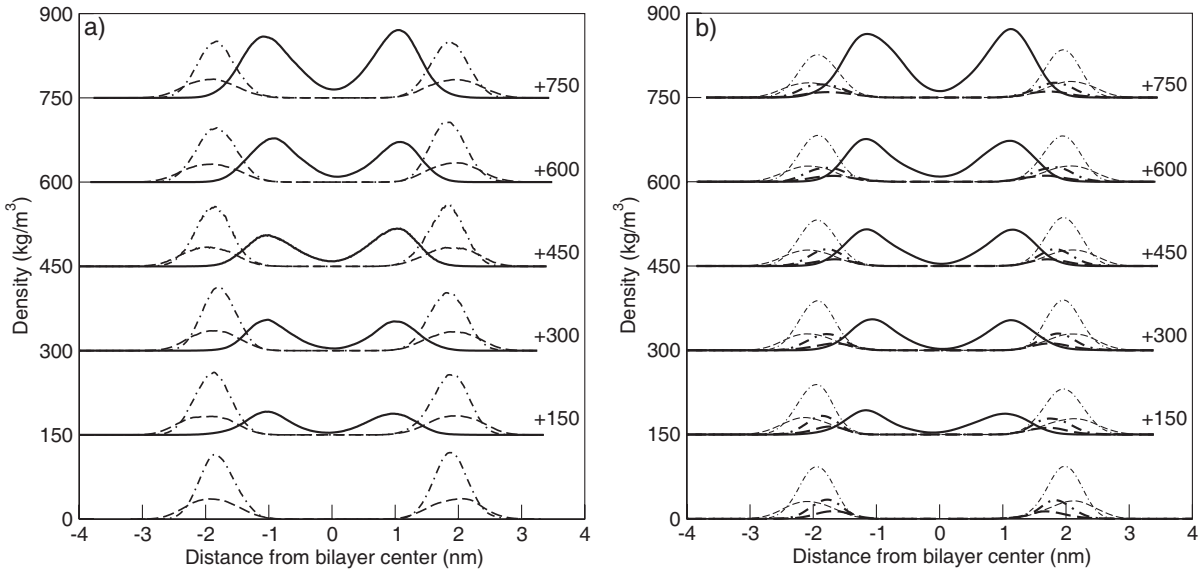

Figure 5.17: Partial density profiles at 323 K and 1 bar for a) LipidP and b) LipidM. The baseline represents system A, and D-H are displaced by 150 kg/m^3 [D (+150), E (+300), F (+450), G (+600), and H (+750)]. In a), DPPC phosphorus and nitrogen atoms are depicted by dot-dash and dash lines, respectively, and capsaicin is represented by bold line. In b), the same line annotations are used, and DPPC and DPPE atoms are distinguished by thin and bold lines, respectively.

LipidM systems that is not affected by increasing compositions. The relative location of the PC and PE headgroups is also shown, where the PE headgroups are closer to the center of the bilayer.

A detailed analysis of the hydrogen bonds formed between capsaicin and the lipid groups was performed. A hydrogen bond is defined by Brady and Schmidt if the maximum donor-acceptor distance of 0.35 nm and minimum angle (donor-hydrogen-acceptor) is 120 degrees [64]. The probability of forming a hydrogen bond is calculated from the number of time-frames when a hydrogen bond occurs (t_{bond}), divided by the total number of time-frames (t_{total}). This value is then normalized by the number of hydrogen donors (N_{donor}),

$$P = \frac{1}{N_{\mathrm{donor}}} \left(\frac{t_{\mathrm{bond}}}{t_{\mathrm{total}}} \right) \tag{5.5}$$

Two functional groups in capsaicin can donate hydrogens to the various oxygen atom acceptors in DPPC and DPPE, namely the vanillyl hydroxyl and the amide groups (see Figure 2.1). The hydroxyl group is expected to form fewer intermolecular hydrogen bonds as a result of the intramolecular hydrogen bond formed with the neighboring anisole group. Figure 5.18 is a bar graph of the various hydrogen bonding probabilities between capsaicin and the lipid oxygen atom acceptors, water, and intramolecular acceptors. The lipid acceptors are O7, O9, O10, and O11 in the phosphate group, ester oxygens O14 and O33, and carbonyl oxygens O16 and O35 in the lipid Sn-2 and Sn-1 acyl tails, respectively (see Figure 2.3). From this figure, it is evident that capsaicin binds with both water and lipids in the interface. As expected, the amide group forms more intermolecular hydrogen bonds than the hydroxyl group. The main binding sites between capsaicin and the lipids are atoms O9 and O10 in the phosphate group and atoms O14 and O16 in the lipid Sn-2 acyl tail. In our molecular representation of the lipids, atoms O7, O9, and O10 all have the same atomic charge (-0.80), whereas the charge for O11 is slightly less (-0.70). As discussed previously, the phosphate group atom O7 in DPPC points away from the center of the bilayer, and thus is unfavorable for forming hydrogen bonds. In DPPE this atom is the main site of intramolecular hydrogen bonds with the ethanolamine group [41]. Atoms O9, O10, and O11 have favorable positions for forming hydrogen bonds, and the preference for O9 and O10 is likely the result of the slightly higher atomic charge. There is also a preference for forming hydrogen bonds with the Sn-2 acyl tail over the Sn-1 acyl tail. The Sn-1 acyl tail has an additional carbon atom between the ester and phosphate groups that causes it to extend further into the bilayer core. As a result, the Sn-2 tail is closer to the interface and in a more favorable configuration to form hydrogen bonds.

The polar atoms in capsaicin also form hydrogen bonds by acting as acceptors. Near the interface, water and the ethanolamine group of DPPE can act as hydrogen donors. The probability of the capsaicin hydroxyl, anisole, amide nitrogen, and carbonyl groups to form hydrogen bonds with water were unaffected by the concentration of capsaicin and lipid composition. For LipidP, the probability of these groups to form a hydrogen bond with water

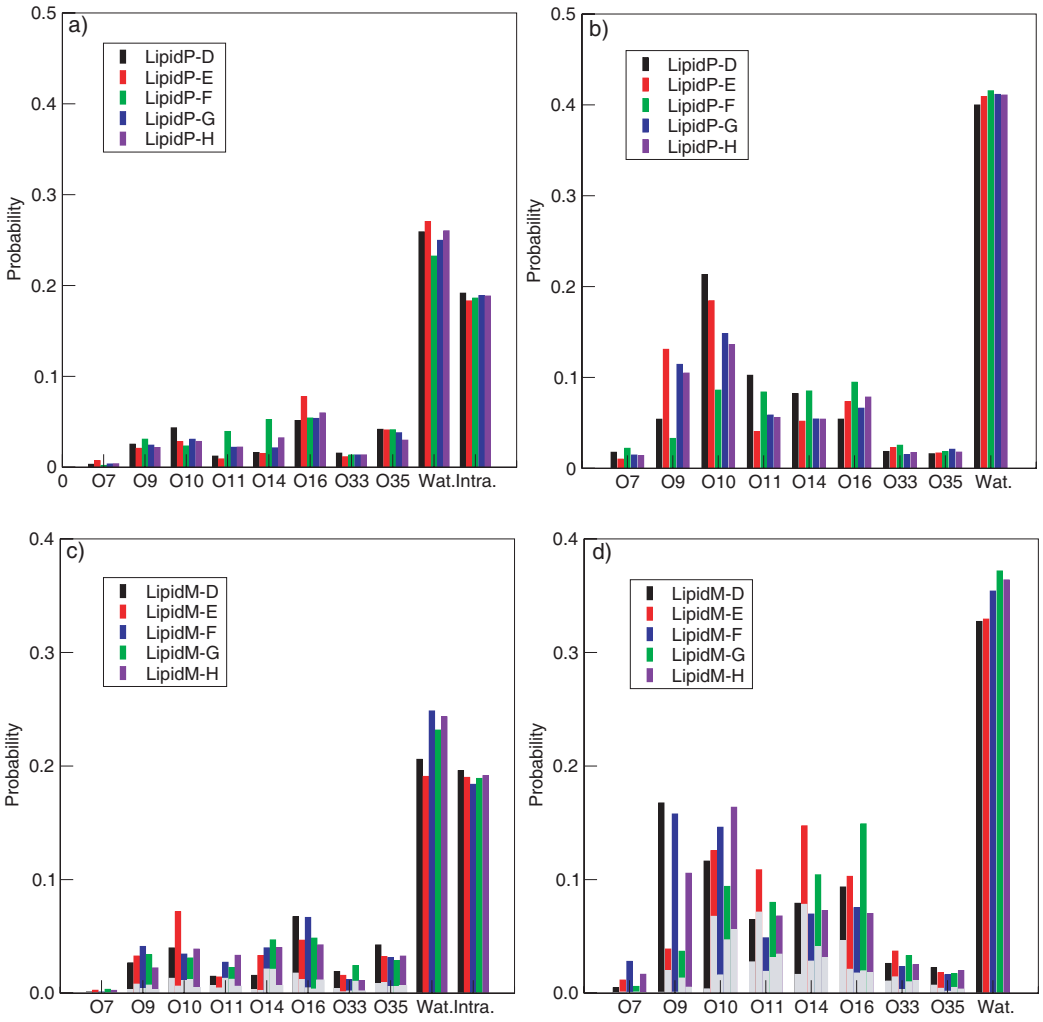

Figure 5.18: Hydrogen bonding probabilities between hydrogen donors in capsaicin and various lipid acceptors, water, and intramolecular acceptors. Probabilities for the vanillyl hydroxyl group acting as a donor are shown for a) LipidP and b) LipidM. Probabilities for the amide nitrogen acting as a donor are shown for c) LipidP and d) LipidM. Lipid oxygen atoms follow the numbering scheme mentioned in the text, where O7, O9, O10, and O11 are phosphate group oxygens; O14 and O33 are ester oxygen atoms, and O16 and O35 are carbonyl oxygen atoms in the Sn-2 and Sn-1 lipid acyl tails, respectively. Hydrogen bonds formed with water are denoted by Wat. and intramolecular hydrogen bonds formed between the hydroxyl and anisole group are denoted by Intra. The fraction of hydrogen bonds formed with DPPE in LipidM systems are shown as gray fractions of the total probability.

was calculated as 0.52 ± 0.02, 0.10 ± 0.01, 0.02 ± 0.01, and 0.62 ± 0.03, respectively, and for LipidM as 0.50 ± 0.03, 0.10 ± 0.01, 0.02 ± 0.01, and 0.57 ± 0.04, respectively. Hydrogen bonds were not identified between the ethanolamine group in DPPE and the capsaicin acceptors.

The hydrogen bonding probabilities for each bilayer system are summarized in Table 5.4, with the probabilities of each group averaged over simulations D-H. The values in this table are weighted by the number of capsaicin molecules (12-40) divided by the total number of capsaicin molecules simulated in systems D-H, causing system H to affect the average more than system D. Based on these averages, the hydroxyl group has equal probabilities of forming hydrogen bonds with water and lipids near the interface, whereas the amide group has a greater preference for binding to lipids. Changing the lipid composition does not effect the behavior of the hydroxyl group, which is shown by the similarity between LipidP and LipidM. The binding of the amide group is affected by lipid composition. The addition of DPPE to the bilayer increases the number of hydrogen bonds formed between the amide group and the lipid ester and carbonyl groups, and decreases the number of hydrogen bonds formed with water. This is attributed to the increased order of the lipid acyl tails in LipidM that restrict the motion of capsaicin in the bilayer (Figure 5.16).

Further evidence of different capsaicin configurations in LipidP and LipidM is shown by the the orientation of the vanillyl group and the alkyl chain of capsaicin (Figure 5.19). A characteristic vector for the orientation of the vanillyl group was defined as a vector pointing from the carbon atom between the vanillyl and amide groups to the oxygen atom of the hydroxyl group, and for the alkyl chain, from the carbonyl carbon to the 8-methyl tail (see Figure 5.19). The angle distribution is relative to the outward normal of each bilayer leaflet. The distributions are averaged over all LipidP and LipidM configurations. The most probable angles formed by the alkyl chain with the bilayer normal are 142 and 150 degrees for LipidP and LipidM, respectively. This distribution is characteristic of lipid acyl tails, and indicates preferential alignment and association of these groups. The increased order of LipidM causes a shift in the angle distribution toward 180 degrees. The probability distribution for the vanillyl group is much broader, but a maximum does occur at approximately 65 and 62

Table 5.4: Average hydrogen bonding probabilities among hydrogen donors in capsaicin and lipid oxygen atoms, water, and intramolecular acceptors. The phosphate group contains atoms O7, O9, O10, and O11; the ester group contains oxygen atoms O14 and O33, and the carbonyl group contains O16 and O35 for the Sn-2 and Sn-1 tails, respectively. Values for LipidP and LipidM are weighted averages for systems D-H.

	Donor			
Acceptor	Hydroxyl Oxygen		Amide Nitrogen	
Group	LipidP	LipidM	LipidP	LipidM
Phosphate	0.080 ± 0.011	0.099 ± 0.015	0.317 ± 0.063	0.319 ± 0.067
Ester	0.043 ± 0.016	0.053 ± 0.013	0.081 ± 0.019	0.119 ± 0.038
Carbonyl	0.096 ± 0.012	0.084 ± 0.015	0.094 ± 0.016	0.114 ± 0.031
Water	0.218 ± 0.014	0.230 ± 0.025	0.410 ± 0.006	0.355 ± 0.020
Intramolecular	0.188 ± 0.003	0.190 ± 0.004	—	—
Total	0.660 ± 0.011	0.656 ± 0.024	0.911 ± 0.038	0.907 ± 0.012
% Lipid	33.0 ± 0.028	36.0 ± 0.020	54.5 ± 0.025	60.8 ± 0.025
% Water	38.5 ± 0.024	35.0 ± 0.027	45.5 ± 0.025	39.2 ± 0.025

degrees for LipidP and LipidM, respectively. The broader distribution is characteristic of this moiety having isotropic motion within the bilayer [23]. This is expected because of the intramolecular bond that can form between the hydroxyl group and neighboring anisole group. The absence or presence of this intramolecular bond determines the hydrophilic or lipophilic nature of this moiety [23]. The previously mentioned hydrogen bond analysis indicates that the probability of forming this intramolecular hydrogen bond is 0.19.

The RDFs of the hydroxyl and amide groups in capsaicin were also calculated to determine the average position of capsaicin in the bilayer relative to the lipid phosphate, carbonyl, and nitrogen containing groups (choline for DPPC and ethanolamine for DPPE). Figure 5.20 shows the RDFs between the capsaicin hydroxyl group, and the lipid phosphate and nitrogen groups for LipidP-H and LipidM-H. In Figure 5.20a, the first maximum in the RDFs occurs at 0.40 and 0.43 nm for the phosphate and choline groups, respectively. For LipidM-H, the shape and location of the first peak for PC atoms was the same as LipidP-H. For the PE phosphorus group, the first maximum occurs at 0.41 nm, and for the ethanolamine group at 0.31 nm. Based on the previously mentioned P-P distance (Table 5.3) and partial

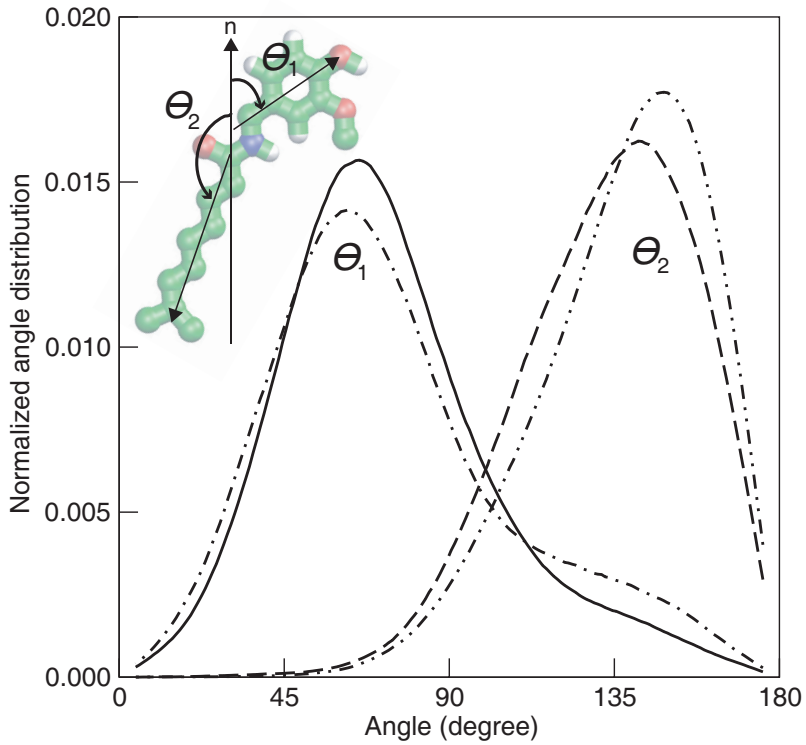

Figure 5.19: Characteristic vector angle distributions for the capsaicin vanillyl group (θ_1) from LipidP (solid) and LipidM (dot-dash) and the nine carbon alkyl chain (θ_2) for LipidP (dash) and LipidM (dot-dot-dash). Each distribution reflects the average over all systems D-H of LipidP or LipidM. The inserted figure depicts the characteristic vectors mentioned in the text. All angles are relative to the outward pointing bilayer normal.

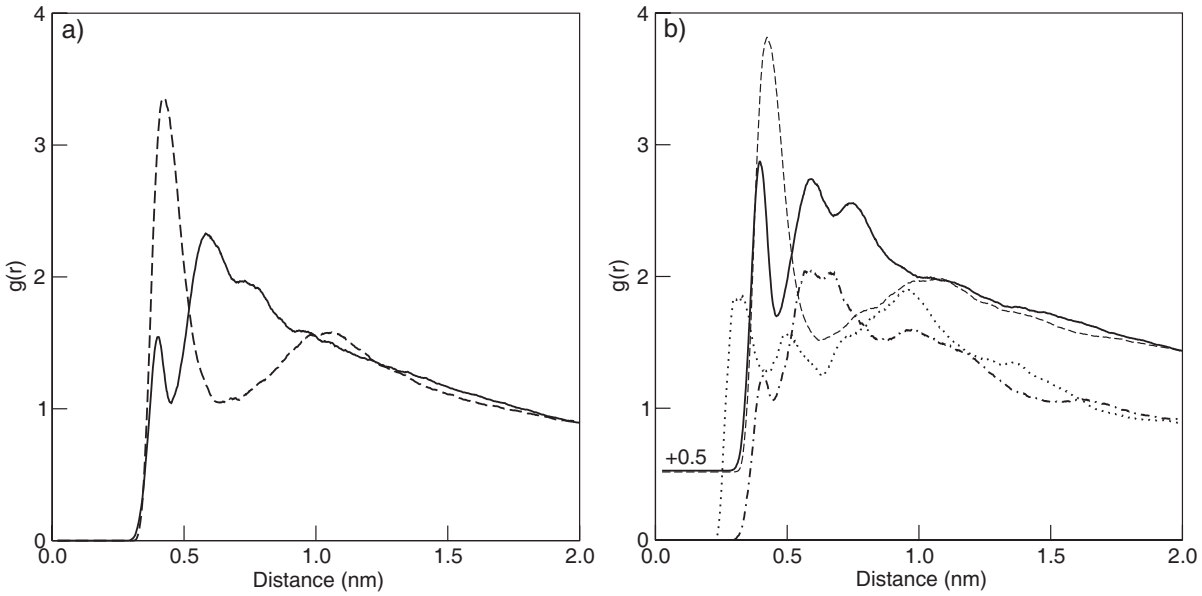

Figure 5.20: Radial distribution functions between the hydroxyl group of capsaicin and a) the lipid phosphate (solid line) and choline (dash line) groups from LipidP-H, and b) the PC phosphate (solid line +0.5), PE phosphate (dot-dash line), choline (dash line +0.5), and ethanolamine (dot line) groups of LipidM-H.

density profiles (Figure 5.17), the ethanolamine group extends further into the bilayer core than the choline group. Since the hydroxyl group is closer to the ethanolamine group, it must be positioned below the interface. From the P-P distance analysis (Table 5.3), the PE-PE distance is approximately 0.20 nm less than the PC-PC distance in LipidM (0.10 nm per leaflet), which is similar to the distances between the RDF maximum of choline and ethanolamine (0.12 nm) in LipidM-H.

RDFs between the amide nitrogen and the lipid phosphate, carbonyl, and nitrogen containing groups are shown in Figure 5.21. Figures 5.21a,b show the RDFs between the phosphate and nitrogen containing groups of LipidP-H and LipidM-H. The distances between the amide nitrogen and the phosphate groups are similar to those observed for the hydroxyl group. The first maximum for the PC phosphate group in LipidP-H occurs at 0.41 nm, and for the PC and PE groups in LipidM-H at 0.41 and 0.42 nm, respectively. This similarity is expected since both groups form hydrogen bonds with the various phosphate group oxygens,

as shown in Figure 5.18 and Table 5.4. For the choline group of LipidP-H the first maximum occurs at 0.54 nm (Figure 5.21a), and for the choline and ethanolamine groups of LipidM-H at 0.53 and 0.44 nm (Figure 5.21b), respectively. Based on these results, the hydroxyl group is closer to the interface, which is supported by the characteristic angle distribution of the vanillyl group (Figure 5.19). This result seems counterintuitive because the hydroxyl and amide groups are equidistant from the phosphate groups, but they have different positions relative to the choline and ethanolamine groups. This effect is attributed to the membrane fluidity. The partial density profiles shown in Figure 5.17 indicate that the location of the phosphorus atoms is represented by a Gaussian distribution with a standard deviation of approximately 0.5 nm. This broad distribution allows the hydroxyl group and the amide nitrogen to bind with the phosphate oxygens, even though the amide group is closer to the center of the bilayer.

The RDFs between the amide nitrogen and the lipid carbonyl groups (Figure 5.21c,d) indicate a preference for binding with the lipid Sn-2 acyl tail in both LipidP-H and LipidM-H. This behavior was also observed in the hydrogen bond analysis previously mentioned (Figure 5.18). The first maximum in the RDFs for the Sn-2 acyl tail occur at 0.32 nm for LipidP-H and at 0.33 nm for both PC and PE in LipidM-H. The location and structure of these peaks suggest the formation of hydrogen bonds, which was previously observed (Figure 5.18). For the Sn-1 acyl tails, this structure is absent.

The RDFs for systems D-F were similar to system H in LipidP, but the dynamic movement of the lipids and capsaicin caused deviations in the local lipid concentration near capsaicin for LipidM systems D-E. These effects were less pronounced in LipidM-H because of the increased concentration of capsaicin. Figure 5.22 shows the RDFs between the amide nitrogen and the phosphate oxygens O9 and O10 (Figure 2.3) for LipidM-E averaged over different time spans from 10 to 30 ns, and from 30 to 50 ns (the area per molecule remained within ± 1 nm of the average value during these time intervals - see Figure 5.14b). From 10 to 30 ns, the main site of interaction is between the O9 group of DPPC and for 30 to 50 ns, the main site is the O9 atom of DPPE. The overall structure of the RDFs is not altered

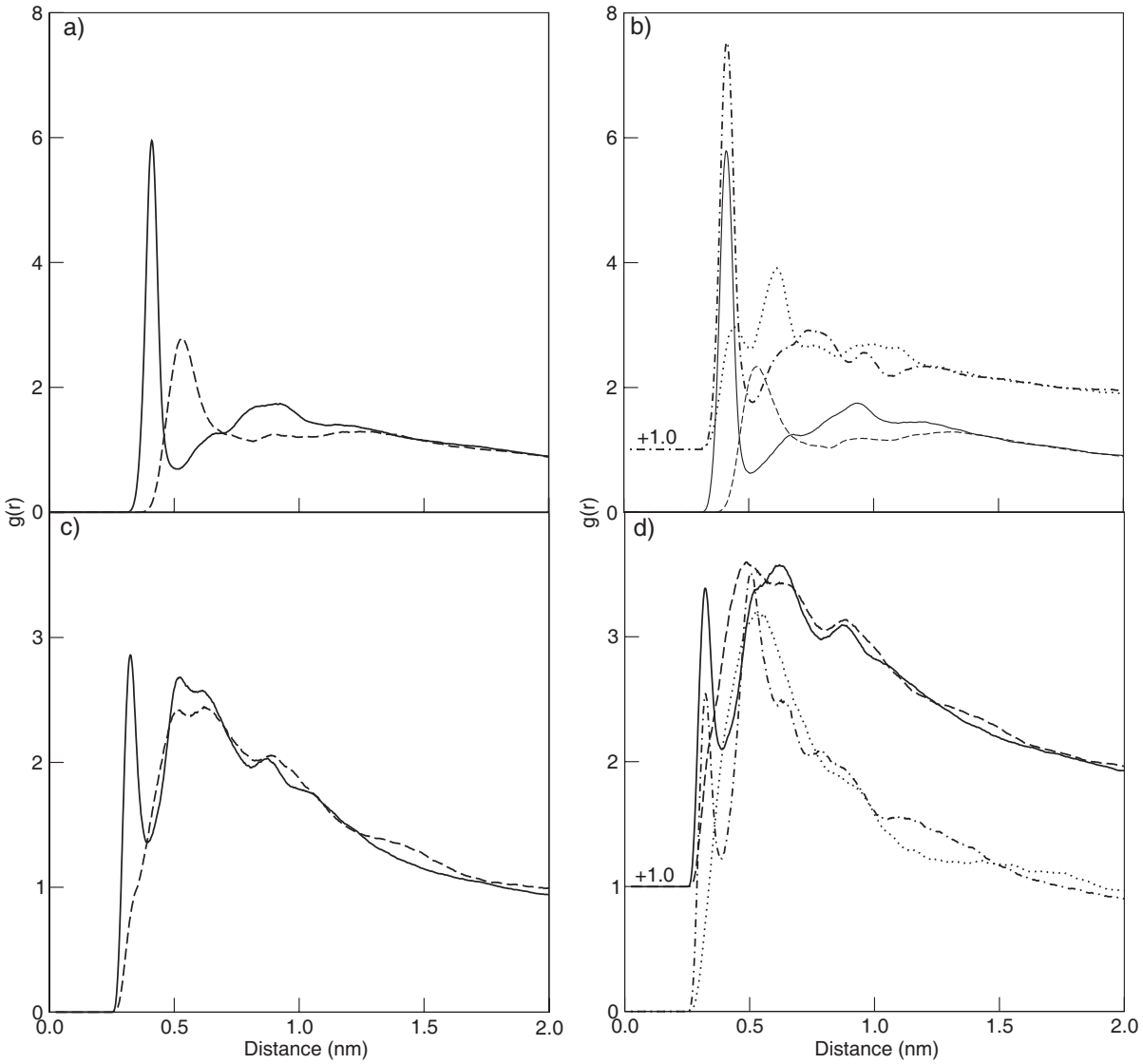

Figure 5.21: Radial distribution functions between the amide nitrogen of capsaicin and a) the lipid phosphate (solid line) and choline (dash line) groups in LipidP-H; b) the PC phosphate (solid line), PE phosphate (dot-dash line +1.0), choline (dash line), and ethanolamine (dot line +1.0) groups in LipidM-H; c) lipid carbonyl groups from the Sn-2 (solid line) and Sn-1 (dash line) acyl tails in LipidP-H; and d) the DPPC Sn-2 (solid line +1.0) and Sn-1 (dash line +1.0) acyl tails and DPPE Sn-2 (dot-dash line) and Sn-1 (dot line) acyl tails.

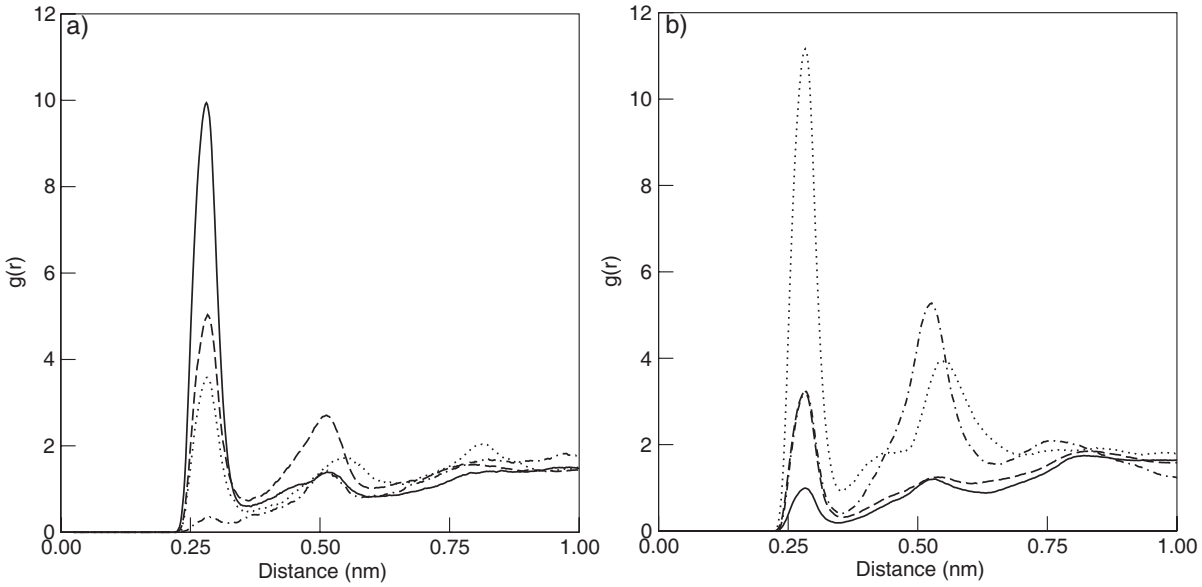

Figure 5.22: Radial distribution functions between the amide nitrogen of capsaicin and a) the PC phosphate oxygens O9 (solid line) and O10 (dash line), and the PE phosphate oxygens O9 (dot-dash line) and O10 (dot line) from LipidP-E. In b) the groups and line annotations are replicated. a) is averaged from 10 to 30 ns, and b) is averaged from 30 to 50 ns.

between the time sets, but the relative contributions change significantly. The RDFs also indicate that there is no preferential binding with DPPC or DPPE.

Studies by Lundbæk *et al.* indicate that capsaicin alters the "stiffness" of the bilayer without effecting the thickness [21]. One indication of bilayer stiffness that can be obtained from simulations is the order parameter. An increase in the order parameter of the lipid tails corresponds to an increase in the stiffness of the bilayer as lipids are packed closer together. Our results do not show a change in the order parameter of the lipid tails, suggesting that the bilayer stiffness is possibly affected by other means. One possible explanation is that capsaicin increases the ability of lipids to repack laterally by creating additional space between the lipid headgroups. Capsaicin resides beneath the lipid/water interface, without contributing to the interfacial density (Figure 5.17). The lateral area of capsaicin (0.35 ± 0.1 nm) creates additional space between the lipid headgroups in the interface which is shown

by the linear increase in the cross-sectional area of the simulation box (Figure 5.15). By increasing this distance, the steric collisions between the lipid headgroups are reduced, which may affect the bilayer fluidity. Tsuchiya suggested that at low concentrations the lipid tails can cooperatively bend and fill the free volume around capsaicin, and at high concentrations, interdigitation of the lipid acyl tails occurs to fill the free volume [18]. These occurrences are attributed to the biphasic behavior observed by Tsuchiya and Meddings *et al.* [16, 18]. For these simulations, interdigitation was not observed, which suggests that the concentrations of capsaicin considered allow cooperative bending of the lipid acyl tails without interdigitation to increase the fluidity of the bilayer.

Decreasing the headgroup density, or volume fraction, in the interface could also account for the increased ion permeability of membranes exposed to capsaicin, as determined by Feigin *et al.* [19]. The rate limiting step for a solute dissolving into the membrane is the diffusion through the interface [47, 48, 92]. The density of the interface is proportional to the activation energy required, and by decreasing this density, the permeability of the bilayer increases. Since ions are small, a slight decrease in the interfacial density is likely to result in an increase in permeability.

The effects of capsaicin on the dynamics of the lipids in the plane of the bilayer were also investigated. The diffusion coefficient was calculated from the mean-squared displacement (Equation 3.17) after the initial relaxation of the lipids (10 to 50 ns). This property is not affected by the presence of capsaicin when compared to pure lipid systems (A), within statistical uncertainty. The average lateral diffusion coefficient for DPPC in LipidP systems is $D_{\mathrm{PC-P}} = 0.272 \pm 0.092 \times 10^{-6}$ cm^2/s, and the values for DPPC and DPPE in LipidM systems are $D_{\mathrm{PC_M}} = 0.230 \pm 0.084 \times 10^{-6}$ cm^2/s and $D_{\mathrm{PE-M}} = 0.212 \pm 0.071 \times 10^{-6}$ cm^2/s. There was not an observable trend in the lateral diffusion coefficients of the lipids with increasing compositions of capsaicin. The average lateral diffusion coefficients of capsaicin are similar to the lipids, and represent the movement of capsaicin being constrained by the lipids. For LipidP and LipidM, the average lateral diffusion coefficients were calculated as $D_{\mathrm{C-P}} = 0.229 \pm 0.120 \times 10^{-6}$ cm^2/s and $D_{\mathrm{C-M}} = 0.345 \pm 0.091 \times 10^{-6}$ cm^2/s.

The lateral movements of capsaicin in the plane of the bilayer are shown in Figures 5.23 and 5.24 for LipidP and LipidM systems, respectively. The colored lines represent the lateral movements of the center of mass for each individual capsaicin molecule. The initial and final position of capsaicin molecules at 10 and 50 ns are shown by open boxes connected by dash lines. The lateral movements of capsaicin are localized for most molecules, which is shown by the high line density in Figures 5.23 and 5.24. The largest distance between the initial and final position of capsaicin was 5.7 nm for LipidP-F and 5.1 nm for LipidM-G. From this figure, it is evident that the lateral movements of capsaicin are random, and lateral phase separation does not occur for the time scales studied. Single capsaicin molecules were observed to diffuse through the bilayer in LipidP-G and LipidM-H, but for most systems, capsaicin remained evenly distributed between each leaflet.

5.4 Conclusions

We have presented a study on the partitioning of capsaicin between an aqueous phase and a lipid bilayer, and the properties of capsaicin in the bilayer. A pure DPPC bilayer and a bilayer containing a 3:1 molar ratio of DPPC to DPPE were used as model cell membranes. Two starting configurations were used to investigate these interactions: capsaicin in the aqueous phase and capsaicin in the bilayer. Capsaicin initially in the aqueous phase resulted in its penetration into the bilayer. The permeability of the bilayer to capsaicin was influenced by the lipid composition and the temperature. Bilayers containing DPPE decreased the permeability, while increasing the temperature had the opposite effect. Diffusion through the interface was the rate limiting step for capsaicin to penetrate the bilayer, and increasing the headgroup density of the interface directly affected the bilayer permeability. This transient behavior caused substantial deformation of the interface.

Capsaicin molecules inserted into the bilayer partitioned to a similar position in

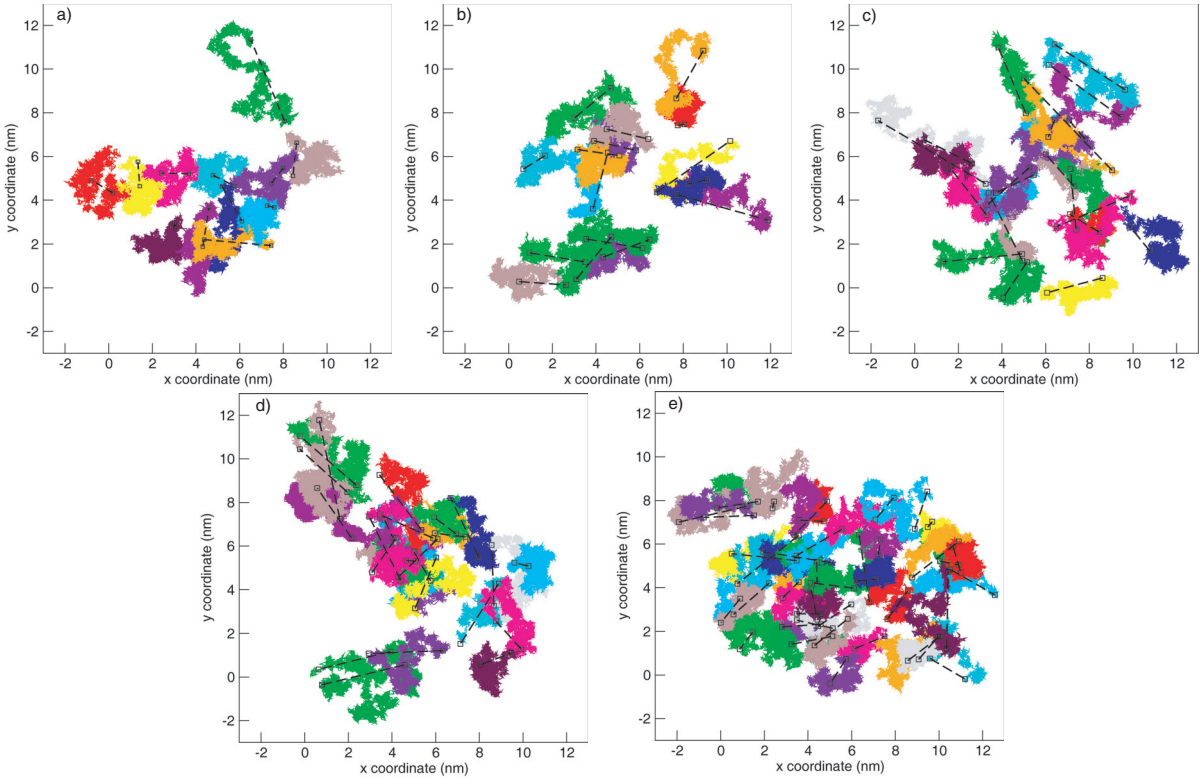

Figure 5.23: Lateral movements of capsaicin in the plane of the bilayer in a) LipidP-D, b) LipidP-E, c) LipidP-F, d) LipidP-G, and e) LipidP-H. The colored lines depict the lateral movements of individual capsaicin molecules and the open boxes, connected by dash lines, are the initial and final position of each molecule at 10 and 50 ns, respectively.

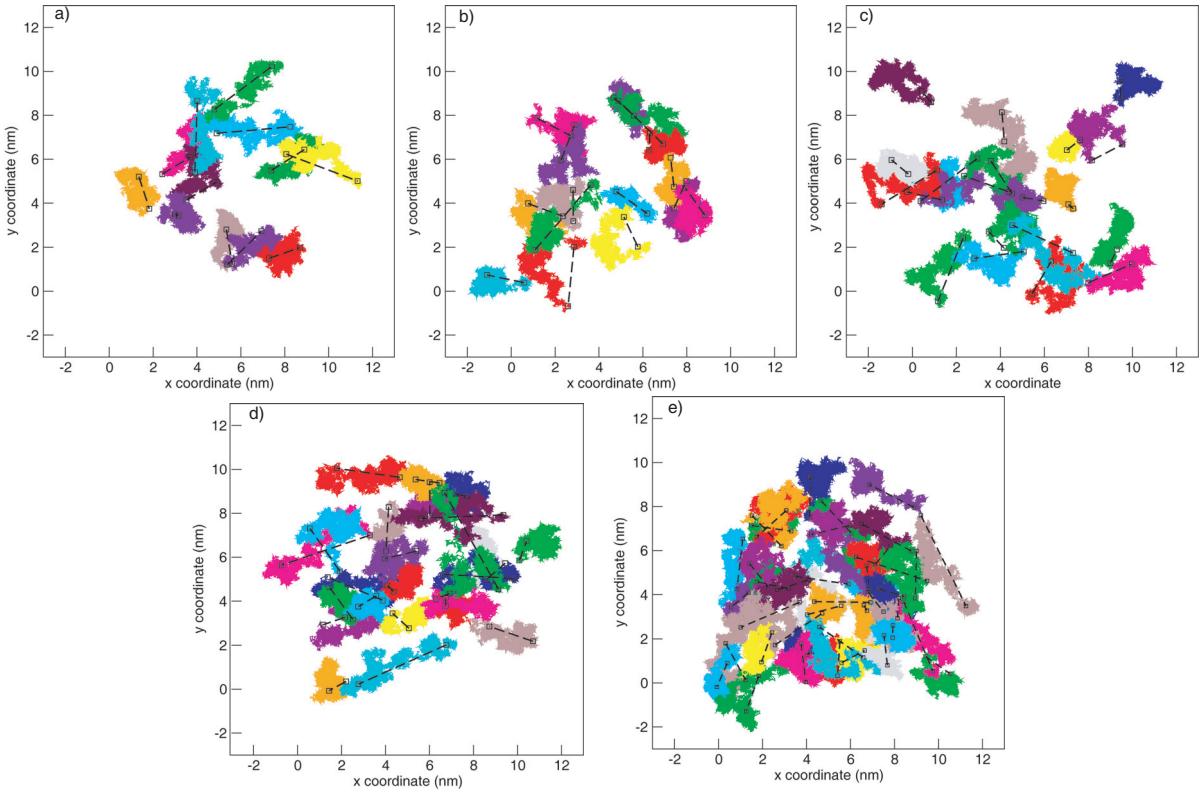

Figure 5.24: Lateral movements of capsaicin in the plane of the bilayer in a) LipidM-D, b) LipidM-E, c) LipidM-F, d) LipidM-G, and e) LipidM-H. The colored lines depict the lateral movements of individual capsaicin molecules and the open boxes, connected by dash lines, are the initial and final position of each molecule at 10 and 50 ns, respectively.

both bilayers. The hydrophobic part of capsaicin aligned with the lipid acyl tails and the hydrophilic hydroxyl and amide groups were distributed below the interface. This configuration allows favorable enthalpic interactions to occur between similar hydrophobic and hydrophilic groups. Capsaicin interacted with the lipids through hydrogen bonding without changing the structure of the lipids. The additional molecular volume of capsaicin in the bilayer separated the lipid headgroups and decreased the interfacial density. The additional spacing between the lipids helps to explain experimental results in the literature where capsaicin was observed to change the fluidity of cell membranes. This study sheds some light on the interactions of capsaicin with lipid bilayers that are in part responsible for its chemosensory action.

Chapter 6

Conclusions and Proposed Future Work

6.1 Conclusions

Molecular dynamics were used to study the properties of capsaicin in model cell membranes. The first part involved the validation of the OPLS force field to describe the molecular interactions of capsaicin. An 1-octanol/water system was used for that purpose, as it is often used in the correlation of membrane permeability. The OPLS all-atom and united-atom force fields quantitatively and qualitatively represented capsaicin and 1-octanol accurately. The 1-octanol/water system formed a bilayer-like structure with a clear interface. Capsaicin molecules that were initially dissolved into the aqueous phase partitioned to the interface, where the hydrophobic part of capsaicin aligned with the interfacial octanol hydrocarbon chains, and the hydrophilic part of capsaicin was exposed to the aqueous phase, where it formed hydrogen bonds with water and interfacial octanol molecules. Both all-atom and united-atom force fields gave similar representations of capsaicin. The united-atom model was chosen as a suitable model to represent capsaicin in the second part of this study dealing with model cell membranes.

The second part involved the study of capsaicin in pure DPPC bilayers and mixed bilayers with a 3:1 molar ratio of DPPC to DPPE. Two methods were used to detail the interactions of capsaicin and the cell membrane: dissolving capsaicin into the aqueous and lipid phases. Capsaicin molecules initially dissolved into the aqueous phase penetrated the bilayer, and the effect of lipid composition and temperature on the permeability of the bilayer were determined. Bilayers with DPPE had a lower permeability than pure DPPC bilayers, while increasing the temperature had the opposite effect. Capsaicin molecules that penetrated the bilayer partitioned to an area beneath the lipid/water interface where the hydrophobic part aligned with the lipid acyl tails, and the hydrophilic part was close to the interface. Capsaicin molecules introduced directly into the bilayer had a similar configuration. At this position in the bilayer, the hydrophilic groups can form hydrogen bonds with the lipids and water in the interface and the hydrophobic tail can be accommodated by favorable enthalpic interactions. The presence of capsaicin did not affect the structure of the bilayer. One important result from the simulations indicates that the interfacial density decreases with increasing concentrations of capsaicin, which may explain experimental studies in which capsaicin increased the permeability of the membrane to ions, and affected the membrane fluidity.

In conclusion, the 1-octanol/water system slightly overestimates the ability of capsaicin to penetrate the bilayer. For similar concentrations of capsaicin dissolved into the aqueous phase, more molecules were integrated into the octanol rich phase than in the bilayer. Diffusion through the interface is the rate limiting step to penetrate the bilayer, where an increase in the interfacial density decreases the permeability. The 1-octanol/water interface forms a bilayer-like structure, but the interface is thinner than that of a bilayer, since it is only composed of hydroxyl groups and hydrating water molecules. The bilayer interface is also denser, and its physical properties vary depending on the lipid composition. The 1-octanol/water system is acceptable for determining the general partitioning behavior of capsaicin between hydrophilic and lipophilic environments; however, it does not provide

atomic detail of the complex interactions associated with diffusion into cell membranes. Another discrepancy between the 1-octanol/water and lipid systems was the effect of capsaicin on the hydrophobic tails of octanol and lipids. The first part of this study showed an increase in the order of interfacial octanol molecules in the presence of capsaicin; however, this result was not replicated for the lipid acyl tails in the bilayers.

Overall, the preference of capsaicin for an amphiphilic environment is well represented by the 1-octanol/water system, but the specific interactions that contribute to the chemosensory action cannot be determined using this system. To fully understand these interactions, an explicit membrane environment with lipids must be investigated. This initial study reveals certain aspects of the chemosensory action of capsaicin. Since the bilayer interface accounts for up to 60% of its volume, slight changes in its properties may substantially affect its function. In order to fully understand the chemosensory action, additional experiments and simulations are needed. The results of this study are useful for invsetigating the chemosensory action of capsaicin and how it occurs. If capsaicin alters the properties of the bilayer or binds to TRPV1 it must interact with the sensory neuron membrane. If changes in the structure of the bilayer cause the chemosensory action, then this study suggests that the changes occur in the interfacial density. If there is a specific interaction site for capsaicin with TRPV1, then the target residues should be present near the lipid/water interface.

6.2 Proposed Future Work

As a result of the considerable amount of evidence for the specific interactions of capsaicin with TRPV1, future simulations should investigate possible binding sites for capsaicin. To date, a high resolution, three dimensional structure of TRPV1 has not been characterized. However, since TRPV1 is a member of the larger TRP family, the structure of this protein can be predicted from sequence alignment, homology modeling, and structure fitting studies of other TRP proteins. A specific binding site has been proposed from amino acid sequence

modification experiments, and this site should be investigated first [14]. Capsaicin should be introduced in the local proximity of this binding site to overcome the relatively slow dynamics of lateral diffusion in the bilayer.

Other molecules that cause a chemosensory action may also provide insight into the action of capsaicin. Menthol, a cold sensation compound, activates receptors in similar ways to capsaicin. Another TRP protein has been isolated as a possible interaction site for menthol that is homologous to TRPV1 [95]. Since both molecules mimic thermal sensations by possible interactions with TRP proteins, their interactions with sensory neurons are likely to be similar. As a result, increasing our understanding of the chemosensory action of one should assist in determining that of the other.

Bibliography

[1] Jordt, S. E., D. D. McKemy, and D. Julius. 2003. Lessons from peppers and peppermint: the molecular logic of thermosensation. *Curr. Opin. Neurobio.* 13:487–492.

[2] Hunt, S. P., and P. W. Mantyh. 2001. The molecular dynamics of pain control. *Nat. Rev. Neurosci.* 2:83–91.

[3] Niemeyer, B. A. 2005. Structure-function analysis of TRPV channels. *Naunyn-Schmiedeberg's Arch. Pharmacol.* 371:285–294.

[4] Caterina, M. J., M. A. Schumacher, M. Tominaga, T. A. Rosen, J. D. Levine, and D. Julius. 1997. The capsaicin receptor: a heat-activated ion channel in the pain pathway. *Nature* 389:816–824.

[5] Szallasi, A., and P. M. Blumberg. 1999. Vanilloid (capsaicin) receptors and mechanisms. *Pharmacol. Reviews* 51:159–211.

[6] Buck, S. H., and T. F. Burks. 1986. The neuropharmacology of capsaicin: review of some recent observations. *Pharmacol. Rev.* 38:179–226.

[7] Jordt, S. E., and D. Julius. 2003. Molecular determinants of ligand interaction with the capsaicin receptor. *J. Neurochem.* 85:4–4.

[8] Krajewska, A. M., and J. J. Powers. 1988. Sensory properties of naturally-occurring capsaicinoids. *J. Food Sci.* 53:902–905.

[9] Johnston, J. C., W. I. F. David, A. J. Markvardsen, and K. Shankland. 2002. A hybrid Monte Carlo method for crystal structure determination from powder diffraction data. *Acta Cryst. Sec. A* 58:441–447.

[10] Thresh, L. T. 1846. Isolation of capsaicin. *Pharm. J.* 6:941.

[11] Scoville, W. L. 1912. Note on capsicum. *J. Amer. Pharm. Assoc.* 1:453.

[12] Surh, Y. J. 2002. More than spice: capsaicin in hot chili peppers makes tumor cells commit suicide. *J. Nat. Cancer Inst.* 94:1263–1265.

[13] Surh, Y. J. 1998. Cancer chemoprevention by dietary phytochemicals: a mechanistic viewpoint. *Cancer J. - France* 11:6–10.

[14] Jordt, S. E., and D. Julius. 2002. Molecular basis for species-specific sensitivity to "hot" chili peppers. *Cell* 108:421–430.

[15] Singer, S., and G. L. Nicolson. 1972. The fluid mosaic model of cell membranes. *Science* 172:720–730.

[16] Meddings, J. B., C. M. Hogaboam, K. Tran, J. D. Reynolds, and J. L. Wallace. 1991. Capsaicin effects on non-neuronal plasma membranes. *Biochim. Biophys. Acta* 1070:43–50.

[17] Aranda, F. J., J. Villalaín, and J. C. Gómez-Fernández. 1995. Capsaicin affects the structure and phase organization of phospholipid membranes. *Biochim. Biophys. Acta* 1234:225–34.

[18] Tsuchiya, H. 2001. Biphasic membrane effects of capsaicin, an active component in *Capsicum* species. *J. Ethnopharmacol.* 75:295–9.

[19] Feigin, A. M., E. V. Aronov, B. P. Bryant, J. H. Teeter, and J. G. Brand. 1995. Capsaicin and its analogs induce ion channels in planar lipid bilayers. *Neuroreport* 6:2134–2136.

[20] Feigin, A. M., E. V. Aronov, J. H. Teeter, and J. G. Brand. 1995. Capsaicin lipid interactions: relationship to biological activity. *Chem. Senses* 20:78–78.

[21] Lundbæ k, J. A., P. Birn, S. E. Tape, G. E. Toombes, R. Sogaard, R. E. Koeppe II, S. M. Gruner, A. J. Hansen, and O. S. Andersen. 2005. Capsaicin regulates voltage-dependent sodium channels by altering lipid bilayer elasticity. *Mol. Pharmacol.* 68:680–9.

[22] De Petrocellis, L., and V. Di Marzo. 2005. Lipids as regulators of the activity of transient receptor potential type V1 (TRPV1) channels. *Life Sci.* 77:1651–1666.

[23] Kogure, K., S. Goto, M. Nishimura, M. Yasumoto, K. Abe, C. Ohiwa, H. Sassa, T. Kusumi, and H. Terada. 2002. Mechanism of potent antiperoxidative effect of capsaicin. *Biochim. Biophys. Acta* 1573:84–92.

[24] Egberts, E., S. J. Marrink, and H. J. C. Berendsen. 1994. Molecular-dynamics simulation of a phospholipid membrane. *Euro. Biophys. J. Biophys. Lett.* 22:423–436.

[25] Debolt, S. E., and P. A. Kollman. 1995. Investigation of structure, dynamics, and solvation in 1-octanol and its water-saturated solution: molecular dynamics and free-energy perturbation studies. *J. Amer. Chem. Soc.* 117:5316–5340.

[26] Jorgensen, W. L., J. D. Madura, and C. J. Swenson. 1984. Optimized intermolecular potential functions for liquid hydrocarbons. *J. Amer. Chem. Soc.* 106:6638–6646.

[27] Jorgensen, W. L. 1986. Optimized intermolecular potential functions for liquid alcohols. *J. Phys. Chem.* 90:1276–1284.

[28] Jorgensen, W. L., and C. J. Swenson. 1985. Optimized intermolecular potential functions for amides and peptides. Hydration of amides. *J. Amer. Chem. Soc.* 107:1489–1496.

[29] Jorgensen, W. L., and C. J. Swenson. 1985. Optimized intermolecular potential functions for amides and peptides. Structure and properties of liquid amides. *J. Amer. Chem. Soc.* 107:569–578.

[30] Jorgensen, W. L., E. R. Laird, T. B. Nguyen, and J. Tiradorives. 1993. Monte Carlo simulations of pure liquid substituted benzenes with OPLS potential functions. *J. Comput. Chem.* 14:206–215.

[31] Jorgensen, W. L., and T. B. Nguyen. 1993. Monte Carlo simulations of the hydration of substituted benzenes with OPLS potential functions. *J. Comp. Chem.* 14:195–205.

[32] Best, S. A., K. M. Merz, and C. H. Reynolds. 1999. Free energy perturbation study of octanol/water partition coefficients: comparison with continuum GB/SA calculations. *J. Phys. Chem. B* 103:714–726.

[33] De Oliveira, C. A. F., C. R. W. Guimarães, and R. B. De Alencastro. 2000. Molecular dynamics study on liquid 1-octanol. *Int. J. Quant. Chem.* 80:999–1006.

[34] De Oliveira, C. A. F., C. R. W. Guimarães, and R. B. De Alencastro. 2002. Molecular dynamics study on liquid 1-octanol. Part 2. Water-saturated 1-octanol solution. *Int. J. Quant. Chem.* 90:786–791.

[35] MacCallum, J. L., and D. P. Tieleman. 2002. Structures of neat and hydrated 1-octanol from computer simulations. *J. Amer. Chem. Soc.* 124:15085–15093.

[36] Steel, W. H., C. L. Beildeck, and R. A. Walker. 2004. Solvent polarity across strongly associating interfaces. *J. Phys. Chem. B* 108:16107–16116.

[37] Benjamin, I. 2004. Polarity of the water/octanol interface. *Chem. Phys. Lett.* 393:453–456.

[38] De Oliveira, C. A. F., C. R. W. Guimãraes, H. De Mello, A. Echevarria, and R. B. De Alencastro. 2005. A molecular dynamics study on liquid 1-octanol. Part 3. Evaluating octanol/water partition coefficients of novel thrombin inhibitors via free-energy perturbations. *Int. J. Quant. Chem.* 102:542–553.

[39] Berger, O., O. Edholm, and F. Jähnig. 1997. Molecular dynamics simulations of a fluid bilayer of dipalmitoylphosphatidylcholine at full hydration, constant pressure, and constant temperature. *Biophys. J.* 72:2002–2013.

[40] Chou, M. Z., T. Mtui, Y. D. Gao, M. Kohler, and R. E. Middleton. 2004. Resiniferatoxin binds to the capsaicin receptor (TRPV1) near the extracellular side of the S4 transmembrane domain. *Biochem.* 43:2501–2511.

[41] Leekumjorn, S., and A. K. Sum. 2006. Molecular dynamics simulations of mixed DPPC/DPPE bilayers. *Biophys. J.* 90:3951-3965.

[42] Leach, A. R. 2001. Molecular Modeling: Principles and Applications. 2nd edition. Pearson Education, Harlow, England.

[43] Lee, B. W., R. Faller, A. K. Sum, I. Vattulainen, M. Patra, and M. Karttunen. 2005. Structural effects of small molecules on phospholipid bilayers investigated by molecular simulations. *Fluid Phase Equil.* 228:135–140.

[44] Bassolino-Klimas, D., H. E. Alper, and T. R. Stouch. 1993. Solute diffusion in lipid bilayer membranes: an atomic level study by molecular dynamics simulation. *Biochem.* 32:12624–37.

[45] Bassolino-Klimas, D., H. Alper, and T. R. Stouch. 1996. Drug-membrane interactions studied by molecular dynamics simulation: size dependence of diffusion. *Drug Des. Discov.* 13:135–41.

[46] Bassolino-Klimas, D., H. E. Alper, and T. R. Stouch. 1995. Mechanism of solute diffusion through lipid bilayer membranes by molecular dynamics simulation. *J. Amer. Chem. Soc.* 117:4118–4129.

[47] Bemporad, D., C. Luttmann, and J. W. Essex. 2005. Behaviour of small solutes and large drugs in a lipid bilayer from computer simulations. *Biochim. Biophys. Acta* 1718:1–21.

[48] Ulander, J., and A. D. Haymet. 2003. Permeation across hydrated DPPC lipid bilayers: simulation of the titrable amphiphilic drug valproic acid. *Biophys. J.* 85:3475–84.

[49] Bemporad, D., J. W. Essex, and C. Luttmann. 2004. Permeation of small molecules through a lipid bilayer: a computer simulation study. *J. Phys. Chem. B* 108:4875–4884.

[50] Bemporad, D., C. Luttmann, and J. W. Essex. 2004. Computer simulation of small molecule permeation across a lipid bilayer: dependence on bilayer properties and solute volume, size, and cross-sectional area. *Biophys. J.* 87:1–13.

[51] Doxastakis, M., A. K. Sum, and J. J. de Pablo. 2005. Modulating membrane properties: the effect of trehalose and cholesterol on a phospholipid bilayer. *J. Phys. Chem. B* 109:24173–24181.

[52] Sum, A. K., R. Faller, and J. J. de Pablo. 2003. Molecular simulation study of phospholipid bilayers and insights of the interactions with disaccharides. *Biophys. J.* 85:2830–44.

[53] Sum, A. K., and J. J. de Pablo. 2003. Molecular simulation study on the influence of dimethylsulfoxide on the structure of phospholipid bilayers. *Biophys. J.* 85:3636–3645.

[54] Berendsen, H. J. C., D. van der Spoel, and R. van Drunen. 1995. GROMACS: a message-passing parallel molecular dynamics implementation. *Comput. Phys. Commun.* 91:43–56.

[55] Lindahl, E., B. Hess, and D. van der Spoel. 2001. GROMACS 3.1: a package for molecular simulation and trajectory analysis. *J. Mol. Model.* 7:306–317.

[56] Jorgensen, W. L., D. S. Maxwell, and J. Tirado-Rives. 1996. Development and testing of the OPLS all-atom force field on conformational energetics and properties of organic liquids. *J. Amer. Chem. Soc.* 118:11225–11236.

[57] Berendsen, H. J. C., J. P. M. Postma, W. van Gunsteren, and J. Hermans. 1981. Intermolecular Forces. Reidel, Dordrecht, The Netherlands.

[58] van der Spoel, D., E. Lindahl, B. Hess, A. R. van Buuren, E. Apol, P. J. Meulenhoff, P. D. Tieleman, A. L. T. M. Sijbers, K. A. Feenstra, R. van Drunen, and H. J. C. Berendsen. 2004. GROMACS User Manuel: Version 3.2. 1st edition. Department of Biophysical Chemistry, Groningen, The Netherlands.

[59] Anézo, C., A. H. de Vries, H. D. Höltje, D. P. Tieleman, and S. J. Marrink. 2003. Methodological issues in lipid bilayer simulations. *J. Phys. Chem. B* 107:9424–9433.

[60] Darden, T., D. York, and L. Pedersen. 1993. Particle Mesh Ewald - an n·log(n) method for Ewald sums in large systems. *J. Chem. Phys.* 98:10089–10092.

[61] Berendsen, H. J. C., J. P. M. Postma, W. F. van Gunsteren, A. Dinola, and J. R. Haak. 1984. Molecular dynamics with coupling to an external bath. *J. Chem. Phys.* 81:3684–3690.

[62] Frenkel, D., and B. Smit. 2002. Understanding Molecular Simulation: From Algorithms to Applications. Second edition. Academic Press, San Diego, CA.

[63] Mukhopadhyay, P., H. J. Vogel, and D. P. Tieleman. 2004. Distribution of pentachlorophenol in phospholipid bilayers: a molecular dynamics study. *Biophys. J.* 86:337–45.

[64] Brady, J. W., and R. K. Schmidt. 1993. The role of hydrogen bonding in carbohydrates: molecular dynamics simulations of maltose in aqueous solution. *J. Phys. Chem.* 97:958–966.

[65] Nagy, I., P. Santha, G. Jancso, and L. Urban. 2004. The role of the vanilloid (capsaicin) receptor (TRPV1) in physiology and pathology. *Euro. J. Pharm.* 500:351–369.

[66] Turgut, C., B. M. Newby, and T. J. Cutright. 2004. Determination of optimal water solubility of capsaicin for its usage as a non-toxic antifoulant. *Enviro. Sci. and Pollut. R.* 11:7–10.

[67] Lide, R. D., editor. 2005. CRC Handbook of Chemistry and Physics, Internet Version 2005. CRC Press, Boca Raton, FL.

[68] Berti, P., S. Cabani, and V. Molica. 1987. Limiting partial molar volumes at 298.15 K of some open chain and cyclic organic compounds in 1-octanol. *Fluid Phase Equilib.* 32:195–203.

[69] Iwahashi, M., Y. Hayashi, N. Hachiya, H. Matsuzawa, and H. Kobayashi. 1993. Self-association of octan-1-ol in the pure liquid state and in decane solutions as observed by viscosity, self-diffusion, nuclear magnetic resonance and near infrared spectroscopy measurements. *J. Chem. Soc. Faraday Trans.* 89:707–712.

[70] Mills, R. 1973. Self-diffusion in normal and heavy water in the range 1-45^o. *J. Phys. Chem.* 77:685–688.

[71] Winter, J., S. Bevan, and E. A. Campbell. 1995. Capsaicin and pain mechanisms. *Brit. J. Anesthesia* 75:157–168.

[72] Lambert, J. W., and A. K. Sum. 2006. Molecular dynamics study of the properties of capsaicin in an 1-octanol/water system. *J. Phys. Chem. B* 110:2351–2357.

[73] Pandit, S. A., D. Bostick, and M. L. Berkowitz. 2004. Complexation of phosphatidylcholine lipids with cholesterol. *Biophys. J.* 86:1345–1356.

[74] Smondyrev, A. M., and M. L. Berkowitz. 1999. Structure of dipalmitoylphosphatidylcholine/cholesterol bilayer at low and high cholesterol concentrations: molecular dynamics simulation. *Biophys. J.* 77:2075–2089.

[75] Nagle, J. F. 1993. Area lipid of bilayers from NMR. *Biophys. J.* 64:1476–1481.

[76] Nagle, J. F., R. T. Zhang, S. Tristram-Nagle, W. J. Sun, H. I. Petrache, and R. M. Suter. 1996. X-ray structure determination of fully hydrated L_α phase dipalmitoylphosphatidylcholine bilayers. *Biophys. J.* 70:1419–1431.

[77] Edholm, O., and J. F. Nagle. 2005. Areas of molecules in membranes consisting of mixtures. *Biophys. J.* 89:1827–1832.

[78] Ikemoto, A., T. Kobayashi, S. Watanabe, and H. Okuyama. 1997. Membrane fatty acid modifications of PC12 cells by arachidonate or docosahexaenoate affect neurite outgrowth but not norepinephrine release. *Neurochem. Res.* 22:671–8.

[79] Wilson, R., and M. V. Bell. 1993. Molecular species composition of glycerophospholipids from white matter of human brain. *Lipids* 28:13–7.

[80] Isaac, G., D. Bylund, J. E. Mansson, K. E. Markides, and J. Bergquist. 2003. Analysis of phosphatidylcholine and sphingomyelin molecular species from brain extracts using capillary liquid chromatography electrospray ionization mass spectrometry. *J. Neurosci. Methods* 128:111–9.

[81] Calderon, R. O., B. Attema, and G. H. DeVries. 1995. Lipid composition of neuronal cell bodies and neurites from cultured dorsal root ganglia. *J. Neurochem.* 64:424–9.

[82] Olsson, N. U., and J. Salem, N. 1997. Molecular species analysis of phospholipids. *J. Chromatogr. B Biomed. Sci. Appl.* 692:245–56.

[83] Hess, B., H. Bekker, H. J. C. Berendsen, and J. G. E. M. Fraajie. 1997. LINCS: a linear constraint solver for molecular simulations. *J. Comput. Chem.* 18:1463–1472.

[84] Miyamoto, S., and P. A. Kollman. 1992. SETTLE: an analytical version of the shake and rattle algorithm for rigid water molecules. *J. Comput. Chem.* 13:952–962.

[85] Petrache, H. I., S. W. Dodd, and M. F. Brown. 2000. Area per lipid and acyl length distributions in fluid phosphatidylcholines determined by ^{2}H NMR spectroscopy. *Biophys. J.* 79:3172–3192.

[86] Feller, S. E. 1997. Computer simulation of a DPPC phospholipid bilayer: structural changes as a function of molecular surface area. *Langmuir* 13:6555–6561.

[87] Song, Y., V. Guallar, and N. A. Baker 2005. Molecular dynamics simulations of salicylate effects on the micro- and mesoscopic properties of a dipalmitoylphosphatidylcholine bilayer. *Biochem.* 44:13425–13438.

[88] Marrink, S. J., and H. J. C. Berendsen 1994. Simulation of water transport through a lipid membrane. *J. Phys. Chem.* 98:4155–4168.

[89] Marrink, S. J., and H. J. C. Berendsen 1996. Permeation process of small molecules across lipid membranes studied by molecular dynamics simulations. *J. Phys. Chem.* 100:16729–16738.

[90] Seelig, J., and A. Seelig. 1974. Dynamic structure of fatty acyl chains in a phospholipid bilayer measured by NMR. *Biochem.* 13:4839–4845.

[91] Patra, M., M. T. Karttunen, M. T. Hyvönen, E. Falck, and I. Vattulainen. 2004. Lipid bilayers driven to a wrong lane in molecular dynamics simulations by subtle changes in long-range electrostatic interactions. *J. Phys. Chem. B* 108:4485–4494.

[92] Israelachvili, J. N., and H. Wennerström. 1992. Entropic forces between amphiphilic surfaces in liquids. *J. Phys. Chem.* 96:520–531.

[93] Tanford, C. 1979. Interfacial free energy and the hydrophobic effect. *Proc. Natl. Acad. Sci. USA* 76:4175–4176.

[94] Seelig, J., and P. Ganz. 1991. Nonclassical hydrophobic effect in membrane binding equilibria. *Biochem.* 30:9354–9359.

[95] Voets, T., G. Droogmans, U. Wissenbach, A. Janssens, V. Flockerzi, and B. Nilius. 2004. The principle of temperature-dependent gating in cold- and heat-sensitive TRP channels. *Nature* 430:748–54.

Appendix A

This Appendix contains the force field parameters for the representations of OPLS AA capsaicin, OPLS UA capsaicin, OPLS AA octanol, modified OPLS UA octanol, DPPC, DPPE, and SPC water.

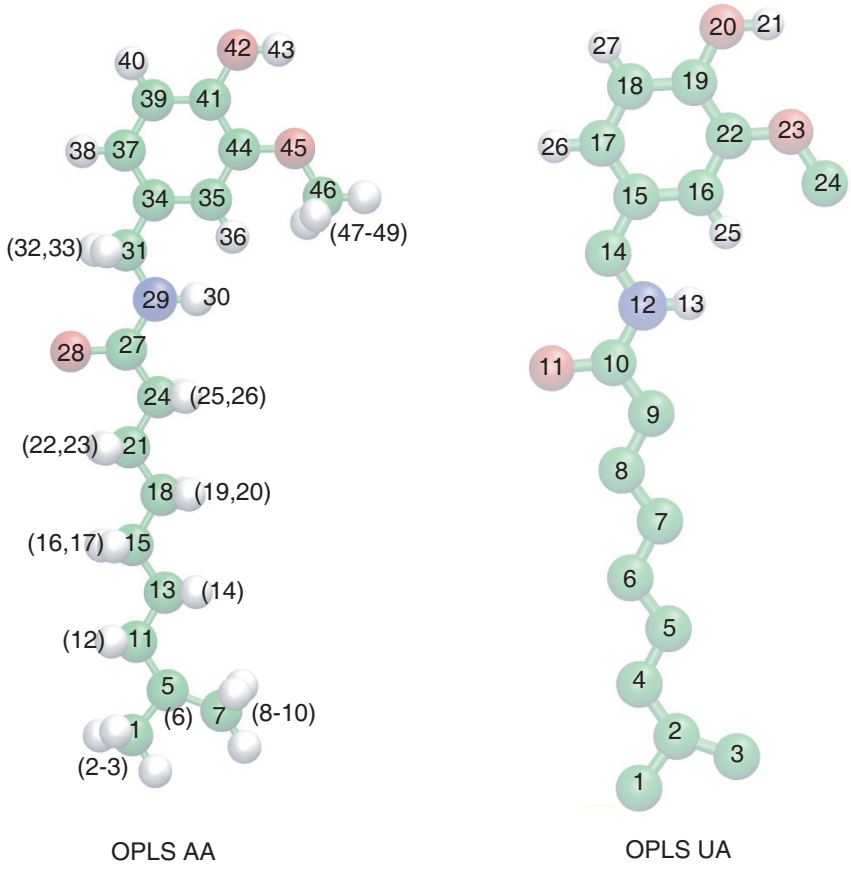

Figure A.1: Atom numbering scheme used for the OPLS AA and UA representations of capsaicin.

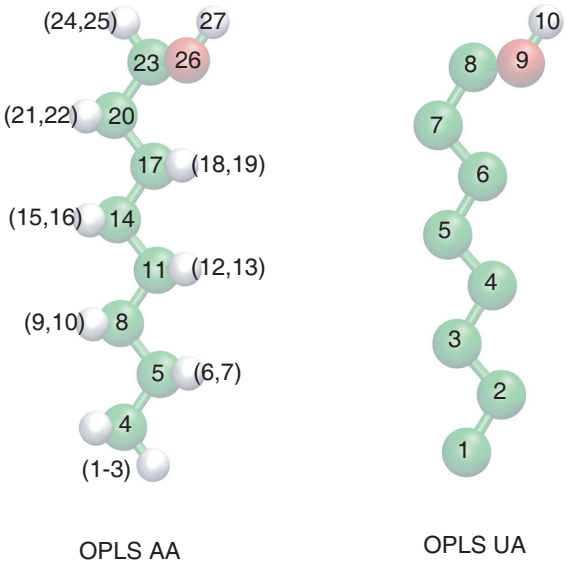

Figure A.2: Atom numbering scheme used for the OPLS AA and UA representations of octanol.

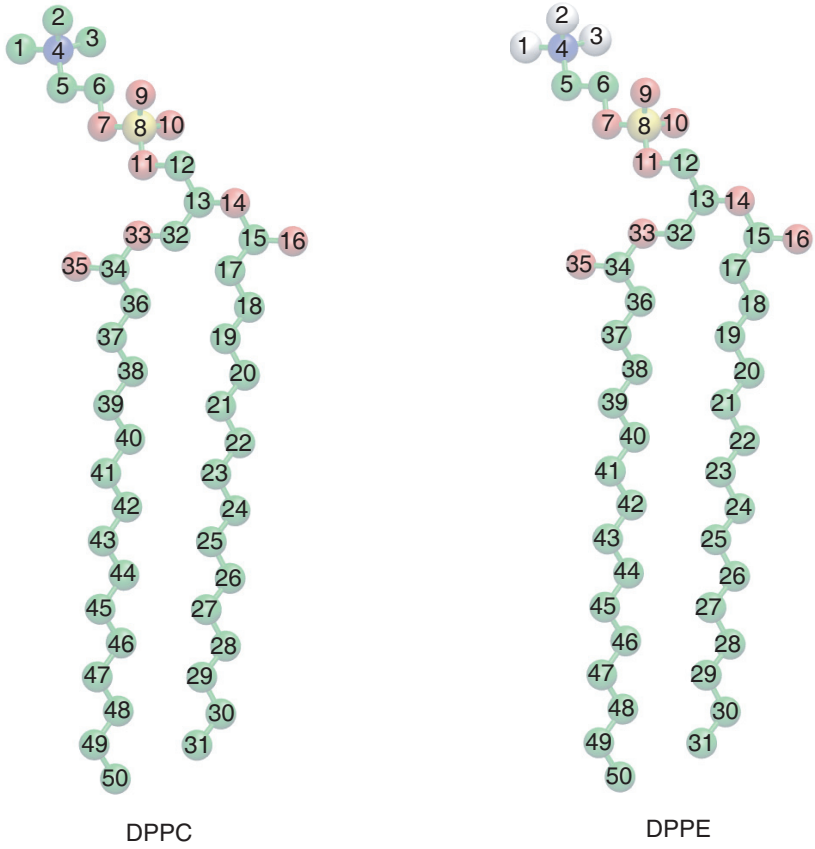

Figure A.3: Atom numbering scheme used for DPPC and DPPE.

A.1 Force Field File Formats

The GROMACS force field file format is explained in this section for files included in Appendix A.2.

A.1.1 Bonded Force Field Formats

```
[ moleculetype ]
; Name nrexcl
CAPS     3
```

This section contains the name of the molecule and the number of exclusions. The name must be consistent with the topology file that is referenced by `grompp` . The number of exclusions indicates the number of bonded atoms to exclude for calculating non-bonded interactions. By specifying `3` , the only atoms separated by three or more bonds have non-bonded interactions.

```
[ atoms ]
;nr type resnr cresid atom cgnr  charge   mass
1   CCT 1 CAPS  CT   1 -0.180  12.0110
```

This section lists the atom number (`nr)` , atom type (`type)` , residue number (`resnr)` , residue identification (`cresid)` , corresponding coordinate file atom type (`atom)` , charge group (`cgnr)` , electronic charge (`charge)` , and molecular mass (`mass)` .

```
[ bonds ]
; ai  aj  fu       c0, c1, ...
  1   2   1    0.1090 284702.4
```

Bonds between atoms are defined by specifying the bonded atom numbers, the bond function, the bond length, and the bond force constant in kJ/mol. For this entry, atoms `1` and `2` are bonded by a harmonic bond potential (`func.  1)` with a bond length of `0.1090` nm and a force constant of 284,702.4 kJ/mol.

```
[ pairs ]
; ai  aj  fu
   2   6   1
```

1,4 pair interactions are explicitly listed with the specified function. Here, the atoms `2` and `6` are separated by three bonds and are considered for 1,4 pair interactions. A function of `1` indicates that these interactions are scaled according to the fudge factors defined in the head force field file.

```
[ angles ]
; ai  aj  ak  fu    c0, c1, ...
  2   1   3    1   107.80 276.329
```

Like bonds, angles are defined by listing the three atoms involved in the angle (`2 1 3`) , the angle function, the angle (degree), and the force constant. For this entry a harmonic potential is used, defined by function 1, with an angle of `107.80` degrees and a force constant of 276.329 kJ/mol.

```
[ dihedrals ]
; ai  aj   ak    al  fu    c0, c1, m, ...
  2    1   5    6  3    0.6280  1.8841   0.0000 -2.5121 0 0
```

Dihedrals are specified for torsion potentials, where four atoms are listed and the type of dihedral is specified by the functions number. Function `1` is a standard potential, `2` is an improper dihedral, and `3` is a Ryckaert-Bellemans potential. For this listing, a Ryckaert-Bellemans potential is defined with six force constants.

A.1.2 Non-bonded Force Field Formats

```
[ atomtypes ]
; name     mass    charge ptype       C6             C12
  CH3     15.0350   0.00  A     +6.9810E-03   +1.9414E-05
```

Non-bonded parameters are included in a separate file, where the parameters for all atoms in a simulation must be listed together. The `name` corresponds to the `atomtype` listed in the [`atoms`] section of the bonded force field parameters. The `mass` and `charge` are redundant, and the `C6` and `C12` entries are the values for the Lennard Jones potential in kJ/mol. C6 and C12 can be calculated from σ and ϵ using the relationship C6 $= 4\epsilon_{i,j}(\sigma_{i,j})^6$ and C12 $= 4\epsilon_{i,j}(\sigma_{i,j})^{12}$.

A.2 Force Field Parameters

A.2.1 Bonded Parameter Files

OPLS AA force field parameters for capsaicin (capsOPLSAA.itp)

```
[ moleculetype ]
; Name nrexcl
CAPS     3

[ atoms ]
;nr type resnr cresid atom cgnr charge   mass
1  CCT 1 CAPS CT 1 -0.180  12.0110
2  CHC 1 CAPS HC 1  0.060   1.0080
3  CHC 1 CAPS HC 1  0.060   1.0080
4  CHC 1 CAPS HC 1  0.060   1.0080
5  CCT 1 CAPS CT 1 -0.060  12.0110
6  CHC 1 CAPS HC 1  0.060   1.0080
7  CCT 1 CAPS CT 1 -0.180  12.0110
8  CHC 1 CAPS HC 1  0.060   1.0080
9  CHC 1 CAPS HC 1  0.060   1.0080
10 CHC 1 CAPS HC 1  0.060   1.0080
11 CCM 1 CAPS CM 2 -0.115  12.0110
12 CHE 1 CAPS HE 2  0.115   1.0080
13 CCM 1 CAPS CM 2 -0.115  12.0110
14 CHE 1 CAPS HE 2  0.115   1.0080
15 CCT 1 CAPS CT 3 -0.120  12.0110
16 CHC 1 CAPS HC 3  0.060   1.0080
17 CHC 1 CAPS HC 3  0.060   1.0080
18 CCT 1 CAPS CT 3 -0.120  12.0110
19 CHC 1 CAPS HC 3  0.060   1.0080
20 CHC 1 CAPS HC 3  0.060   1.0080
21 CCT 1 CAPS CT 3 -0.120  12.0110
22 CHC 1 CAPS HC 3  0.060   1.0080
23 CHC 1 CAPS HC 3  0.060   1.0080
24 CCT 1 CAPS CT 3 -0.120  12.0110
25 CHC 1 CAPS HC 3  0.060   1.0080
26 CHC 1 CAPS HC 3  0.060   1.0080
27 CC 1 CAPS C   4  0.500  12.0110
28 CO 1 CAPS O   4 -0.500  15.9994
29 CN 1 CAPS N   4 -0.500  14.0067
30 CH 1 CAPS H   4  0.300   1.0080
31 CCT 1 CAPS CT 4  0.030  12.0110
32 CHC 1 CAPS HC 4  0.060   1.0080
33 CHC 1 CAPS HC 4  0.060   1.0080
34 CCA 1 CAPS CA 5  0.015  12.0110
35 CCA 1 CAPS CA 5 -0.115  12.0110
36 CHA 1 CAPS HA 5  0.115   1.0080
37 CCA 1 CAPS CA 6 -0.115  12.0110
38 CHA 1 CAPS HA 6  0.115   1.0080
39 CCA 1 CAPS CA 6 -0.160  12.0110
40 CHA 1 CAPS HA 6  0.115   1.0080
41 CCA 1 CAPS CA 7  0.150  12.0110
42 COH 1 CAPS OH 7 -0.585  15.9994
43 CHO 1 CAPS HO 7  0.435   1.0080
44 CCA 1 CAPS CA 8  0.100  12.0110
45 COS 1 CAPS OS 8 -0.285  15.9994
46 CCA 1 CAPS CA 8  0.085  12.0110
47 CHC 1 CAPS HC 8  0.060   1.0080
48 CHC 1 CAPS HC 8  0.060   1.0080
49 CHC 1 CAPS HC 8  0.060   1.0080

[ bonds ]
; ai  aj  fu    c0, c1, ...
1   2 1 0.1090 284702.4
1   3 1 0.1090 284702.4
1   4 1 0.1090 284702.4
1   5 1 0.1529 224412.5
5   6 1 0.1090 284702.4
5   7 1 0.1529 224412.4
7   8 1 0.1090 284702.4
7   9 1 0.1090 284702.4
7  10 1 0.1090 284702.4
5  11 1 0.1510 265443.1
11 12 1 0.1080 284702.4
11 13 1 0.1340 459710.6
13 14 1 0.1080 284702.4
13 15 1 0.1510 265443.1
15 16 1 0.1090 284702.4
15 17 1 0.1090 284702.4
15 18 1 0.1529 224412.5
18 19 1 0.1090 284702.4
18 20 1 0.1090 284702.4
18 21 1 0.1529 224412.5
21 22 1 0.1090 284702.4
21 23 1 0.1090 284702.4
21 24 1 0.1529 224412.5
24 25 1 0.1090 284702.4
24 26 1 0.1090 284702.4
24 27 1 0.1522 265443.1
27 28 1 0.1229 477295.2
27 29 1 0.1335 410306.4
29 30 1 0.1010 363412.2
29 31 1 0.1449 282190.3
31 32 1 0.1090 284702.4
31 33 1 0.1090 284702.4
31 34 1 0.1510 265443.1
34 35 1 0.1400 392721.8
34 37 1 0.1400 392721.8
35 36 1 0.1080 307311.1
35 44 1 0.1400 392721.8
37 38 1 0.1080 307311.1
37 39 1 0.1400 392721.8
39 40 1 0.1080 307311.1
39 41 1 0.1400 392721.8
41 42 1 0.1364 376812.0
41 44 1 0.1400 392721.8
42 43 1 0.0945 463060.1
44 45 1 0.1364 376812.0
45 46 1 0.1364  376812.0
46 47 1 0.1080 307311.1
46 48 1 0.1080 307311.1
46 49 1 0.1080 307311.1

[ pairs ]
; ai  aj  fu
   2   6   1
   2   7   1
   2  11   1
   3   6   1
   3   7   1
   3  11   1
   4   6   1
   4   7   1
   4  11   1
   8   1   1
   8   6   1
   8   1   1
   9   1   1
   9   6   1
   9  11   1
  10   1   1
  10   6   1
  10  11   1
   1   8   1
   1   9   1
   1  10   1
   1  12   1
   7  12   1
   1  13   1
   7  13   1
   6  12   1
   6  13   1
   5  14   1
   5  15   1
  11  16   1
  11  17   1
  11  18   1
  12  14   1
  12  15   1
  13  19   1
  13  20   1
  13  21   1
  14  16   1
  14  17   1
```

```
  14  18   1
  15  22   1
  15  23   1
  15  24   1
  16  19   1
  16  20   1
  16  21   1
  17  19   1
  17  20   1
  17  21   1
  18  25   1
  18  26   1
  18  27   1
  19  22   1
  19  23   1
  19  24   1
  20  22   1
  20  23   1
  20  24   1
  21  28   1
  21  29   1
  22  25   1
  22  26   1
  22  27   1
  23  25   1
  23  26   1
  23  27   1
  24  30   1
  24  31   1
  25  28   1
  25  29   1
  26  28   1
  26  29   1
  27  32   1
  27  33   1
  27  34   1
  28  30   1
  28  31   1
  29  35   1
  29  37   1
  30  32   1
  30  33   1
  30  34   1
  31  36   1
  31  44   1
  31  38   1
  31  39   1
  32  35   1
  32  37   1
  33  35   1
  33  37   1
  34  45   1
  34  40   1
  34  41   1
  35  38   1
  35  39   1
  35  42   1
  35  46   1
  36  37   1
  36  41   1
  36  45   1
  37  42   1
  37  44   1
  38  40   1
  38  41   1
  39  43   1
  39  45   1
  40  42   1
  40  44   1
  41  46   1
  42  45   1
  43  44   1
  44  47   1
  44  48   1
  44  49   1

[ angles ]
; ai  aj  ak  fu    c0, c1, ...
2   1 3  1 107.80 276.329
2   1 4  1 107.80 276.329
3   1 4  1 107.80 276.329
2   1 5  1 110.70 314.010
3   1 5  1 110.70 314.010
4   1 5  1 110.70 314.010
1   5 7  1 112.70 488.600
8   7 9  1 107.80 276.329
8   7 10 1 107.80 276.329
9   7 10 1 107.80 276.329
8   7 5  1 110.70 314.010
9   7 5  1 110.70 314.010
10  7 5  1 110.70 314.010
1   5 6  1 110.70 314.010
7   5 6  1 110.70 314.010
1   5 11 1 111.10 527.537
7   5 11 1 111.10 527.537
6   5 11 1 110.70 314.010
5  11 12 1 117.00  293.076
5  11 13 1 124.00  586.152
11 13 14 1 120.00 293.076
11 13 15 1 124.00  586.152
12 11 13 1 120.00 293.076
13 15 16 1 109.50 293.076
13 15 17 1 109.50  293.076
13 15 18 1 111.10 527.537
14 13 15 1 117.00  293.076
15 18 19 1 110.70 314.010
15 18 20 1 110.70 314.010
15 18 21 1 112.70 488.600
16 15 17 1 107.80 276.329
16 15 18 1 110.70 314.010
17 15 18 1 110.70 314.010
18 21 22 1 110.70 314.010
18 21 23 1 110.70 314.010
18 21 24 1 112.70 488.600
19 18 20 1 107.80 276.329
19 18 21 1 110.70 314.010
20 18 21 1 110.70 314.010
21 24 25 1 110.70 314.010
21 24 26 1 110.70 314.010
21 24 27 1 111.10  527.537
22 21 23 1 107.80 276.329
22 21 24 1 110.70 314.010
23 21 24 1 110.70 314.010
24 27 28 1 120.40  669.888
24 27 29 1 116.60  586.152
25 24 26 1 107.80 276.329
25 24 27 1 110.70 314.010
26 24 27 1 110.70 314.010
27 29 30 1 119.80 293.076
27 29 31 1 121.90 418.680
28 27 29 1 122.90 669.888
29 31 32 1 109.50 293.076
29 31 33 1 109.50 293.076
29 31 34 1 109.70  669.888
30 29 31 1 118.40  318.197
31 34 35 1 120.00 586.152
31 34 37 1 120.00 586.152
32 31 33 1 107.80 276.329
32 31 34 1 109.50 293.076
33 31 34 1 109.50 293.076
34 35 36 1 120.00 293.076
34 35 44 1 120.00 527.537
34 37 38 1 120.00 293.076
34 37 39 1 120.00 527.537
35 44 45 1 120.00 586.152
35 44 41 1 120.00 527.537
36 35 44 1 120.00 293.076
37 39 40 1 120.00 293.076
37 39 41 1 120.00 527.537
38 37 39 1 120.00 293.076
39 41 42 1 120.00  586.152
39 41 44 1 120.00 527.537
40 39 41 1 120.00 293.076
41 42 43 1 113.00  293.076
41 44 45 1 120.00 586.152
42 41 44 1 120.00 586.152
44 45 46 1 111.00  628.020
45 46 47 1 109.50 293.076
45 46 48 1 109.50 293.076
45 46 49 1 109.50 293.076
47 46 48 1 107.80 276.329
47 46 49 1 107.80 276.329
48 46 49 1 107.80 276.329

[ dihedrals ]
; ai  aj  ak  al  fu    c0, c1, m, ...
2   1 5   6 3  0.6280  1.8841   0.0000 -2.5121 0 0
2   1 5   7 3  0.6280  1.8841   0.0000 -2.5121 0 0
2   1 5  11 3  0.6280  1.8841   0.0000 -2.5121 0 0
3   1 5   6 3  0.6280  1.8841   0.0000 -2.5121 0 0
3   1 5   7 3  0.6280  1.8841   0.0000 -2.5121 0 0
3   1 5  11 3  0.6280  1.8841   0.0000 -2.5121 0 0
4   1 5   6 3  0.6280  1.8841   0.0000 -2.5121 0 0
4   1 5   7 3  0.6280  1.8841   0.0000 -2.5121 0 0
```

```
4   1 5  11 3  0.6280  1.8841   0.0000 -2.5121 0 0
8   7 5   1 3  0.6280  1.8841   0.0000 -2.5121 0 0
8   7 5   6 3  0.6280  1.8841   0.0000 -2.5121 0 0
8   7 5  11 3  0.6280  1.8841   0.0000 -2.5121 0 0
9   7 5   1 3  0.6280  1.8841   0.0000 -2.5121 0 0
9   7 5   6 3  0.6280  1.8841   0.0000 -2.5121 0 0
9   7 5  11 3  0.6280  1.8841   0.0000 -2.5121 0 0
10  7 5   1 3  0.6280  1.8841   0.0000 -2.5121 0 0
10  7 5   6 3  0.6280  1.8841   0.0000 -2.5121 0 0
10  7 5  11 3  0.6280  1.8841   0.0000 -2.5121 0 0
1   5 7   8 3  0.6280  1.8841   0.0000 -2.5121 0 0
1   5 7   9 3  0.6280  1.8841   0.0000 -2.5121 0 0
1   5 7  10 3  0.6280  1.8841   0.0000 -2.5121 0 0
1   5 11 12 3  0.6680  1.9941   0.0000 -2.6621 0 0
7   5 11 12 3  0.6680  1.9941   0.0000 -2.6620 0 0
1   5 11 13 3  0.5275 -6.4016  -1.6957  7.5697 0 0
7   5 11 13 3  0.5275 -6.4016  -1.6957  7.5697 0 0
6   5 11 12 3  0.6657  1.9971   0.0000 -2.6620 0 0
6   5 11 13 3 -0.7787 -2.3362   0.0000  3.1150 0 0
5  11 13 14 3 58.6152  0.0000 -58.6152  0.0000 0 0
5  11 13 15 3 58.6152  0.0000 -58.6152  0.0000 0 0
11 13 15 16 3 -0.7787 -2.3362   0.0000  3.1150 0 0
11 13 15 17 3 -0.7787 -2.3362   0.0000  3.1150 0 0
11 13 15 18 3  0.5275 -6.4016  -1.6957  7.5697 0 0
12 11 13 14 3  0.6280  1.8841   0.0000 -2.5121 0 0
12 11 13 15 3 58.6152  0.0000 -58.6152  0.0000 0 0
13 15 18 19 3  0.7662  2.2986   0.0000 -3.0647 0 0
13 15 18 20 3  0.7662  2.2986   0.0000 -3.0647 0 0
13 15 18 21 3  2.9308 -1.4654   0.2093 -1.6747 0 0
14 13 15 16 3  0.6280  1.8841   0.0000 -2.5121 0 0
14 13 15 17 3  0.6280  1.8841   0.0000 -2.5121 0 0
14 13 15 18 3  0.6657  1.9971   0.0000 -2.6620 0 0
15 18 21 22 3  0.6280  1.8841   0.0000 -2.5121 0 0
15 18 21 23 3  0.6280  1.8841   0.0000 -2.5121 0 0
15 18 21 24 3  2.9308 -1.4654   0.2093 -1.6747 0 0
16 15 18 19 3  0.6280  1.8841   0.0000 -2.5121 0 0
16 15 18 20 3  0.6280  1.8841   0.0000 -2.5121 0 0
16 15 18 21 3  0.6280  1.8841   0.0000 -2.5121 0 0
17 15 18 19 3  0.6280  1.8841   0.0000 -2.5121 0 0
17 15 18 20 3  0.6280  1.8841   0.0000 -2.5121 0 0
17 15 18 21 3  0.6280  1.8841   0.0000 -2.5121 0 0
18 21 24 25 3  0.6280  1.8841   0.0000 -2.5121 0 0
18 21 24 26 3  0.6280  1.8841   0.0000 -2.5121 0 0
18 21 24 27 3 -4.9635  6.2907   1.3105 -2.6377 0 0
19 18 21 22 3  0.6280  1.8841   0.0000 -2.5121 0 0
19 18 21 23 3  0.6280  1.8841   0.0000 -2.5121 0 0
19 18 21 24 3  0.6280  1.8841   0.0000 -2.5121 0 0
20 18 21 22 3  0.6280  1.8841   0.0000 -2.5121 0 0
20 18 21 23 3  0.6280  1.8841   0.0000 -2.5121 0 0
20 18 21 24 3  0.6280  1.8841   0.0000 -2.5121 0 0
21 24 27 28 3  4.8818  0.0000  -4.8818  0.0000 0 0
21 24 27 29 3  4.8358 -7.6577   1.6831  1.1388 0 0
22 21 24 25 3  0.6280  1.8841   0.0000 -2.5121 0 0
22 21 24 26 3  0.6280  1.8841   0.0000 -2.5121 0 0
22 21 24 27 3 -0.2093 -0.6280   0.0000  0.8374 0 0
23 21 24 25 3  0.6280  1.8841   0.0000 -2.5121 0 0
23 21 24 26 3  0.6280  1.8841   0.0000 -2.5121 0 0
23 21 24 27 3 -0.2093 -0.6280   0.0000  0.8374 0 0
24 27 29 30 3 20.5153  0.0000 -20.5153  0.0000 0 0
24 27 29 31 3 30.3083 -4.8148 -25.4934  0.0000 0 0
25 24 27 28 3  0.0000  0.0000   0.0000  0.0000 0 0
25 24 27 29 3  0.0000  0.0000   0.0000  0.0000 0 0
26 24 27 28 3  0.0000  0.0000   0.0000  0.0000 0 0
26 24 27 29 3  0.0000  0.0000   0.0000  0.0000 0 0
27 29 31 32 3 -0.2910 -0.8730   0.0000  1.1639 0 0
27 29 31 33 3 -0.2910 -0.8730   0.0000  1.1639 0 0
27 29 31 34 3 -4.7102  2.9224   1.7878  0.0000 0 0
28 27 29 30 3 20.5153  0.0000 -20.5153  0.0000 0 0
28 27 29 31 3 25.4934  0.0000 -25.4934  0.0000 0 0
29 31 34 35 3  0.0000  0.0000   0.0000  0.0000 0 0
29 31 34 37 3  0.0000  0.0000   0.0000  0.0000 0 0
30 29 31 32 3  0.0000  0.0000   0.0000  0.0000 0 0
30 29 31 33 3  0.0000  0.0000   0.0000  0.0000 0 0
30 29 31 34 3  0.0000  0.0000   0.0000  0.0000 0 0
31 34 35 36 3 30.3543  0.0000 -30.3543  0.0000 0 0
31 34 35 44 3 30.3543  0.0000 -30.3543  0.0000 0 0
31 34 37 38 3 30.3543  0.0000 -30.3543  0.0000 0 0
31 34 37 39 3 30.3543  0.0000 -30.3543  0.0000 0 0
32 31 34 35 3  0.0000  0.0000   0.0000  0.0000 0 0
32 31 34 37 3  0.0000  0.0000   0.0000  0.0000 0 0
33 31 34 35 3  0.0000  0.0000   0.0000  0.0000 0 0
33 31 34 37 3  0.0000  0.0000   0.0000  0.0000 0 0
34 35 44 41 3 30.3543  0.0000 -30.3543  0.0000 0 0
34 35 44 45 3 30.3543  0.0000 -30.3543  0.0000 0 0
34 37 39 40 3 30.3543  0.0000 -30.3543  0.0000 0 0
34 37 39 41 3 30.3543  0.0000 -30.3543  0.0000 0 0
35 34 37 38 3 30.3543  0.0000 -30.3543  0.0000 0 0
35 34 37 39 3 30.3543  0.0000 -30.3543  0.0000 0 0
35 44 41 39 3 30.3543  0.0000 -30.3543  0.0000 0 0
35 44 41 42 3 30.3543  0.0000 -30.3543  0.0000 0 0
35 44 45 46 3 12.5604  0.0000 -12.5604  0.0000 0 0
36 35 34 37 3 30.3543  0.0000 -30.3543  0.0000 0 0
36 35 44 41 3 30.3543  0.0000 -30.3543  0.0000 0 0
36 35 44 45 3 30.3543  0.0000 -30.3543  0.0000 0 0
37 39 41 42 3 30.3543  0.0000 -30.3543  0.0000 0 0
37 39 41 44 3 30.3543  0.0000 -30.3543  0.0000 0 0
38 37 39 40 3 30.3543  0.0000 -30.3543  0.0000 0 0
38 37 39 41 3 30.3543  0.0000 -30.3543  0.0000 0 0
39 41 42 43 3  7.0422  0.0000  -7.0422  0.0000 0 0
39 41 44 45 3 30.3543  0.0000 -30.3543  0.0000 0 0
40 39 41 42 3 30.3543  0.0000 -30.3543  0.0000 0 0
40 39 41 44 3 30.3543  0.0000 -30.3543  0.0000 0 0
41 44 45 46 3 12.5604  0.0000 -12.5604  0.0000 0 0
42 41 44 45 3 30.3543  0.0000 -30.3543  0.0000 0 0
43 42 41 44 3  7.0422  0.0000  -7.0422  0.0000 0 0
44 45 46 47 3  1.5910  4.7730   0.0000 -6.3640 0 0
44 45 46 48 3  1.5910  4.7730   0.0000 -6.3640 0 0
44 45 46 49 3  1.5910  4.7730   0.0000 -6.3640 0 0
```

OPLS UA force field parameters for capsaicin (capsOPLSUA.itp)

```
[ moleculetype ]
; Name nrexcl
CAPS     3

[ atoms ]
;   nr      type  resnr resid  atom  cgnr    charge      mass
     1       CH3      1  CAPS    CAU     1     0.000   15.0350
     2      CHS3      1  CAPS    CAT     1     0.000   13.0190
     3       CH3      1  CAPS    CAV     1     0.000   15.0350
     4      CHS2      1  CAPS    CAS     2     0.000   13.0190
     5      CHS2      1  CAPS    CAR     2     0.000   13.0190
     6       CH2      1  CAPS    CAQ     2     0.000   14.0270
     7       CH2      1  CAPS    CAP     3     0.000   14.0270
     8       CH2      1  CAPS    CAO     3     0.000   14.0270
     9       CH2      1  CAPS    CAN     3     0.000   14.0270
    10         C      1  CAPS    CAL     4     0.500   12.0110
    11         O      1  CAPS    OAM     4    -0.500   15.9994
    12         N      1  CAPS    NAK     5    -0.570   14.0067
    13         H      1  CAPS    HAB     5     0.370    1.0080
    14      CH2A      1  CAPS    CAJ     5     0.185   14.0270
    15       CAS      1  CAPS    CAC     6     0.015   12.0110
    16        CA      1  CAPS    CAD     6    -0.115   13.0190
    17        CA      1  CAPS    CAB     7    -0.115   13.0190
    18        CA      1  CAPS    CAA     7    -0.115   13.0190
    19       COH      1  CAPS    CAF     8     0.150   12.0110
    20        OH      1  CAPS    OAG     8    -0.585   15.9994
    21        HO      1  CAPS    HAA     8     0.435    1.0080
    22       COA      1  CAPS    CAE     9     0.135   12.0110
    23        OA      1  CAPS    OAH     9    -0.385   15.9994
    24      CH3A      1  CAPS    CAI     9     0.250   15.0350
    25        HA      1  CAPS    HAC     6     0.115    1.0080
    26        HA      1  CAPS    HAD     7     0.115    1.0080
    27        HA      1  CAPS    HAE     7     0.115    1.0080

[ bonds ]
; ai  aj  fu    c0, c1, ...
   1   2   1    0.153    224412.5
   2   3   1    0.153    224412.5
   2   4   1    0.150    265443.1
   4   5   1    0.134    459710.6
   5   6   1    0.150    265443.1
   6   7   1    0.153    224412.5
   7   8   1    0.153    224412.5
   8   9   1    0.153    224412.5
   9  10   1    0.152    265443.1
  10  11   1    0.123    477295.2
  10  12   1    0.134    410306.4
  12  13   1    0.096    363412.2
  12  14   1    0.145    282190.3
  14  15   1    0.153    265443.1
  15  16   1    0.140    392721.8
  15  17   1    0.140    392721.8
  16  22   1    0.140    392721.8
  17  18   1    0.140    392721.8
  18  19   1    0.140    392721.8
  19  20   1    0.136    392721.8
  19  22   1    0.140    392721.8
```

```
  20   21    1    0.096    463060.1
  22   23    1    0.136    376812.0
  23   24    1    0.143    376812.0
  25   16    1    0.108    307311.1
  26   17    1    0.108    307311.1
  27   18    1    0.108    307311.1

[ pairs ]
; ai aj fu
   1    5    1
   3    5    1
   2    6    1
   4    7    1
   8    5    1
   9    6    1
  10    7    1
   8   11    1
   8   12    1
   9   13    1
   9   14    1
  11   13    1
  11   14    1
  13   15    1
  15   10    1
  14   18    1
  14   22    1
  15   19    1
  15   23    1
  17   20    1
  17   12    1
  18   21    1
  18   23    1
  16   24    1
  19   24    1
  14   25    1
  14   26    1
  15   27    1
  16   26    1
  17   25    1
  19   26    1
  20   27    1
  23   25    1
  22   21    1
  20   23    1
  20   16    1
  26   27    1
  12   16    1
  16   18    1
  17   22    1
  19   25    1
  22   27    1

[ angles ]
; ai  aj  ak  fu    c0, c1, ...
   1   2   3   1    112.7       488.600
   1   2   4   1    111.1       527.537
   3   2   4   1    111.1       527.537
   2   4   5   1    124.0       586.152
   4   5   6   1    124.0       586.152
   5   6   7   1    111.1       527.537
   6   7   8   1    112.7       488.600
   7   8   9   1    112.7       488.600
   8   9  10   1    111.1       527.537
   9  10  11   1    120.4       669.888
   9  10  12   1    116.6       586.152
  11  10  12   1    122.9       669.888
  10  12  13   1    119.8       293.076
  10  12  14   1    121.9       418.680
  13  12  14   1    118.4       318.197
  12  14  15   1    109.7       669.888
  14  15  16   1    120.0       586.152
  14  15  17   1    120.0       586.152
  16  15  17   1    120.0       527.537
  15  16  22   1    120.0       527.537
  15  17  18   1    120.0       527.537
  17  18  19   1    120.0       527.537
  18  19  20   1    120.0       586.152
  18  19  22   1    120.0       527.537
  20  19  22   1    120.0       586.152
  19  20  21   1    109.0       593.076
  16  22  19   1    120.0       527.537
  16  22  23   1    120.0       586.152
  19  22  23   1    120.0       586.152
  22  23  24   1    111.0       628.020
  25  16  15   1    120.0       293.076
  25  16  22   1    120.0       293.076
  26  17  15   1    120.0       293.076
  26  17  18   1    120.0       293.076
  27  18  17   1    120.0       293.076
  27  18  19   1    120.0       293.076

[ dihedrals ]
; ai  aj  ak  al  fu    c0, c1, m, ...
   1   2   4   5   3      0.5275  -6.4016  -1.6957   7.5697   0.0   0.0
   3   2   4   5   3      0.5275  -6.4016  -1.6957   7.5697   0.0   0.0
   2   4   5   6   3     58.6152   0.0000 -58.6152   0.0000   0.0   0.0
   4   5   6   7   3      0.5275  -6.4016  -1.6957   7.5697   0.0   0.0
   8   7   6   5   3      2.9308  -1.4654   0.2093  -1.6747   0.0   0.0
   9   8   7   6   3      2.9308  -1.4654   0.2093  -1.6747   0.0   0.0
  10   9   8   7   3     -4.9635   6.2907   1.3105  -2.6377   0.0   0.0
   8   9  10  11   3      4.8818   0.0000  -4.8818   0.0000   0.0   0.0
   8   9  10  12   3      4.8358  -7.6577   1.6831   1.1388   0.0   0.0
   9  10  12  13   3     20.5153   0.0000 -20.5153   0.0000   0.0   0.0
   9  10  12  14   3     30.3083  -4.8148 -25.4934   0.0000   0.0   0.0
  11  10  12  13   3     20.5153   0.0000 -20.5153   0.0000   0.0   0.0
  11  10  12  14   3     25.4934   0.0000 -25.4934   0.0000   0.0   0.0
  13  12  14  15   3      0.0000   0.0000   0.0000   0.0000   0.0   0.0
  15  14  12  10   3     -4.7102   2.9224   1.7878   0.0000   0.0   0.0
  14  15  17  18   3     30.3543   0.0000 -30.3543   0.0000   0.0   0.0
  14  15  16  22   3     30.3543   0.0000 -30.3543   0.0000   0.0   0.0
  15  17  18  19   3     30.3543   0.0000 -30.3543   0.0000   0.0   0.0
  15  16  22  19   3     30.3543   0.0000 -30.3543   0.0000   0.0   0.0
  15  16  22  23   3     30.3543   0.0000 -30.3543   0.0000   0.0   0.0
  17  18  19  20   3     30.3543   0.0000 -30.3543   0.0000   0.0   0.0
  17  15  14  12   3      0.0000   0.0000   0.0000   0.0000   0.0   0.0
  18  19  20  21   3     14.6440   0.0000 -14.6440   0.0000   0.0   0.0
  18  19  22  23   3     30.3543   0.0000 -30.3543   0.0000   0.0   0.0
  16  22  23  24   3      9.2050   0.0000  -9.2050   0.0000   0.0   0.0
  19  22  23  24   3      9.2050   0.0000  -3.2050   0.0000   0.0   0.0
  14  15  16  25   3     30.3543   0.0000 -30.3543   0.0000   0.0   0.0
  14  15  17  26   3     30.3453   0.0000 -30.3543   0.0000   0.0   0.0
  15  17  18  27   3     30.3453   0.0000 -30.3543   0.0000   0.0   0.0
  16  15  17  26   3     30.3453   0.0000 -30.3543   0.0000   0.0   0.0
  17  15  16  25   3     30.3453   0.0000 -30.3453   0.0000   0.0   0.0
  19  18  17  26   3     30.3453   0.0000 -30.3453   0.0000   0.0   0.0
  20  19  18  27   3     30.3453   0.0000 -30.3453   0.0000   0.0   0.0
  23  22  16  25   3     30.3453   0.0000 -30.3453   0.0000   0.0   0.0
  22  19  20  21   3     14.6440   0.0000 -14.6440   0.0000   0.0   0.0
  20  19  22  23   3     30.3453   0.0000 -30.3453   0.0000   0.0   0.0
  20  19  22  16   3     30.3453   0.0000 -30.3453   0.0000   0.0   0.0
  26  17  18  27   3     30.3453   0.0000 -30.3453   0.0000   0.0   0.0
  12  14  15  16   3      0.0000   0.0000   0.0000   0.0000   0.0   0.0
  16  15  17  18   3     30.3453   0.0000 -30.3453   0.0000   0.0   0.0
  16  22  19  18   3     30.3453   0.0000 -30.3453   0.0000   0.0   0.0
  17  15  16  22   3     30.3453   0.0000 -30.3453   0.0000   0.0   0.0
  17  18  19  22   3     30.3453   0.0000 -30.3453   0.0000   0.0   0.0
  19  22  16  25   3     30.3453   0.0000 -30.3453   0.0000   0.0   0.0
  22  19  18  27   3     30.3453   0.0000 -30.3453   0.0000   0.0   0.0
```

OPLS AA force field parameters for octanol (octOPLSAA.itp)

```
[ moleculetype ]
; Name nrexcl
OCT      3

[ atoms ]
;   nr       type  resnr resid  atom  cgnr    charge      mass
     1        OHC      1  OCT     OH1     1     0.060     1.00800
     2        OHC      1  OCT     OH2     1     0.060     1.00800
     3        OHC      1  OCT     OH3     1     0.060     1.00800
     4        OCT      1  OCT     OCA     1    -0.180    12.01100
     5        OCT      1  OCT     OCB     2    -0.120    12.01100
     6        OHC      1  OCT     OH4     2     0.060     1.00800
     7        OHC      1  OCT     OH5     2     0.060     1.00800
     8        OCT      1  OCT     OCC     3    -0.120    12.01100
     9        OHC      1  OCT     OH6     3     0.060     1.00800
    10        OHC      1  OCT     OH7     3     0.060     1.00800
    11        OCT      1  OCT     OCD     4    -0.120    12.01100
    12        OHC      1  OCT     OH8     4     0.060     1.00800
    13        OHC      1  OCT     OH9     4     0.060     1.00800
    14        OCT      1  OCT     OCE     5    -0.120    12.01100
    15        OHC      1  OCT     OH10    5     0.060     1.00800
    16        OHC      1  OCT     OH11    5     0.060     1.00800
    17        OCT      1  OCT     OCF     6    -0.120    12.01100
    18        OHC      1  OCT     OH12    6     0.060     1.00800
    19        OHC      1  OCT     OH13    6     0.060     1.00800
    20        OCT      1  OCT     OCG     7    -0.120    12.01100
```

```
    21       OHC     1  OCT     OH14    7    0.060    1.00800
    22       OHC     1  OCT     OH15    7    0.060    1.00800
    23       OOC     1  OCT     OCH     8    0.145   12.01100
    24       OHC     1  OCT     OH16    8    0.060    1.00800
    25       OHC     1  OCT     OH17    8    0.060    1.00800
    26       OOH     1  OCT     OAI     8   -0.683   15.99940
    27       OHO     1  OCT     HAA     8    0.418    1.00800

[ bonds ]
; ai  aj  fu    c0, c1, ...
   4   1   1    0.10900   284512.0 ;
   4   2   1    0.10900   284512.0 ;
   4   3   1    0.10900   284512.0 ;
   4   5   1    0.15290   224262.4 ;
   5   6   1    0.10900   284512.0 ;
   5   7   1    0.10900   284512.0 ;
   5   8   1    0.15290   224262.4 ;
   8   9   1    0.10900   284512.0 ;
   8  10   1    0.10900   284512.0 ;
   8  11   1    0.15290   224262.4 ;
  11  12   1    0.10900   284512.0 ;
  11  13   1    0.10900   284512.0 ;
  11  14   1    0.15290   224262.4 ;
  14  15   1    0.10900   284512.0 ;
  14  16   1    0.10900   284512.0 ;
  14  17   1    0.15290   224262.4 ;
  17  18   1    0.10900   284512.0 ;
  17  19   1    0.10900   284512.0 ;
  17  20   1    0.15290   224262.4 ;
  20  21   1    0.10900   284512.0 ;
  20  22   1    0.10900   284512.0 ;
  20  23   1    0.15290   224262.4 ;
  23  24   1    0.10900   284512.0 ;
  23  25   1    0.10900   284512.0 ;
  23  26   1    0.14100   267776.0 ;
  26  27   1    0.09450   462750.4 ;

[ pairs ]
; ai  aj  fu    c0, c1, ...
   1   8   1 ;
   2   8   1 ;
   3   8   1 ;
   1   6   1 ;
   2   6   1 ;
   3   6   1 ;
   1   7   1 ;
   2   7   1 ;
   3   7   1 ;
   4  11   1 ;
   4   9   1 ;
   4  10   1 ;
   5  12   1 ;
   5  13   1 ;
   5  14   1 ;
   6   9   1 ;
   6  10   1 ;
   6  11   1 ;
   7   9   1 ;
   7  10   1 ;
   7  11   1 ;
   8  15   1 ;
   8  16   1 ;
   8  17   1 ;
   9  12   1 ;
   9  13   1 ;
   9  14   1 ;
  10  12   1 ;
  10  13   1 ;
  10  14   1 ;
  11  18   1 ;
  11  19   1 ;
  11  20   1 ;
  12  15   1 ;
  12  16   1 ;
  12  17   1 ;
  13  15   1 ;
  13  16   1 ;
  13  17   1 ;
  14  21   1 ;
  14  22   1 ;
  14  23   1 ;
  15  18   1 ;
  15  19   1 ;
  15  20   1 ;
  16  18   1 ;
  16  19   1 ;
  16  20   1 ;
  17  24   1 ;
  17  25   1 ;
  17  26   1 ;
  18  21   1 ;
  18  22   1 ;
  18  23   1 ;
  19  21   1 ;
  19  22   1 ;
  19  23   1 ;
  20  27   1 ;
  21  24   1 ;
  21  25   1 ;
  21  26   1 ;
  22  24   1 ;
  22  25   1 ;
  22  26   1 ;
  24  27   1 ;
  25  27   1 ;

[ angles ]
; ai  aj  ak  fu    c0, c1, ...
   1   4   2   1    107.8       552.288 ;
   1   4   3   1    107.8       552.288 ;
   2   4   3   1    107.8       552.288 ;
   1   4   5   1    110.7       627.600 ;
   2   4   5   1    110.7       627.600 ;
   3   4   5   1    110.7       627.600 ;
   4   5   6   1    110.7       627.600 ;
   4   5   7   1    110.7       627.600 ;
   4   5   8   1    112.7       976.273 ;
   6   5   7   1    107.8       552.288 ;
   6   5   8   1    110.7       627.600 ;
   7   5   8   1    110.7       627.600 ;
   5   8   9   1    110.7       627.600 ;
   5   8  10   1    110.7       627.600 ;
   5   8  11   1    112.7       976.546 ;
   9   8  10   1    107.8       552.288 ;
   9   8  11   1    110.7       627.600 ;
  10   8  11   1    110.7       627.600 ;
   8  11  12   1    110.7       627.600 ;
   8  11  13   1    110.7       627.600 ;
   8  11  14   1    112.7       976.546 ;
  12  11  13   1    107.8       552.288 ;
  12  11  14   1    110.7       627.600 ;
  13  11  14   1    110.7       627.600 ;
  11  14  15   1    110.7       627.600 ;
  11  14  16   1    110.7       627.600 ;
  11  14  17   1    112.7       976.546 ;
  15  14  16   1    107.8       552.288 ;
  15  14  17   1    110.7       627.600 ;
  16  14  17   1    110.7       627.600 ;
  14  17  18   1    110.7       627.600 ;
  14  17  19   1    110.7       627.600 ;
  14  17  20   1    112.7       976.546 ;
  18  17  19   1    107.8       552.288 ;
  18  17  20   1    110.7       627.600 ;
  19  17  20   1    110.7       627.600 ;
  17  20  21   1    110.7       627.600 ;
  17  20  22   1    110.7       627.600 ;
  17  20  23   1    112.7       976.546 ;
  21  20  22   1    107.8       552.288 ;
  21  20  23   1    110.7       627.600 ;
  22  20  23   1    110.7       627.600 ;
  20  23  24   1    110.7       627.600 ;
  20  23  25   1    110.7       627.600 ;
  20  23  26   1    109.5       836.800 ;
  24  23  25   1    107.8       552.288 ;
  24  23  26   1    109.5       585.760 ;
  25  23  26   1    109.5       585.760 ;
  23  26  27   1    108.5       920.480 ;

[ dihedrals ]
; ai  aj  ak  al fu    c0, c1, m, ...
  1   4   5   8  3   0.62760   1.88280   0.00000  -2.51040  0.0  0.0
  2   4   5   8  3   0.62760   1.88280   0.00000  -2.51040  0.0  0.0
  3   4   5   8  3   0.62760   1.88280   0.00000  -2.51040  0.0  0.0
  1   4   5   6  3   0.62760   1.88280   0.00000  -2.51040  0.0  0.0
  2   4   5   6  3   0.62760   1.88280   0.00000  -2.51040  0.0  0.0
  3   4   5   6  3   0.62760   1.88280   0.00000  -2.51040  0.0  0.0
  1   4   5   7  3   0.62760   1.88280   0.00000  -2.51040  0.0  0.0
  2   4   5   7  3   0.62760   1.88280   0.00000  -2.51040  0.0  0.0
  3   4   5   7  3   0.62760   1.88280   0.00000  -2.51040  0.0  0.0
  4   5   8  11  3   2.92880  -1.46440   0.20920  -1.67360  0.0  0.0
  4   5   8   9  3   0.62760   1.88280   0.00000  -2.51040  0.0  0.0
  4   5   8  10  3   0.62760   1.88280   0.00000  -2.51040  0.0  0.0
  5   8  11  12  3   0.62760   1.88280   0.00000  -2.51040  0.0  0.0
  5   8  11  13  3   0.62760   1.88280   0.00000  -2.51040  0.0  0.0
```

```
  5   8  11  14   3   2.92880  -1.46440   0.20920  -1.67360  0.0  0.0
  6   5   8   9   3   0.62760   1.88280   0.00000  -2.51040  0.0  0.0
  6   5   8  10   3   0.62760   1.88280   0.00000  -2.51040  0.0  0.0
  6   5   8  11   3   0.62760   1.88280   0.00000  -2.51040  0.0  0.0
  7   5   8   9   3   0.62760   1.88280   0.00000  -2.51040  0.0  0.0
  7   5   8  10   3   0.62760   1.88280   0.00000  -2.51040  0.0  0.0
  7   5   8  11   3   0.62760   1.88280   0.00000  -2.51040  0.0  0.0
  8  11  14  15   3   0.62760   1.88280   0.00000  -2.51040  0.0  0.0
  8  11  14  16   3   0.62760   1.88280   0.00000  -2.51040  0.0  0.0
  8  11  14  17   3   2.92880  -1.46440   0.20920  -1.67360  0.0  0.0
  9   8  11  12   3   0.62760   1.88280   0.00000  -2.51040  0.0  0.0
  9   8  11  13   3   0.62760   1.88280   0.00000  -2.51040  0.0  0.0
  9   8  11  14   3   0.62760   1.88280   0.00000  -2.51040  0.0  0.0
 10   8  11  12   3   0.62760   1.88280   0.00000  -2.51040  0.0  0.0
 10   8  11  13   3   0.62760   1.88280   0.00000  -2.51040  0.0  0.0
 10   8  11  14   3   0.62760   1.88280   0.00000  -2.51040  0.0  0.0
 11  14  17  18   3   0.62760   1.88280   0.00000  -2.51040  0.0  0.0
 11  14  17  19   3   0.62760   1.88280   0.00000  -2.51040  0.0  0.0
 11  14  17  20   3   2.92880  -1.46440   0.20920  -1.67360  0.0  0.0
 12  11  14  15   3   0.62760   1.88280   0.00000  -2.51040  0.0  0.0
 12  11  14  16   3   0.62760   1.88280   0.00000  -2.51040  0.0  0.0
 12  11  14  17   3   0.62760   1.88280   0.00000  -2.51040  0.0  0.0
 13  11  14  15   3   0.62760   1.88280   0.00000  -2.51040  0.0  0.0
 13  11  14  16   3   0.62760   1.88280   0.00000  -2.51040  0.0  0.0
 13  11  14  17   3   0.62760   1.88280   0.00000  -2.51040  0.0  0.0
 14  17  20  21   3   0.62760   1.88280   0.00000  -2.51040  0.0  0.0
 14  17  20  22   3   0.62760   1.88280   0.00000  -2.51040  0.0  0.0
 14  17  20  23   3   2.92880  -1.46440   0.20920  -1.67360  0.0  0.0
 15  14  17  18   3   0.62760   1.88280   0.00000  -2.51040  0.0  0.0
 15  14  17  19   3   0.62760   1.88280   0.00000  -2.51040  0.0  0.0
 15  14  17  20   3   0.62760   1.88280   0.00000  -2.51040  0.0  0.0
 16  14  17  18   3   0.62760   1.88280   0.00000  -2.51040  0.0  0.0
 16  14  17  19   3   0.62760   1.88280   0.00000  -2.51040  0.0  0.0
 16  14  17  20   3   0.62760   1.88280   0.00000  -2.51040  0.0  0.0
 17  20  23  24   3   0.62760   1.88280   0.00000  -2.51040  0.0  0.0
 17  20  23  25   3   0.62760   1.88280   0.00000  -2.51040  0.0  0.0
 17  20  23  26   3   2.92880   2.93716   0.00000  -3.91622  0.0  0.0
 18  17  20  21   3   0.62760   1.88280   0.00000  -2.51040  0.0  0.0
 18  17  20  22   3   0.62760   1.88280   0.00000  -2.51040  0.0  0.0
 18  17  20  23   3   0.62760   1.88280   0.00000  -2.51040  0.0  0.0
 19  17  20  21   3   0.62760   1.88280   0.00000  -2.51040  0.0  0.0
 19  17  20  22   3   0.62760   1.88280   0.00000  -2.51040  0.0  0.0
 19  17  20  23   3   0.62760   1.88280   0.00000  -2.51040  0.0  0.0
 20  23  26  27   3  -0.44350   3.83255   0.72801  -4.11705  0.0  0.0
 21  20  23  24   3   0.62760   1.88280   0.00000  -2.51040  0.0  0.0
 21  20  23  25   3   0.62760   1.88280   0.00000  -2.51040  0.0  0.0
 21  20  23  26   3   0.97905   2.93716   0.00000  -3.91622  0.0  0.0
 22  20  23  24   3   0.62760   1.88280   0.00000  -2.51040  0.0  0.0
 22  20  23  25   3   0.62760   1.88280   0.00000  -2.51040  0.0  0.0
 22  20  23  26   3   0.97905   2.93716   0.00000  -3.91622  0.0  0.0
 24  23  26  27   3   0.94140   2.82420   0.00000  -3.76560  0.0  0.0
 25  23  26  27   3   0.94140   2.82420   0.00000  -3.76560  0.0  0.0
```

Modified OPLS UA force field parameters for octanol (octOPLSUA.itp)

```
[ moleculetype ]
; Name nrexcl
OCT      3

[ atoms ]
;   nr       type  resnr resid  atom  cgnr    charge      mass
     1        OC3      1  OCT     cAA     1     0.000   15.0350
     2        OC2      1  OCT     cAB     1     0.000   14.0270
     3        OC2      1  OCT     cAC     1     0.000   14.0270
     4        OC2      1  OCT     cAD     2     0.000   14.0270
     5        OC2      1  OCT     cAE     2     0.000   14.0270
     6        OC2      1  OCT     cAF     3     0.000   14.0270
     7        OC2      1  OCT     cAG     3     0.000   14.0270
     8        OOC      1  OCT     cAH     4     0.265   14.0270
     9        OOA      1  OCT     oAI     4    -0.700   15.9994
    10        OHO      1  OCT     hAA     4     0.435    1.0080

[ bonds ]
; ai  aj  fu    c0, c1, ...
   1   2   1    0.1530    334720.0
   2   3   1    0.1530    334720.0
   3   4   1    0.1530    334720.0
   4   5   1    0.1530    334720.0
   5   6   1    0.1530    334720.0
   6   7   1    0.1530    334720.0
   7   8   1    0.1530    334720.0
   8   9   1    0.1430    334720.0
   9  10   1    0.0945    313800.0

[ pairs ]
; ai  aj  fu    c0, c1, ...
   1   4   1
   2   5   1
   3   6   1
   4   7   1
   5   8   1
   6   9   1
   7  10   1

[ angles ]
; ai  aj  ak  fu    c0, c1, ...
   1   2   3   1    112.0        263.59
   2   3   4   1    112.0        263.59
   3   4   5   1    112.0        263.59
   4   5   6   1    112.0        263.59
   5   6   7   1    112.0        263.59
   6   7   8   1    112.0        263.59
   7   8   9   1    108.0        334.72
   8   9  10   1    108.5        230.12

[ dihedrals ]
; ai  aj  ak  al  fu    c0, c1, m, ...
   4   3   2   1   3   8.367 16.818 1.134 -26.318 0 0
   5   4   3   2   3   8.367 16.818 1.134 -26.318 0 0
   6   5   4   3   3   8.367 16.818 1.134 -26.318 0 0
   7   6   5   4   3   8.367 16.818 1.134 -26.318 0 0
   8   7   6   5   3   8.367 16.818 1.134 -26.318 0 0
   9   8   7   6   3   6.983 17.736 0.887 -25.606 0 0
   7   8   9  10   3   2.822  2.943 0.485  -6.250 0 0
```

Force field parameters for DPPC (DPPC.itp)

```
[ moleculetype ]
;Name        nrexcl
DPPC           3

[atoms]
;   nr    type   resnr  residu    atom    cgnr       charge ;
     1     LC3N       1    DPPC      C1       1        0.40
     2     LC3N       1    DPPC      C2       1        0.40
     3     LC3N       1    DPPC      C3       1        0.40
     4      LNL       1    DPPC      N4       1       -0.50
     5      LC2       1    DPPC      C5       1        0.30
     6     LC2O       1    DPPC      C6       2        0.40
     7      LOS       1    DPPC      O7       2       -0.80
     8       LP       1    DPPC      P8       2        1.70
     9      LOM       1    DPPC      O9       2       -0.80
    10      LOM       1    DPPC     O10       2       -0.80
    11      LOS       1    DPPC     O11       2       -0.70
    12     LC2O       1    DPPC     C12       3        0.40
    13     LCH1       1    DPPC     C13       3        0.30
    14      LOS       1    DPPC     O14       3       -0.70
    15       LC       1    DPPC     C15       3        0.70
    16      LO2       1    DPPC     O16       3       -0.70
    17     LCH2       1    DPPC     C17       4        0.0
    18     LCH2       1    DPPC     C18       5        0.0
    19     LCH2       1    DPPC     C19       6        0.0
    20     LCH2       1    DPPC     C20       7        0.0
    21     LCH2       1    DPPC     C21       8        0.0
    22     LCH2       1    DPPC     C22       9        0.0
    23     LCH2       1    DPPC     C23      10        0.0
    24     LCH2       1    DPPC     C24      11        0.0
    25     LCH2       1    DPPC     C25      12        0.0
    26     LCH2       1    DPPC     C26      13        0.0
    27     LCH2       1    DPPC     C27      14        0.0
    28     LCH2       1    DPPC     C28      15        0.0
    29     LCH2       1    DPPC     C29      16        0.0
    30     LCH2       1    DPPC     C30      17        0.0
    31     LCH3       1    DPPC     C31      18        0.0
    32     LC2O       1    DPPC     C32      19        0.50
    33      LOS       1    DPPC     O33      19       -0.70
    34       LC       1    DPPC     C34      19        0.80
    35      LO2       1    DPPC     O35      19       -0.60
    36     LCH2       1    DPPC     C36      20        0.0
    37     LCH2       1    DPPC     C37      21        0.0
    38     LCH2       1    DPPC     C38      22        0.0
    39     LCH2       1    DPPC     C39      23        0.0
    40     LCH2       1    DPPC     C40      24        0.0
    41     LCH2       1    DPPC     C41      25        0.0
```

```
    42     LCH2       1    DPPC      C42       26       0.0
    43     LCH2       1    DPPC      C43       27       0.0
    44     LCH2       1    DPPC      C44       28       0.0
    45     LCH2       1    DPPC      C45       19       0.0
    46     LCH2       1    DPPC      C46       30       0.0
    47     LCH2       1    DPPC      C47       31       0.0
    48     LCH2       1    DPPC      C48       32       0.0
    49     LCH2       1    DPPC      C49       33       0.0
    50     LCH3       1    DPPC      C50       34       0.0

[bonds]
;  ai    aj funct
    1     4     1
    2     4     1
    3     4     1
    4     5     1
    5     6     1
    6     7     1
    7     8     1
    8     9     1
    8    10     1
    8    11     1
   11    12     1
   12    13     1
   13    14     1
   13    32     1
   14    15     1
   15    16     1
   15    17     1
   17    18     1
   18    19     1
   19    20     1
   20    21     1
   21    22     1
   22    23     1
   23    24     1
   24    25     1
   25    26     1
   26    27     1
   27    28     1
   28    29     1
   29    30     1
   30    31     1
   32    33     1
   33    34     1
   34    35     1
   34    36     1
   36    37     1
   37    38     1
   38    39     1
   39    40     1
   40    41     1
   41    42     1
   42    43     1
   43    44     1
   44    45     1
   45    46     1
   46    47     1
   47    48     1
   48    49     1
   49    50     1

[ pairs ]
;ai aj funct     c0           c1           c2           c3
  1  6  1  1.0324742e-03  3.5181067e-06  1.0324742e-03  3.5181067e-06
  2  6  1  1.0324742e-03  3.5181067e-06  1.0324742e-03  3.5181067e-06
  3  6  1  1.0324742e-03  3.5181067e-06  1.0324742e-03  3.5181067e-06
  4  7  1  3.2949910e-04  3.0539735e-07  3.2949910e-04  3.0539735e-07
  5  8  1  1.1086361e-03  3.4535341e-06  1.1086361e-03  3.4535341e-06
  6  9  1  5.1901029e-04  7.3857637e-07  5.1901029e-04  7.3857637e-07
  6 10  1  5.1901029e-04  7.3857637e-07  5.1901029e-04  7.3857637e-07
  6 11  1  4.8624808e-04  7.2038415e-07  4.8624808e-04  7.2038415e-07
  7 12  1  4.8624808e-04  7.2038415e-07  4.8624808e-04  7.2038415e-07
  8 13  1  7.5842381e-04  2.1771004e-06  7.5842381e-04  2.1771004e-06
  9 12  1  5.1901029e-04  7.3857637e-07  5.1901029e-04  7.3857637e-07
 10 12  1  5.1901029e-04  7.3857637e-07  5.1901029e-04  7.3857637e-07
 11 14  1  2.5916250e-04  1.8892500e-07  2.5916250e-04  1.8892500e-07
 11 32  1  4.8624808e-04  7.2038415e-07  4.8624808e-04  7.2038415e-07
 12 15  1  7.4539997e-04  2.1568903e-06  7.4539997e-04  2.1568903e-06
 12 33  1  4.8624808e-04  7.2038415e-07  4.8624808e-04  7.2038415e-07
 13 16  1  3.2011832e-04  1.4405955e-06  3.2011832e-04  1.4405955e-06
 13 17  1  6.0697598e-04  2.0682859e-06  6.0697598e-04  2.0682859e-06
 13 34  1  5.5338320e-04  1.6012958e-06  5.5338320e-04  1.6012958e-06
 14 18  1  4.3576181e-04  7.3062136e-07  4.3576181e-04  7.3062136e-07
 14 33  1  2.5916250e-04  1.8892500e-07  2.5916250e-04  1.8892500e-07
 15 19  1  6.6800642e-04  2.1875414e-06  6.6800642e-04  2.1875414e-06
 15 32  1  7.4539997e-04  2.1568903e-06  7.4539997e-04  2.1568903e-06
 16 18  1  3.8642497e-04  1.9680076e-06  3.8642497e-04  1.9680076e-06
 32 35  1  4.3119519e-04  1.9404326e-06  4.3119519e-04  1.9404326e-06
 32 36  1  8.1758876e-04  2.7859100e-06  8.1758876e-04  2.7859100e-06
 33 37  1  4.3576181e-04  7.3062136e-07  4.3576181e-04  7.3062136e-07
 34 38  1  6.6800642e-04  2.1875414e-06  6.6800642e-04  2.1875414e-06
 35 37  1  3.8642497e-04  1.9680076e-06  3.8642497e-04  1.9680076e-06

[ angles ]
;  ai    aj    ak funct           c0           c1
    1     4     2     1
    1     4     3     1
    1     4     5     1
    2     4     3     1
    2     4     5     1
    3     4     5     1
    4     5     6     1
    5     6     7     1
    6     7     8     1
    7     8     9     1
    7     8    10     1
    7     8    11     1
    8    11    12     1
    9     8    10     1
    9     8    11     1
   10     8    11     1
   11    12    13     1
   12    13    14     1
   12    13    32     1
   13    14    15     1
   13    32    33     1
   14    13    32     1
   14    15    16     1
   14    15    17     1
   15    17    18     1
   16    15    17     1
   17    18    19     1
   18    19    20     1
   19    20    21     1
   20    21    22     1
   21    22    23     1
   22    23    24     1
   23    24    25     1
   24    25    26     1
   25    26    27     1
   26    27    28     1
   27    28    29     1
   28    29    30     1
   29    30    31     1
   32    33    34     1
   33    34    35     1
   33    34    36     1
   34    36    37     1
   35    34    36     1
   36    37    38     1
   37    38    39     1
   38    39    40     1
   39    40    41     1
   40    41    42     1
   41    42    43     1
   42    43    44     1
   43    44    45     1
   44    45    46     1
   45    46    47     1
   46    47    48     1
   47    48    49     1
   48    49    50     1

[ dihedrals ]
;  ai    aj    ak    al funct    (func=2 is improper dihedral)
   13    14    32    12   2         35.264        334.72
   15    14    17    16   2          0.0          167.36
   34    33    36    35   2          0.0          167.36

[ dihedrals ]
;ai  aj  a   al funct  phi0  cp mult (func=1 is normal, 3=R-B)
  1   4   5   6    1    0       3.766   3
  4   5   6   7    1    0       5.858   3
  5   6   7   8    1    0       3.766   3
  6   7   8   11   1    0       1.046   3
  6   7   8   11   1    0       3.138   2
  7   8   11  12   1    0       1.046   3
  7   8   11  12   1    0       3.138   2
  8   11  12  13   1    0       3.766   3
  11  12  13  14   1    0       2.092   2
  11  12  13  32   1    0       5.858   3
  11  12  13  32   1    0       0.418   2
  12  13  32  33   1    0       5.858   3
```

```
  12   13   32   33    1    0       0.418   2
  12   13   14   15    1    0       3.766   3
  13   32   33   34    1    0       3.766   3
  13   14   15   17    1    180    16.736   2
  14   13   32   33    1    0       2.092   2
  14   15   17   18    1    0       0.418   6
  15   17   18   19    1    0       5.858   3
  17   18   19   20    3    9.2789 12.156 -13.120 -3.0597 26.240 -31.495
  18   19   20   21    3    9.2789 12.156 -13.120 -3.0597 26.240 -31.495
  19   20   21   22    3    9.2789 12.156 -13.120 -3.0597 26.240 -31.495
  20   21   22   23    3    9.2789 12.156 -13.120 -3.0597 26.240 -31.495
  21   22   23   24    3    9.2789 12.156 -13.120 -3.0597 26.240 -31.495
  22   23   24   25    3    9.2789 12.156 -13.120 -3.0597 26.240 -31.495
  23   24   25   26    3    9.2789 12.156 -13.120 -3.0597 26.240 -31.495
  24   25   26   27    3    9.2789 12.156 -13.120 -3.0597 26.240 -31.495
  25   26   27   28    3    9.2789 12.156 -13.120 -3.0597 26.240 -31.495
  26   27   28   29    3    9.2789 12.156 -13.120 -3.0597 26.240 -31.495
  27   28   29   30    3    9.2789 12.156 -13.120 -3.0597 26.240 -31.495
  28   29   30   31    3    9.2789 12.156 -13.120 -3.0597 26.240 -31.495
  13   32   33   34    1    0       3.766   3
  32   33   34   36    1    180    16.736   2
  33   34   36   37    1    0       0.418   6
  34   36   37   38    1    0       5.858   3
  36   37   38   39    3    9.2789 12.156 -13.120 -3.0597 26.240 -31.495
  37   38   39   40    3    9.2789 12.156 -13.120 -3.0597 26.240 -31.495
  38   39   40   41    3    9.2789 12.156 -13.120 -3.0597 26.240 -31.495
  39   40   41   42    3    9.2789 12.156 -13.120 -3.0597 26.240 -31.495
  40   41   42   43    3    9.2789 12.156 -13.120 -3.0597 26.240 -31.495
  41   42   43   44    3    9.2789 12.156 -13.120 -3.0597 26.240 -31.495
  42   43   44   45    3    9.2789 12.156 -13.120 -3.0597 26.240 -31.495
  43   44   45   46    3    9.2789 12.156 -13.120 -3.0597 26.240 -31.495
  44   45   46   47    3    9.2789 12.156 -13.120 -3.0597 26.240 -31.495
  45   46   47   48    3    9.2789 12.156 -13.120 -3.0597 26.240 -31.495
  46   47   48   49    3    9.2789 12.156 -13.120 -3.0597 26.240 -31.495
  47   48   49   50    3    9.2789 12.156 -13.120 -3.0597 26.240 -31.495
```

Force field parameters for DPPE (DPPE.itp)

```
[ moleculetype ]
;Name        nrexcl
DPPE          3

[atoms]
;   nr     type   resnr  residu    atom    cgnr       charge ;
     1     LH3N       1    DPPE      H1        1        0.40
     2     LH3N       1    DPPE      H2        1        0.40
     3     LH3N       1    DPPE      H3        1        0.40
     4      LNL       1    DPPE     N4E        1       -0.50
     5      LC2       1    DPPE     C5E        1        0.30
     6     LC2O       1    DPPE     C6E        2        0.40
     7      LOS       1    DPPE     O7E        2       -0.80
     8       LP       1    DPPE     P8E        2        1.70
     9      LOM       1    DPPE     O9E        2       -0.80
    10      LOM       1    DPPE    O10E        2       -0.80
    11      LOS       1    DPPE    O11E        2       -0.70
    12     LC2O       1    DPPE    C12E        3        0.40
    13     LCH1       1    DPPE    C13E        3        0.30
    14      LOS       1    DPPE    O14E        3       -0.70
    15       LC       1    DPPE    C15E        3        0.70
    16      LO2       1    DPPE    O16E        3       -0.70
    17     LCH2       1    DPPE    C17E        4        0.0
    18     LCH2       1    DPPE    C18E        5        0.0
    19     LCH2       1    DPPE    C19E        6        0.0
    20     LCH2       1    DPPE    C20E        7        0.0
    21     LCH2       1    DPPE    C21E        8        0.0
    22     LCH2       1    DPPE    C22E        9        0.0
    23     LCH2       1    DPPE    C23E       10        0.0
    24     LCH2       1    DPPE    C24E       11        0.0
    25     LCH2       1    DPPE    C25E       12        0.0
    26     LCH2       1    DPPE    C26E       13        0.0
    27     LCH2       1    DPPE    C27E       14        0.0
    28     LCH2       1    DPPE    C28E       15        0.0
    29     LCH2       1    DPPE    C29E       16        0.0
    30     LCH2       1    DPPE    C30E       17        0.0
    31     LCH3       1    DPPE    C31E       18        0.0
    32     LC2O       1    DPPE    C32E       19        0.50
    33      LOS       1    DPPE    O33E       19       -0.70
    34       LC       1    DPPE    C34E       19        0.80
    35      LO2       1    DPPE    O35E       19       -0.60
    36     LCH2       1    DPPE    C36E       20        0.0
    37     LCH2       1    DPPE    C37E       21        0.0
    38     LCH2       1    DPPE    C38E       22        0.0
    39     LCH2       1    DPPE    C39E       23        0.0
    40     LCH2       1    DPPE    C40E       24        0.0
    41     LCH2       1    DPPE    C41E       25        0.0
    42     LCH2       1    DPPE    C42E       26        0.0
    43     LCH2       1    DPPE    C43E       27        0.0
    44     LCH2       1    DPPE    C44E       28        0.0
    45     LCH2       1    DPPE    C45E       29        0.0
    46     LCH2       1    DPPE    C46E       30        0.0
    47     LCH2       1    DPPE    C47E       31        0.0
    48     LCH2       1    DPPE    C48E       32        0.0
    49     LCH2       1    DPPE    C49E       33        0.0
    50     LCH3       1    DPPE    C50E       34        0.0

[bonds]
;  ai    aj funct
    1     4     1
    2     4     1
    3     4     1
    4     5     1
    5     6     1
    6     7     1
    7     8     1
    8     9     1
    8    10     1
    8    11     1
   11    12     1
   12    13     1
   13    14     1
   13    32     1
   14    15     1
   15    16     1
   15    17     1
   17    18     1
   18    19     1
   19    20     1
   20    21     1
   21    22     1
   22    23     1
   23    24     1
   24    25     1
   25    26     1
   26    27     1
   27    28     1
   28    29     1
   29    30     1
   30    31     1
   32    33     1
   33    34     1
   34    35     1
   34    36     1
   36    37     1
   37    38     1
   38    39     1
   39    40     1
   40    41     1
   41    42     1
   42    43     1
   43    44     1
   44    45     1
   45    46     1
   46    47     1
   47    48     1
   48    49     1
   49    50     1

[ pairs ]
;ai aj funct     c0           c1             c2             c3
  4  7  1  3.2949910e-04  3.0539735e-07  3.2949910e-04  3.0539735e-07
  5  8  1  1.1086361e-03  3.4535341e-06  1.1086361e-03  3.4535341e-06
  6  9  1  5.1901029e-04  7.3857637e-07  5.1901029e-04  7.3857637e-07
  6 10  1  5.1901029e-04  7.3857637e-07  5.1901029e-04  7.3857637e-07
  6 11  1  4.8624808e-04  7.2038415e-07  4.8624808e-04  7.2038415e-07
  7 12  1  4.8624808e-04  7.2038415e-07  4.8624808e-04  7.2038415e-07
  8 13  1  7.5842381e-04  2.1771004e-06  7.5842381e-04  2.1771004e-06
  9 12  1  5.1901029e-04  7.3857637e-07  5.1901029e-04  7.3857637e-07
 10 12  1  5.1901029e-04  7.3857637e-07  5.1901029e-04  7.3857637e-07
 11 14  1  2.5916250e-04  1.8892500e-07  2.5916250e-04  1.8892500e-07
 11 32  1  4.8624808e-04  7.2038415e-07  4.8624808e-04  7.2038415e-07
 12 15  1  7.4539997e-04  2.1568903e-06  7.4539997e-04  2.1568903e-06
 12 33  1  4.8624808e-04  7.2038415e-07  4.8624808e-04  7.2038415e-07
 13 16  1  3.2011832e-04  1.4405955e-06  3.2011832e-04  1.4405955e-06
 13 17  1  6.0697598e-04  2.0682859e-06  6.0697598e-04  2.0682859e-06
 13 34  1  5.5338320e-04  1.6012958e-06  5.5338320e-04  1.6012958e-06
 14 18  1  4.3576181e-04  7.3062136e-07  4.3576181e-04  7.3062136e-07
 14 33  1  2.5916250e-04  1.8892500e-07  2.5916250e-04  1.8892500e-07
 15 19  1  6.6800642e-04  2.1875414e-06  6.6800642e-04  2.1875414e-06
 15 32  1  7.4539997e-04  2.1568903e-06  7.4539997e-04  2.1568903e-06
```

```
 16 18   1  3.8642497e-04   1.9680076e-06   3.8642497e-04   1.9680076e-06
 32 35   1  4.3119519e-04   1.9404326e-06   4.3119519e-04   1.9404326e-06
 32 36   1  8.1758876e-04   2.7859100e-06   8.1758876e-04   2.7859100e-06
 33 37   1  4.3576181e-04   7.3062136e-07   4.3576181e-04   7.3062136e-07
 34 38   1  6.6800642e-04   2.1875414e-06   6.6800642e-04   2.1875414e-06
 35 37   1  3.8642497e-04   1.9680076e-06   3.8642497e-04   1.9680076e-06

[ angles ]
;  ai    aj    ak funct           c0           c1
    1     4     2     1
    1     4     3     1
    1     4     5     1
    2     4     3     1
    2     4     5     1
    3     4     5     1
    4     5     6     1
    5     6     7     1
    6     7     8     1
    7     8     9     1
    7     8    10     1
    7     8    11     1
    8    11    12     1
    9     8    10     1
    9     8    11     1
   10     8    11     1
   11    12    13     1
   12    13    14     1
   12    13    32     1
   13    14    15     1
   13    32    33     1
   14    13    32     1
   14    15    16     1
   14    15    17     1
   15    17    18     1
   16    15    17     1
   17    18    19     1
   18    19    20     1
   19    20    21     1
   20    21    22     1
   21    22    23     1
   22    23    24     1
   23    24    25     1
   24    25    26     1
   25    26    27     1
   26    27    28     1
   27    28    29     1
   28    29    30     1
   29    30    31     1
   32    33    34     1
   33    34    35     1
   33    34    36     1
   34    36    37     1
   35    34    36     1
   36    37    38     1
   37    38    39     1
   38    39    40     1
   39    40    41     1
   40    41    42     1
   41    42    43     1
   42    43    44     1
   43    44    45     1
   44    45    46     1
   45    46    47     1
   46    47    48     1
   47    48    49     1
   48    49    50     1

[ dihedrals ]
;  ai    aj    ak    al funct    (func=2 is improper dihedral)
   13    14    32    12    2         35.264        334.72
   15    14    17    16    2          0.0          167.36
   34    33    36    35    2          0.0          167.36

[ dihedrals ]
;ai   aj   ak   al funct phi0 cp   mult (func=1 is nornal, 3=R-B)
  1    4    5    6    1    0        3.766    3
  4    5    6    7    1    0        5.858    3
  5    6    7    8    1    0        3.766    3
  6    7    8   11    1    0        1.046    3
  6    7    8   11    1    0        3.138    2
  7    8   11   12    1    0        1.046    3
  7    8   11   12    1    0        3.138    2
  8   11   12   13    1    0        3.766    3
 11   12   13   14    1    0        2.092    2
 11   12   13   32    1    0        5.858    3
 11   12   13   32    1    0        0.418    2
 12   13   32   33    1    0        5.858    3
 12   13   32   33    1    0        0.418    2
 12   13   14   15    1    0        3.766    3
 13   32   33   34    1    0        3.766    3
 13   14   15   17    1    180     16.736    2
 14   13   32   33    1    0        2.092    2
 14   15   17   18    1    0        0.418    6
 15   17   18   19    1    0        5.858    3
 17   18   19   20    3    9.2789  12.156  -13.120  -3.0597   26.240  -31.495
 18   19   20   21    3    9.2789  12.156  -13.120  -3.0597   26.240  -31.495
 19   20   21   22    3    9.2789  12.156  -13.120  -3.0597   26.240  -31.495
 20   21   22   23    3    9.2789  12.156  -13.120  -3.0597   26.240  -31.495
 21   22   23   24    3    9.2789  12.156  -13.120  -3.0597   26.240  -31.495
 22   23   24   25    3    9.2789  12.156  -13.120  -3.0597   26.240  -31.495
 23   24   25   26    3    9.2789  12.156  -13.120  -3.0597   26.240  -31.495
 24   25   26   27    3    9.2789  12.156  -13.120  -3.0597   26.240  -31.495
 25   26   27   28    3    9.2789  12.156  -13.120  -3.0597   26.240  -31.495
 26   27   28   29    3    9.2789  12.156  -13.120  -3.0597   26.240  -31.495
 27   28   29   30    3    9.2789  12.156  -13.120  -3.0597   26.240  -31.495
 28   29   30   31    3    9.2789  12.156  -13.120  -3.0597   26.240  -31.495
 13   32   33   34    1    0        3.766    3
 32   33   34   36    1    180     16.736    2
 33   34   36   37    1    0        0.418    6
 34   36   37   38    1    0        5.858    3
 36   37   38   39    3    9.2789  12.156  -13.120  -3.0597   26.240  -31.495
 37   38   39   40    3    9.2789  12.156  -13.120  -3.0597   26.240  -31.495
 38   39   40   41    3    9.2789  12.156  -13.120  -3.0597   26.240  -31.495
 39   40   41   42    3    9.2789  12.156  -13.120  -3.0597   26.240  -31.495
 40   41   42   43    3    9.2789  12.156  -13.120  -3.0597   26.240  -31.495
 41   42   43   44    3    9.2789  12.156  -13.120  -3.0597   26.240  -31.495
 42   43   44   45    3    9.2789  12.156  -13.120  -3.0597   26.240  -31.495
 43   44   45   46    3    9.2789  12.156  -13.120  -3.0597   26.240  -31.495
 44   45   46   47    3    9.2789  12.156  -13.120  -3.0597   26.240  -31.495
 45   46   47   48    3    9.2789  12.156  -13.120  -3.0597   26.240  -31.495
 46   47   48   49    3    9.2789  12.156  -13.120  -3.0597   26.240  -31.495
 47   48   49   50    3    9.2789  12.156  -13.120  -3.0597   26.240  -31.495
```

Bond and angle parameters for DPPC and DPPE

```
[ bondtypes ]
  ; i     j  func     b0          kb
  LNL LC3N     1    0.147      376560
  LNL  LC2     1    0.147      376560
  LC2 LC2O     1    0.153      334720
  LOS LC2O     1    0.143      251040
  LOS   LP     1    0.161      251040
  LOM   LP     1    0.148      376560
  LO2   LC     1    0.123      502080
 LCH1 LC2O     1    0.153      334720
  LOS LCH1     1    0.143      251040
  LOS   LC     1    0.136      376560
   LC LCH2     1    0.153      334720
 LCH2 LCH3     1    0.153      334720
 LCH2 LCH2     1    0.153      334720
  LNL LH3N     1    0.100      374468
 LCH1 LCH2     1    0.153      334720
 LCH1 LCH1     1    0.139      418400

[ angletypes ]
  ; i     j     k    func   c0          c1
 LC3N   LNL  LC3N     1   109.5        334.72
 LC3N   LNL   LC2     1   109.5        376.56
  LNL   LC2  LC2O     1   109.5        460.24
  LC2  LC2O   LOS     1   109.5        460.24
 LC2O   LOS    LP     1   120.0        397.48
  LOS    LP  LOM     1   109.6        397.48
  LOS    LP  LOS     1   103.0        397.48
  LOM    LP  LOM     1   120.0        585.76
  LOS  LC2O  LCH1     1   111.0        460.24
 LC2O  LCH1   LOS     1   109.5        460.24
 LC2O  LCH1  LC2O     1   109.5        460.24
 LCH1   LOS    LC     1   120.0        418.40
 LC2O   LOS    LC     1   120.0        418.40
  LOS    LC   LO2     1   124.0        502.08
  LOS    LC  LCH2     1   115.0        502.08
  LO2    LC  LCH2     1   121.0        502.08
   LC  LCH2  LCH2     1   111.0        460.24
 LCH2  LCH2  LCH2     1   111.0        460.24
 LCH2  LCH2  LCH3     1   111.0        460.24
 LH3N   LNL  LH3N     1   109.5        334.72
 LH3N   LNL   LC2     1   109.5        376.56
 LCH1  LCH1  LCH2     1   120.0        502.08
 LCH1  LCH2  LCH2     1   111.0        460.24
```

SPC force field parameters for water (SPC.itp)

```
[ moleculetype ]
; molname nrexcl
WAT 2

[ atoms ]
;   nr   type  resnr residue  atom   cgnr     charge       mass
     1    OW    1 WAT     OW      1      -0.82
     2    HW    1 WAT    HW1      1       0.41
     3    HW    1 WAT    HW2 1       0.41

#ifdef FLEXIBLE
[ bonds ]
; i j funct length force.c.
1 2 1 0.1 345000 0.1     345000
1 3 1 0.1 345000 0.1     345000

[ angles ]
; i j k funct angle force.c.
2 1 3 1 109.47 383 109.47 383
#else
[ settles ]
; OW funct doh dhh
1 1 0.1 0.16333

[ exclusions ]
1 2 3
2 1 3
3 1 2
#endif
```

A.2.2 Non-bonded Parameter Files

OPLS AA non-bonded parameters for capsaicin (capsOPLSAAnb.itp)

```
[ atomtypes ]
; name      mass  charge  ptype     C6            C12
  CCT     12.0110   0.00     A   +2.0305E-03   +3.7326E-06
  CHC      1.0080   0.00     A   +1.2266E-04   +2.9946E-08
  CCM     12.0110   0.00     A   +2.5480E-03   +5.0991E-06
  CHE      1.0080   0.00     A   +1.0092E-04   +2.0270E-08
  CC      12.0110   0.00     A   +4.8900E-03   +1.3599E-05
  CO      15.9994   0.00     A   +2.3650E-03   +1.5910E-06
  CN      14.0067   0.00     A   +3.3550E-03   +3.9536E-06
  CH       1.0080   0.00     A   +0.0000E+00   +0.0000E+00
  CCA     12.0110   0.00     A   +2.3463E-03   +4.6966E-06
  CHA      1.0080   0.00     A   +9.6013E-05   +2.4677E-08
  COH     15.9994   0.00     A   +2.3840E-03   +1.9955E-06
  CHO      1.0080   0.00     A   +0.0000E+00   +0.0000E+00
  COS     15.9994   0.00     A   +1.3950E-03   +8.2956E-07
```

OPLS UA non-bonded parameters for capsaicin (capsOPLSUAnb.itp)

```
[ atomtypes ]
; name      mass    charge ptype      C6            C12
  CH3     15.0350   0.00   A     +6.9810E-03   +1.9414E-05
  CHS3    13.0190   0.00   A     +4.3600E-03   +1.4199E-05
  CHS2    13.0190   0.00   A     +5.7950E-03   +1.7450E-05
  CH2     14.0270   0.00   A     +7.0020E-03   +2.4830E-05
  C       12.0110   0.00   A     +4.8870E-03   +1.3589E-05
  O       15.9994   0.00   A     +2.3640E-03   +1.5898E-06
  N       14.0067   0.00   A     +3.3530E-03   +3.9511E-06
  H        1.0080   0.00   A     +0.0000E+00   +0.0000E+00
  CH2A    14.0270   0.00   A     +5.9460E-03   +1.7903E-05
  CA      12.0110   0.00   A     +2.3450E-03   +4.6937E-06
  CAS     12.0110   0.00   A     +2.3450E-03   +4.6937E-06
  HA       1.0080   0.00   A     +1.0083E-04   +2.0253E-08
  COH     12.0110   0.00   A     +2.3450E-03   +4.6937E-06
  OH      15.9994   0.00   A     +2.3820E-03   +1.9942E-06
  HO       1.0080   0.00   A     +0.0000E+00   +0.0000E+00
  COA     12.0110   0.00   A     +2.3450E-03   +4.6937E-06
```

OPLS AA non-bonded parameters for octanol (octOPLSAAnb.itp)

```
[ atomtypes ]
; name      mass    charge ptype      C6            C12
  OCT     12.0110   0.00   A     +2.0305E-03   +3.7326E-06
  OHC      1.0080   0.00   A     +1.2258E-04   +2.9926E-08
  OOC     12.0110   0.00   A     +2.0305E-03   +3.7326E-06
  OOH     15.9994   0.00   A     +2.6244E-03   +2.4208E-06
  OHO      1.0080   0.00   A     +0.0000E-00   +0.0000E-00
```

OPLS UA non-bonded parameters for octanol (octOPLSUAnb.itp)

```
[ atomtypes ]
; name      mass    charge ptype      C6            C12
  OC3     15.0350   0.00   A     +8.9020E-03   +3.1564E-05
  OC2     14.0270   0.00   A     +7.0030E-03   +2.4849E-05
  OOC     14.0270   0.00   A     +7.0030E-03   +2.4849E-05
  OOA     15.9994   0.00   A     +2.3820E-03   +1.9942E-06
  OHO      1.0080   0.00   A     +0.0000E-00   +0.0000E-00
```

Non-bonded parameters for DPPC and DPPE (LIPIDnb.itp)

```
[ atomtypes ]
; name     mass    charge ptype      C6           C12
  LC3N    15.0350   0.000  A   +0.93477E-02   +0.36047E-04
  LNL     14.0067   0.000  A   +0.33514E-02   +0.39494E-05
  LC2     14.0270   0.000  A   +0.85953E-02   +0.30478E-04
  LC2O    14.0270   0.000  A   +0.72985E-02   +0.21975E-04
  LOS     15.9994   0.000  A   +0.20733E-02   +0.15114E-05
  LP      30.9738   0.000  A   +0.91516E-02   +0.25045E-04
  LOM     15.9994   0.000  A   +0.23621E-02   +0.15887E-05
  LCH1    13.0190   0.000  A   +0.40226E-02   +0.12112E-04
  LC      12.0110   0.000  A   +0.48722E-02   +0.13549E-04
  LO2     15.9994   0.000  A   +0.16304E-02   +0.10966E-04
  LCH2    14.0270   0.000  A   +0.58616E-02   +0.22604E-04
  LCH3    15.0350   0.000  A   +0.87924E-02   +0.33906E-04
  LH3N     1.0080   0.000  A   +0.00000E+00   +0.00000E+00
```

Non-bonded parameters for SPC Water (SPCnb.itp)

```
[ atomtypes ]
; name     mass    charge ptype      C6           C12
  OW    15.99940   0.000  A   +0.26171E-02   +0.26331E-05
  HW     1.00800   0.000  A   +0.00000E+00   +0.00000E+00
```

A.2.3 General Force Field Parameter Files

OPLS UA force field parameters (ffOPLSUA.itp)

```
[ defaults ]
; nbfunc comb-rule gen-pairs  fudgeLJ   fudgeQQ
    1      1         yes       0.125      0.5
```

OPLS AA force field parameters (ffOPLSAA.itp)

```
[ defaults ]
; nbfunc comb-rule gen-pairs  fudgeLJ   fudgeQQ
    1      1        yes       0.5        0.5
```

Each force field has specific parameters that are needed to describe the treatment of the van der Waals potential and the 1,4 pair interactions. In GROMACS, these parameters are defined in a separate file shown above. The value of `nbfunc` determines the treatment of the van der Waals interactions. For this example, `nbfunc 1` defines the Lennard Jones potential using C6 and C12 parameters. The `comb-rule` defines the combination rule that is used to combine the C6 and C12 parameters of non-bonded interactions. For this example, `comb-rule 1` defines the combination rule to be a geometric average. The `fudgeLJ` and `FudgeQQ` values are the scaling factors for the Lennard Jones and Coulombic interactions, respectively. For the Lipids, the pairs are listed explicitly in the bonded parameter files in Appendix A.2.

Appendix B

This Appendix contains information supporting Chapter 3

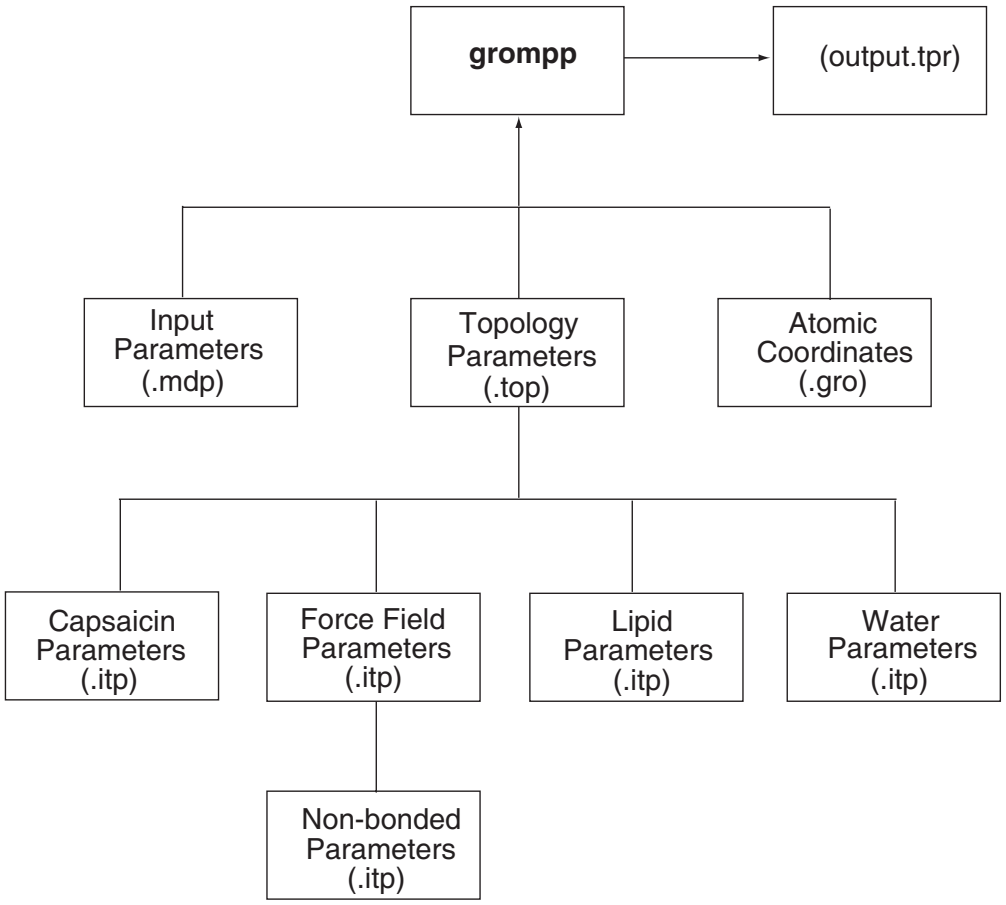

Figure B.1: Flow chart showing the required files for `grompp` , the GROMACS utility that generates the file needed for both energy minimization and molecular dynamics.

In GROMACS, the `grompp` utility generates a `.tpr` file that is needed to perform molecular dynamics. The inputs to this file contain the simulation parameters, atomic coordinates, and force field parameters. Figure B.1 shows a flowchart depicting the input files needed for `grompp` , and the dependencies required for each files.

Energy minimization input file (min.mdp)

```
; VARIOUS PREPROCESSING OPTIONS
title                    = Title of System
; Location of C preprocessor
cpp                      = /lib/cpp
include                  = -I../../ffdppccaps

; RUN CONTROL PARAMETERS
;choose method, steep = steepest descent
integrator               = steep

; ENERGY MINIMIZATION OPTIONS
; Maximum force tolerance and initial displacement
emtol                    = 10
emstep                   = 0.01
; Max number of iterations
niter                    = 20000

; OUTPUT CONTROL OPTIONS
; Output frequency for coords (x), velocities (v) and forces (f)
nstxout                  = 10
nstvout                  = 0
nstfout                  = 0
; Output frequency for energies to log file and energy file
nstlog                   = 1
nstenergy                = 1
; Output frequency and precision for xtc file
nstxtcout                = 10
xtc-precision            = 1000

; NEIGHBORSEARCHING PARAMETERS
; nblist update frequency
nstlist                  = 10
; ns algorithm (simple or grid)
ns_type                  = grid
; Periodic boundary conditions: xyz (default), no (vacuum)
; or full (infinite systems only)
pbc                      = xyz
; nblist cut-off
rlist                    = 1.0

; OPTIONS FOR ELECTROSTATICS AND VDW
; Method for doing electrostatics
coulombtype              = cut-off
rcoulomb                 = 1.5
; Method for doing Van der Waals
vdw-type                 = Cut-off
; cut-off lengths
rvdw                     = 1.0
; Apply long range dispersion corrections for Energy and Pressure
DispCorr                 = EnerPres
; Spacing for the PME/PPPM FFT grid
fourierspacing           = 0.12
; EWALD/PME/PPPM parameters
pme_order                = 8
ewald_rtol               = 1e-05
ewald_geometry           = 3d
optimize_fft             = yes

; OPTIONS FOR WEAK COUPLING ALGORITHMS
; Temperature coupling
tcoupl                   = berendsen
```

```
; Groups to couple separately
tc_grps                  = CAPS DPPC WAT
; Time constant (ps) and reference temperature (K)
tau_t                    = 0.1 0.1 0.1
ref_t                    = 323 323 323
; Pressure coupling
Pcoupl                   = berendsen
Pcoupltype               = anisotropic
; Time constant (ps), compressibility (1/bar) and reference P (bar)
tau_p                    = 2.0
compressibility          = 4.6e-5 4.6e-5 4.6e-5 0.0 0.0 0.0
ref_p                    = 1.0 1.0 1.0 0.0 0.0 0.0

; GENERATE VELOCITIES FOR STARTUP RUN
gen_vel                  = no
gen_temp                 = 323
gen_seed                 = -1

; OPTIONS FOR BONDS
constraints              = all-bonds
; Type of constraint algorithm
constraint_algorithm     = lincs
; Use successive overrelaxation to reduce the number of shake iterations
Shake-SOR                = no
; Relative tolerance of shake
shake-tol                = 0.0001
; Highest order in the expansion of the constraint coupling matrix
lincs-order              = 4
```

Energy minimization input file (min.mdp)

```
; VARIOUS PREPROCESSING OPTIONS
title                    = Capsaicin / DPPC / DPPE /Water
; Preprocessor - specify a full path if necessary.
cpp                      = /usr/bin/cpp
; Location of referenced force field files
include                  = -I../forcefield

; RUN CONTROL PARAMETERS
; choose method, md = molecular dynamics leap frog algorithm
integrator               = md
; Start time and timestep in ps
tinit                    = 0
dt                       = 0.002
; number of MD steps
nsteps                   = 5000000

; OUTPUT CONTROL OPTIONS
; Output frequency for coords (x), velocities (v) and forces (f)
nstxout                  = 2000
nstvout                  = 2000
nstfout                  = 0
; Checkpointing helps you continue after crashes
nstcheckpoint            = 1000
; Output frequency for energies to log file and energy file
nstlog                   = 2000
nstenergy                = 2000
; Output frequency and precision for xtc file
nstxtcout                = 2000
xtc-precision            = 1000

; NEIGHBORSEARCHING PARAMETERS
; nblist update frequency
nstlist                  = 10
; ns algorithm (simple or grid)
ns_type                  = grid
; Periodic boundary conditions: xyz (default), no (vacuum)
; or full (infinite systems only)
pbc                      = xyz
; nblist cut-off
rlist                    = 0.9
domain-decomposition     = no

; OPTIONS FOR ELECTROSTATICS AND VDW
; Method for doing electrostatics
coulombtype              = PME
; switching function length (nm)
rcoulomb-switch          = 0
; coulomb real space cut-off (nm)
rcoulomb                 = 0.9
; Method for doing Van der Waals
vdw-type                 = Cut-off
; cut-off lengths
rvdw-switch              = 0
rvdw                     = 0.9
; Apply long range dispersion corrections for Energy and Pressure
DispCorr                 = EnerPres
; Spacing for the PME FFT grid
fourierspacing           = 0.12
        = 0
; PME parameters
pme_order                = 4
```

```
ewald_rtol              = 1e-05
ewald_geometry          = 3d
epsilon_surface         = 0
optimize_fft            = yes

; OPTIONS FOR WEAK COUPLING ALGORITHMS
; Temperature coupling
tcoupl                  = berendsen
; Groups to couple separately
tc_grps                 = CAPS DPPC DPPE WAT
; Time constant (ps) and reference temperature (K)
tau_t                   = 0.1 0.1 0.1 0.1
ref_t                   = 323 323 323 323
; Pressure coupling
Pcoupl                  = berendsen
Pcoupltype              = semiisotropic
; Time constant (ps), compressibility (1/bar) and reference P (bar)
tau_p                   = 2.0
compressibility         = 4.6e-5 4.6e-5
ref_p                   = 1.0 1.0

; GENERATE VELOCITIES FOR STARTUP RUN
gen_vel                 = yes
gen_temp                = 323
gen_seed                = -1

; OPTIONS FOR BONDS
constraints             = all-bonds
; Type of constraint algorithm
constraint_algorithm    = lincs
```

Coordinate file (coordinate.gro)

The GROMACS coordinate file format contains the residue number, residue name, atom name, atom number; the Cartesian x, y, and z coordinates in (nm), and the x, y, and z components of the atoms velocity, respectively. The coordinate file atom sequence in the residue and the atom name must match those used in the force field files in Appendix A. The first and second lines of the coordinate file contain a description of the system and the number of atoms, respectively. The last line is the size of the simulation box vectors (nm) in the Cartesian coordinates.

```
System Title
35948
    1CAPS   CAU    1   4.656   1.995   3.736  0.0265 -0.1085  0.3090
    1CAPS   CAT    2   4.706   1.896   3.631  0.2568  0.1075  0.2137
    1CAPS   CAV    3   4.810   1.977   3.553  0.2599  0.0606  0.1696
    1CAPS   CAS    4   4.763   1.762   3.669 -0.1338 -0.2601 -0.4823
    1CAPS   CAR    5   4.793   1.712   3.790 -0.3178 -0.4920 -0.5323
    1CAPS   CAQ    6   4.849   1.576   3.820  0.1197 -0.2800 -0.3885
    1CAPS   CAP    7   4.890   1.567   3.967 -0.9153  0.3824 -0.0507
    1CAPS   CAO    8   4.860   1.432   4.033 -0.3679 -0.0706 -0.7184
    1CAPS   CAN    9   4.710   1.410   4.050 -0.3262  0.2189  0.0570
    .
    .
    .
    .
  7949WAT    OW34946   1.767   5.011   4.979  0.5752  0.1669 -0.7412
  7949WAT   HW135947   1.753   4.929   5.034  1.2965  0.3121 -0.3333
  7949WAT   HW235948   1.692   5.075   4.995  0.9869  0.3784  0.3920
   8.33582  10.04338   6.70828
```

Topology file (topology.top)

The topology file contains the number of molecules by type present in the simulation box. The force field parameters for these molecules must be referenced, where their location is defined in the `include = -I../forcefield` line of the `.mdp` file. The `[ system ]` section is the name of the system. The `[ molecules ]` section must contain the number of each molecule type in the simulation box in the order they appear in the coordinate file. In this example the are 12 capsaicin, 192 DPPC, 64 DPPE, and 9549 water molecules.

```
; topology for a mixed bilayer with 256 lipids, 7680 SPC water
; molecules, and 12 capsaicin molecules


; Files that must be included.  The location of these files must
; be specified in the MD parameter .mdp file.
#include "ffOPLSUA.itp"
#include "DPPC.itp"
#include "DPPE.itp"
#include "SPC.itp"
#include "capsOPLSUA.itp"

[ system ]
; name
Pure DPPC bilayer with 256 lipids and 7680 water molecules

[ molecules ]
; name  number
CAPS     12
DPPC     192
DPPE     64
WAT      9549
```

Appendix C

This Appendix contains files used to insert capsaicin into the 1-octanol/water and lipid systems.

The insert.sh file references the insert.pl file. The file names for the configuration of 1-octanol/water or the lipid bilayers are hard coded as `system.gro` , and the configuration containing capsaicin is hard coded as `infile.gro` .

File (insert.sh)

```
cut -b 1-5 infile.gro > 1
cut -b 6-9 infile.gro > 2
cut -b 10-15 infile.gro > 3
cut -b 16-46 infile.gro > 4
paste --delimiters=' ' 1 2 3 4 > input.gro
cut -b 1-5 system.gro > 1
cut -b 6-9 system.gro > 2
cut -b 10-15 system.gro > 3
cut -b 16- system.gro > 4
paste --delimiters=' ' 1 2 3 4 > sys.gro
./insert.pl -f input.gro -s sys.gro -fo insertout.gro -xc 5.67 -yc 6.21 -zc 9.5 -fo outfile.gro -fo2 outfile2.gro -vdw 0.13
rm 1
rm 2
rm 3
rm 4
cut -b 1-5 finaloutput.gro > 11
cut -b 7-11 finaloutput.gro > 22
cut -b 13-17 finaloutput.gro > 33
cut -b 19- finaloutput.gro > 44
paste --delimiters= 11 22 33 44 > system_out.gro
rm 11
rm 22
rm 33
rm 44
```

File (insert.pl)

```
#!/usr/bin/perl

#set up parsable command line
%argh = @ARGV ;

# Usage : Arguments
# -f  : Required Gro File containing coordinates of single molocule for inserting
# -o    : Required Final output file
# -fo   : File containing new coordinates of insert molocule w.r.t defined center
# -fo2  : Gro File containing insert molocule's contribution to final gro configuration
# -fo3  : Temporary output file of total system ( optional for checking work )
# -fo4  : Final output file, feeds into check.gro ( optional at this point )
# -inmol: Required residue name of inserted molocule ex. DPPC, WATER, CAPS ...
# -s    : Required Gro File containing system that molecules are to be inserted into
# -zl   : Lower limit of z
# -zu   : upper limit of z
# -xc   : Required x-coordinate for center of insertion
# -yc   : Required y-coordinate for center of insertion
# -zc   : Required z-coordinate for center of insertion
# -vdw  : Required Van Der Waals radius or deletion radius

# parse
# define input file ; molocule for inserting
if (defined($argh{"-f"})){
    $infile = $argh{"-f"} ;
} else {
    print " input file not set (-f) - using input.gro\n" ;
    $infile = "input.gro" ;
}
# Final output file name
if (defined($argh{"-o"})){
    $finaloutput = $argh{"-o"} ;
} else {
    print " final output file not set (-o) - using finaloutput.gro\n" ;
    $finaloutput = "finaloutput.gro" ;
}

# define output file name for newly inserted molocule coordinates
if (defined($argh{"-fo"})){
    $outfile = $argh{"-fo"} ;
} else {
    print " output file not set (-fo) - using outfile.gro\n" ;
    $infile = "outfile.gro" ;
}
# Temporary outfile for checking work
```

```
if (defined($argh{"-fo2"})){
    $outfile2 = $argh{"-fo2"} ;
} else {
    print " output file not set (-fo2) - using outfile2.gro\n" ;
    $outfile2 = "outfile2.gro" ;
}
# Final out put file
if (defined($argh{"-fo3"})){
    $outfile3 = $argh{"-fo3"} ;
} else {
    print " output file not set (-fo3) - using outfile3.gro\n" ;
    $outfile3 = "outfile3.gro" ;
}
# For real this time, this is the final file
if (defined($argh{"-fo4"})){
    $outfile4 = $argh{"-fo4"} ;
} else {
    print " output file not set (-fo3) - using outfile4.gro\n" ;
    $outfile4 = "outfile4.gro" ;
}

# Keep log of 1's for residues, this is just a check file
if (defined($argh{"-keep"})){
    $keepit = $argh{"-keep"} ;
} else {
    print " output file not set (-keep) - using bilayerout.gro\n" ;
    $keepit = "keepit.itp" ;
}


# define residue name for insert molocule; must be compatible with -f file
if (defined($argh{"-inmol"})){
    $inmol = $argh{"-inmol"} ;
} else {
    print " Insert Molocule not set (-inmol) - using CAPS \n" ;
    $inmol = "CAPS";
}
# define system that molocule is being inserted into
if (defined($argh{"-s"})){
    $system = $argh{"-s"} ;
} else {
    print " System not set (-s) - using system.gro \n" ;
    $system = "system.gro";
}

# Lower limit in z; based on non-water phase limitations
if (defined($argh{"-zl"})){
    $zl = $argh{"-zl"} ;
} else {
    print " Lower limit z not set (-zl) - using 0 \n" ;
    $z1 = 0 ;
}
# Upper limit in z ; based on non-water phase limitations
if (defined($argh{"-zu"})){
    $zu = $argh{"-zu"} ;
} else {
    print " Upper limit z not set (-zl) - using 0 \n" ;
    $zu = 0 ;
}
# Define x, y, and z coordinate for center of insert molocule
if (defined($argh{"-xc"})){
    $xc = $argh{"-xc"} ;
} else {
    print " x insert coordinate not set (option -xc) - using 0 \n" ;
    $xc = 0 ;
}
if (defined($argh{"-yc"})){
    $yc = $argh{"-yc"} ;
} else {
    print " y insert coordinate not set (option -yc) - using 0 \n" ;
    $yc = 0 ;
}
if (defined($argh{"-zc"})){
    $zc = $argh{"-zc"} ;
} else {
    print " z insert coordinate not set (option -zc) - using 0 \n" ;
    $zc = 0 ;
}
# define the Van der Waals radius for deletion sphere
if (defined($argh{"-vdw"})){
    $rvdw = $argh{"-vdw"} ;
} else {
    print " Van der Waals radius not set (option -rvdw) - using 0.12 nm \n" ;
    $rvdw = 0.12;
}

open(IN, "$infile") or die "cant open $infile (-f argument)" ;
```

```
@lines = (<IN>);
$nr = scalar @lines;
$first = $lines[0];
$totalatom = $lines[1];
$box = $lines[-1];
($boxX,$boxY,$boxZ) = split(' ',$box);
$end = $nr - 1;
$endend = $nr -3;
@splice = splice(@lines,2,$endend);
close(IN);

# get average values of x, y, and z for $infile molocule, this is the center
$avz = 0 ;
$avx = 0 ;
$avy = 0 ;
$ct = 0.001 ;
for ($i=0;$i<$endend;$i++)
{
    $_ = $splice[$i];
    ($resnr,$res,$name,$anr,$x,$y,$z,$dum1,$dum2,$dum3) = split(' ',$splice[$i]);
#    next unless $res eq $inmol;
    $avz += $z ;
    $avx += $x ;
    $avy += $y ;
    $ct += 1 ;
}
$avz /= $ct ;
$avx /= $ct ;
$avy /= $ct ;

# Define a transfer matrix based on center of molocule

$transfer = "transfer.itp" ;

open(OUT, ">$transfer") or die "can't open $transfer " ;

for ($j=0;$j<$endend;$j++)
{
    $_ = $lines[$j];
    ($resnr,$res,$name,$anr,$x,$y,$z,$dum1,$dum2,$dum3) = split(' ',$splice[$j]);
#    next unless $res eq $inmol;
    $transX = $x - $avx;
    $transY = $y - $avy;
    $transZ = $z - $avz;
    printf OUT "%1.3f %1.3f %1.3f\n",$transX,$transY,$transZ;
}

close(OUT);

# Define new coordinates of insert molocule based on defined xc, yc, and zc (transfer)

$transfermatrix ="transfer.itp";

open(TR, "$transfermatrix") or die "can't open $transfermatrix for adapting insert molocule " ;
@tlines = (<TR>);
chomp(@tlines);
$tnr = scalar @tlines;
close(TR);

$newx = 0;
$newy = 0;
$newz = 0;
$xc = $xc;
$yc = $yc;
$zc = $zc;

open(NEW, ">$outfile") or die "can't open $outfile for writing insert molocule coordinates " ;

for ($t=0;$t<($tnr);$t++)
{
$_ = $tlines[$t];
($xt,$yt,$zt) = split(' ',$tlines[$t]);
$newx = $xc + $xt;
$newy = $yc + $yt;
$newz = $zc + $zt;
printf NEW "%1.3f  %1.3f  %1.3f\n ",$newx,$newy,$newz;
}

close(NEW);

# make new coordinate file for newly centered insert molocule

@splice2 = splice(@lines,2,$end);

open(NEW2, "$outfile") or die "cant open $outfile (-fo argument) for finalizing molocule coordinates" ;
@n2lines = (<NEW2>);
chomp(@n2lines);
```

```
$n2nr = scalar @n2lines;
close(NEW2);

open(OUT2, ">$outfile2") or die " can't open $outfile2 ";

for ($n=0;$n<$tnr;$n++)
{
$_ = $n2lines[$n];
  ($xi,$yi,$zi) = split(' ',$n2lines[$n]);
$_ = $splice2[$n];
($resnr,$res,$name,$anr,$x,$y,$z,$dum1,$dum2,$dum3) = split(' ',$splice[$n]);
# next unless $res eq $inmol;
printf OUT2 "%5d %-4s %6s %5d %7.5s %7.5s %7.5s\n",$resnr,$res,$name,$anr,$xi,$yi,$zi;
}

close(OUT2);

open(IN2, "$system") or die "cant open $system (-s argument)" ;
@slines = (<IN2>);
$snr = scalar @slines;
close(IN2);

$subs = "WAT" ;
$maxRes = 0 ;
$minRes = 1000000 ;

for ($k=0;$k<$snr;$k++)
{
    $_ = $slines[$k];
    ($resnr,$res,$name,$anr,$x,$y,$z,$dum1,$dum2,$dum3) = split(' ',$slines[$k]);
    next unless $res eq $subs;
    if ($resnr > $maxRes){
$maxRes = $resnr;
    }else{
$maxRes = $maxRes;
    }
    if ($resnr < $minRes){
        $minRes = $resnr;
    }else{
        $minRes = $minRes;
    }
}

$rvdw = $rvdw;

# Cut residues with atoms that are within rvdw distance of any insert molocule atom
#($xt - $rvdw) <= $x && $x <= ($xt + $rvdw) && ($yt - $rvdw) <= $y
#   && $y<= ($yt + $rvdw) && ($zt - $rvdw) < $z && $z <= ($zt + $rvdw) &&

for ($k=0;$k<$snr;$k++)
{
$_ = $slines[$k];
($resnr,$res,$name,$anr,$x,$y,$z,$dum1,$dum2,$dum3) = split(' ',$slines[$k]);
# next unless $res eq $subs;
for ($t=0;$t<($tnr-1);$t++)
{
        $_ = $n2lines[$t];
      ($xt,$yt,$zt) = split(' ',$n2lines[$t]);
        if (sqrt(($x-$xt)*($x-$xt) + ($y-$yt)*($y-$yt) + ($z-$zt)*($z-$zt)) < $rvdw )
        {
                $keep[$resnr] += 1;
                print STDERR "removing residue $resnr\n";
        }else{ $keep[$resnr] -= 0;
        }

}
}

open(FIN, ">$outfile3" ) or die "can't open outfile3 $outfile3 -fo3 argument" ;


for ($l=0;$l<$snr;$l++)
{
$_ = $slines[$l];
($resnr,$res,$name,$anr,$x,$y,$z,$dum1,$dum2,$dum3) = split(' ',$slines[$l]);
if ( $keep[$resnr] < 1 )
{
print FIN $slines[$l];
}
}

close(FIN);

open(OU2, "$outfile2" ) ;
@o2lines = (<OU2>);
close(OU2);
```

```
open(OU3, "$outfile3" ) ;
@fflines = (<OU3>);
$fnr = scalar @fflines;
$fend = $fnr - 3;
$felines = @fflines[-1];
@filines = splice(@fflines,0,2);
@flines = splice(@fflines,0,$fend);
close(OU3);

open(OU4, ">$outfile4" ) ;
print OU4 @filines;
print OU4 @o2lines;
print OU4 @flines;
print OU4 $felines;
close(OU4);

open(CHK, "$outfile4") ;
@chk = (<CHK>);
$chklines = scalar @chk;
$nbratoms = $chklines - 3;
$header = @chk[0];
$na = @chk[1];
$bodylength = $chklines -2;
@body = splice(@chk,2,$bodylength);
close(CHK);

open(FO, ">$finaloutput" );
print FO $header;
print FO "$nbratoms\n";
print FO @body;
close(FO);

exit(0);
```

VITA

The author, Joseph Walter Lambert, was born on September 12, 1981 in Anderson, SC. He graduated from Providence High School in Charlotte, NC in 1999 with Honors and then attended the Citadel where he majored in Biology. After one year, the author transferred to the University of South Carolina to major in Chemical Engineering. He graduated from the University of South Carolina with a Bachelors of Science degree in Chemical Engineering. During his undergraduate studies, the author participated in the cooperative education program with Milliken Co. and undergraduate research with Dr. John W. Weidner. In August 2004, the author began graduate studies at Virginia Tech where his Masters of Science degree was completed in the Summer I semester of 2006 under the supervision of Dr. Amadeu K. Sum. The author is currently employed at Michelin North America in Greenville, SC as a research and development engineer.